Oak Ridge National Laboratory
12/10/2019, 1000 hrs
MDF Room 325

Smart Additive Manufacturing

Modeling, Sensing, and Analytics for Zero Part Defects

Prahalada Rao, Ph.D.

rao@unl.edu
Cell: 814–384–9676

Mechanical and Materials Engineering
University of Nebraska-Lincoln

Acknowledgements

Dr. Scott Smith

THE UNIVERSITY OF TENNESSEE KNOXVILLE

Dr. Chad E. Duty
&
Dr. S.S. Babu

“If I have seen a littler further it is by standing on the shoulder of giants”

Acknowledgements

National Science Foundation (NSF)
CMMI 1752069 (CAREER)
CMMI-1719388
CMMI-1739696
CMMI-1920245 (MRI)

NSF INTERN-ship program at
Edison Welding Institute and
Lawrence Livermore National Laboratory

Acknowledgements

Students

Reza Yavari

Jordan Severson

Aniruddha Gaikwad

Mohammad Montazeri

Colleagues

Dr. Kevin Cole (UNL)

Dr. Abdalla Nassar (Penn State)

Dr. Linkan Bian (Mississippi State)

Dr. Paul Hooper (Imperial College, London)

My scholastic passion: Manufacturing, Sensing, and Analytics.

Neurophysiology

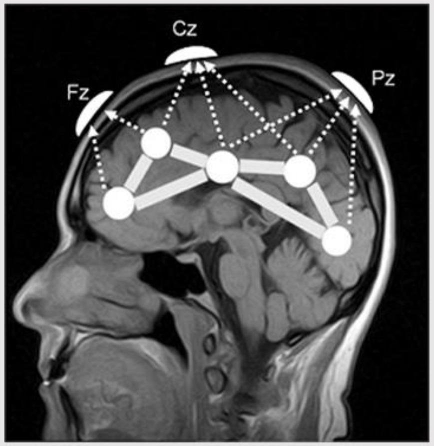

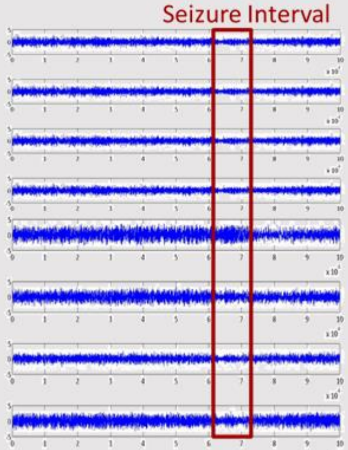

Metal Additive Manufacturing (AM)

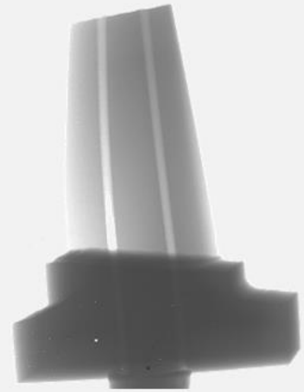

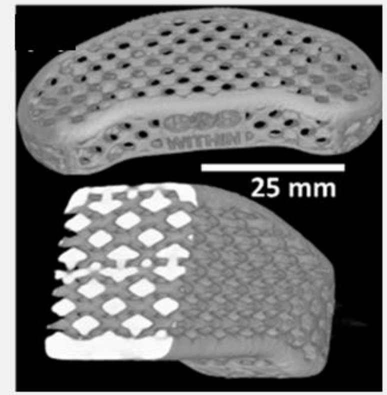

Ultraprecision Machining and Polishing Graduate Studies

Diamond Turning

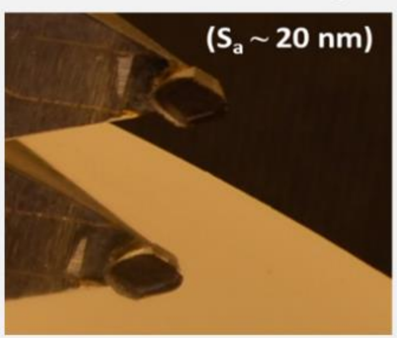

Polishing

Polymer Additive Manufacturing and Aerosol Jet Printing

Printed Electronics

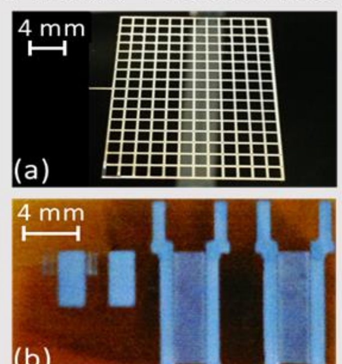

Fused Filament

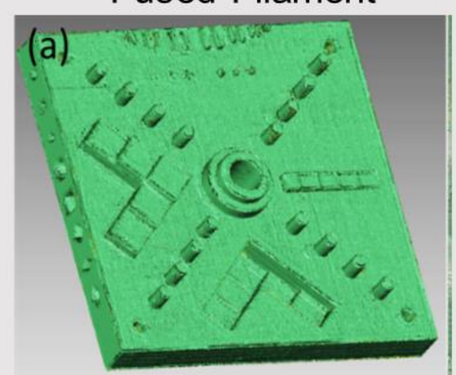

My research goal is to make flaw-free AM parts.

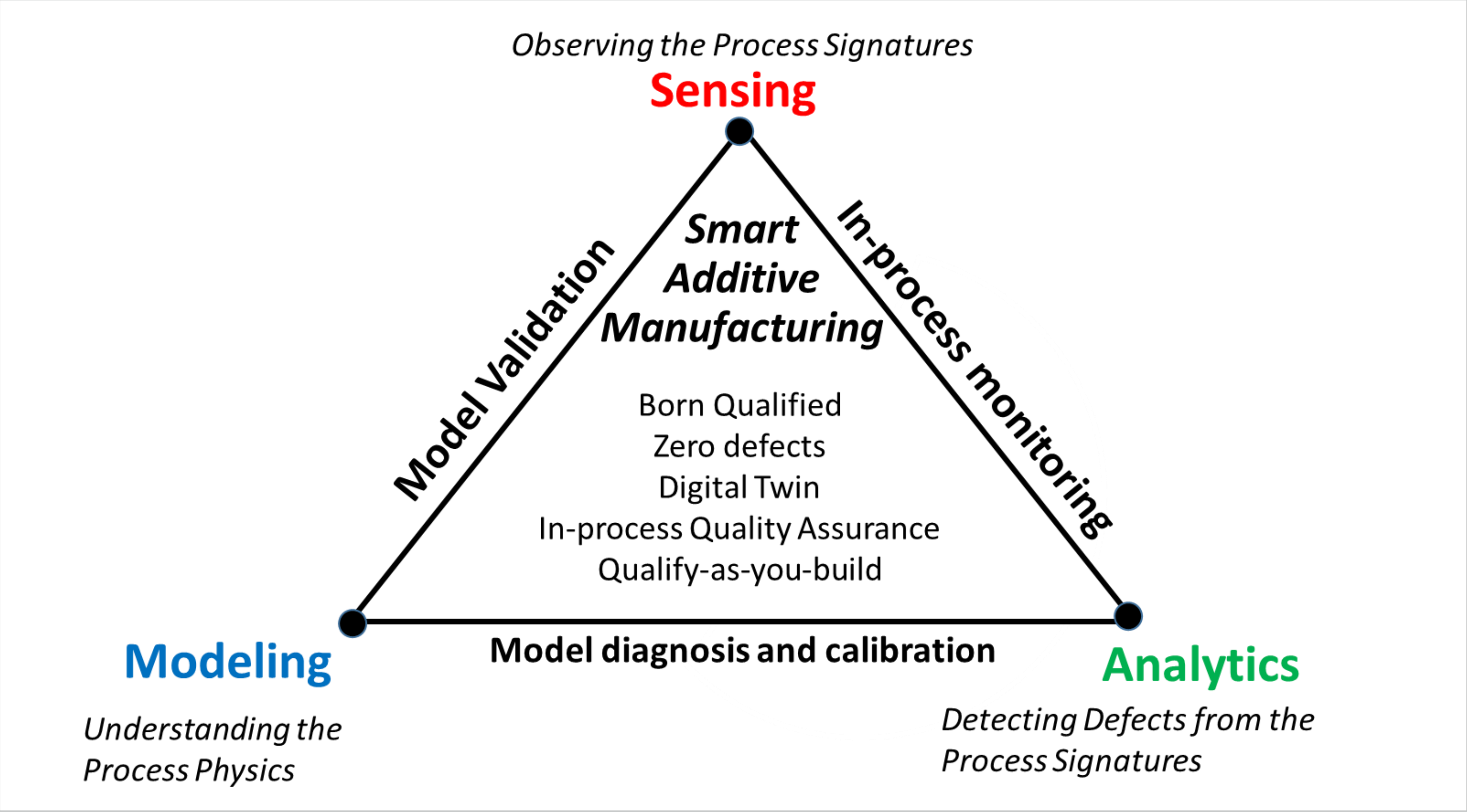

Prior Work with Oakridge

Using graph theory to quantify the dimensional variation between parts from point cloud data.

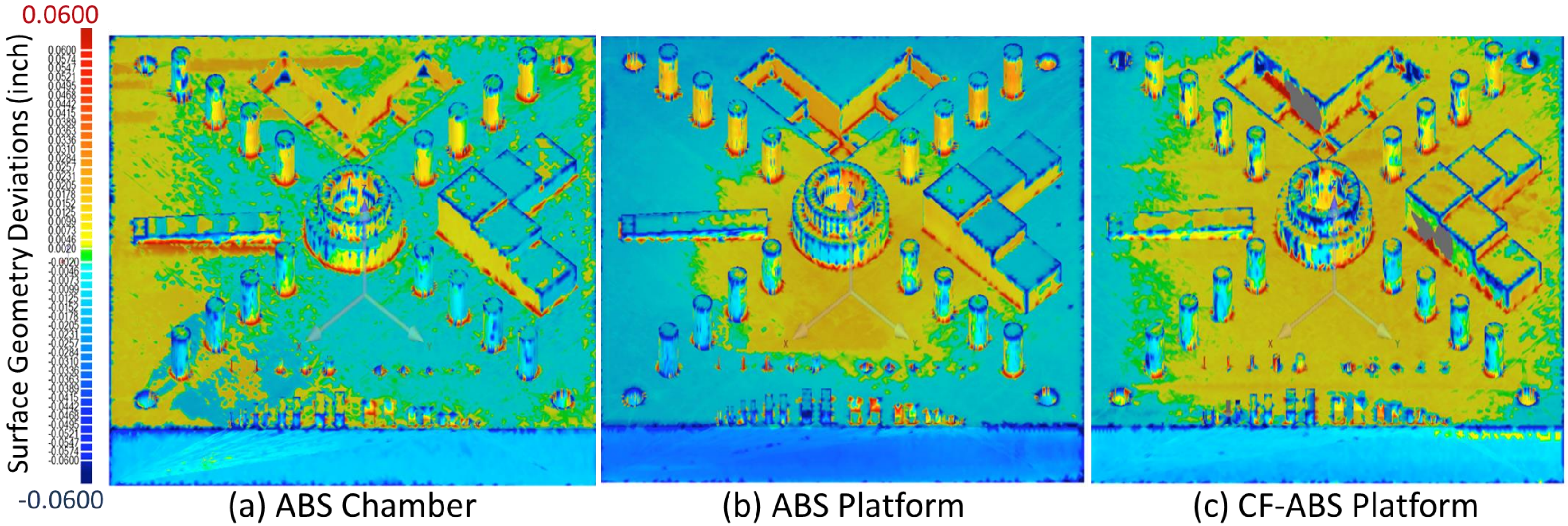

Tell what went wrong, where it went wrong, and by how much?

P. Rao, Z. Kong, **V. Kunc, R. Smith, C. Duty**, Assessment of Dimensional Integrity and Spatial Defect Localization in Additive Manufacturing (AM) using *Spectral Graph Theory (SGT)*. *ASME Transactions, Journal of Manufacturing Science and Engineering*. 138(5), doi: 10.1115/1.4031574

LINK

This presentation has two parts.

Part I: Ultrafast thermal modeling in AM using graph theory (Slide 15 – 70).

Part II: Combining thermal modeling with data analytics (Slide 71 – 83).

This work has been published

A.C. Gaikwad, R. Yavari, M. Montazeri, K. Cole, L. Bian, P. Rao,
Toward the Digital Twin in Metal Additive Manufacturing – Integrating Thermal Simulations, Sensing, and Analytics to Detect Process Faults,
IISE Transactions (Accepted)
10.1080/24725854.2019.1701753

R. Yavari, K. Cole, P. Rao
Thermal Modeling in Metal Additive Manufacturing using Graph Theory.
ASME Transactions, Journal of Manufacturing Science and Engineering
2019, Vol. 141, pp. 0710071-20.
10.1115/1.4043648

Ultrafast Thermal Simulation of Metal Additive Manufacturing

Simulate the thermal field in AM in near real-time using graph theory.

- Mesh-free, discrete modeling.
- Faster and error within 10% of finite element analysis.

Graph Theory
18 minutes

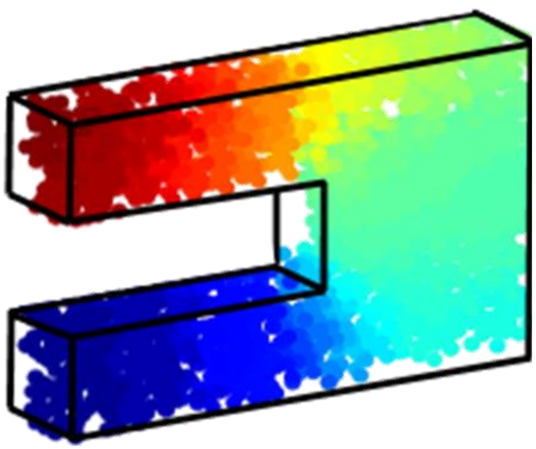

Finite Element (Abaqus)
180 minutes

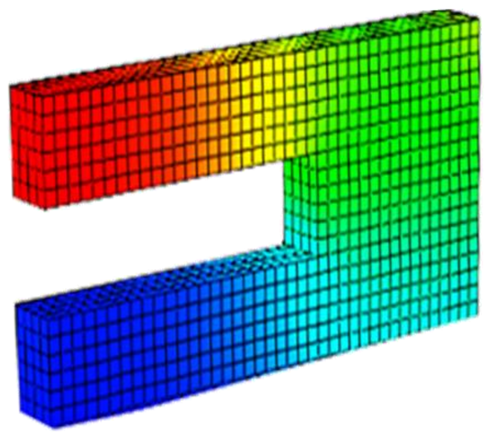

Commercial Code
30 minutes

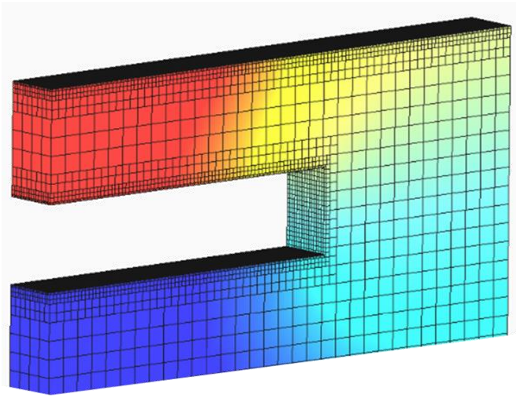

Decreasing flexibility and ability to tinker

Objective and Hypothesis

Solve the heat diffusion equation using graph theory.

$$\rho c_p \frac{\partial \mathrm{T}(x,y,z,t)}{\partial t} - k\left(\frac{\partial^2}{\partial x^2} + \frac{\partial^2}{\partial y^2} + \frac{\partial^2}{\partial z^2}\right)\mathrm{T}(x,y,z,t) = \mathrm{E}_V$$

Hypothesis

The heat equation is solved using graph theory.

Outcome

Graph theory takes 1/10th of time to converge than finite element analysis within acceptable error (10%).

Application to Flaw Detection: Digital Twin
In-process sensor data + Theoretical Simulations → Defect prediction

Actual Part

Sensor Data

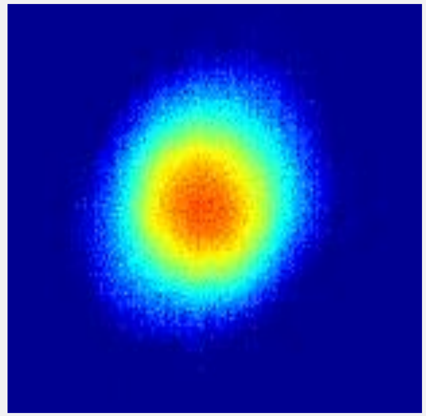

+

Part Temperature predicted from simulation

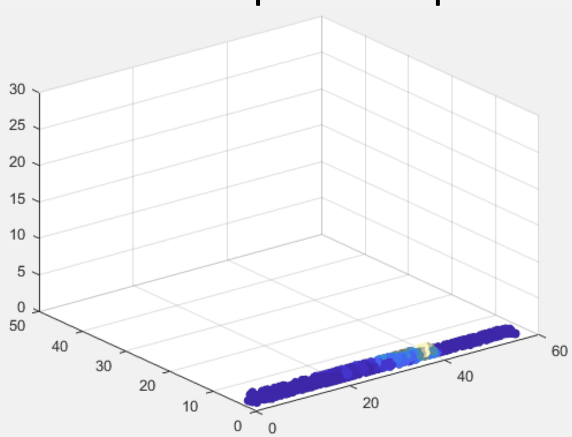

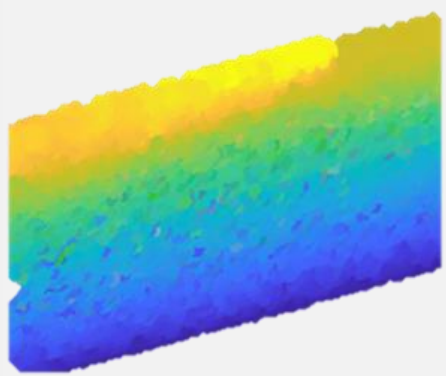

Prediction of pores.

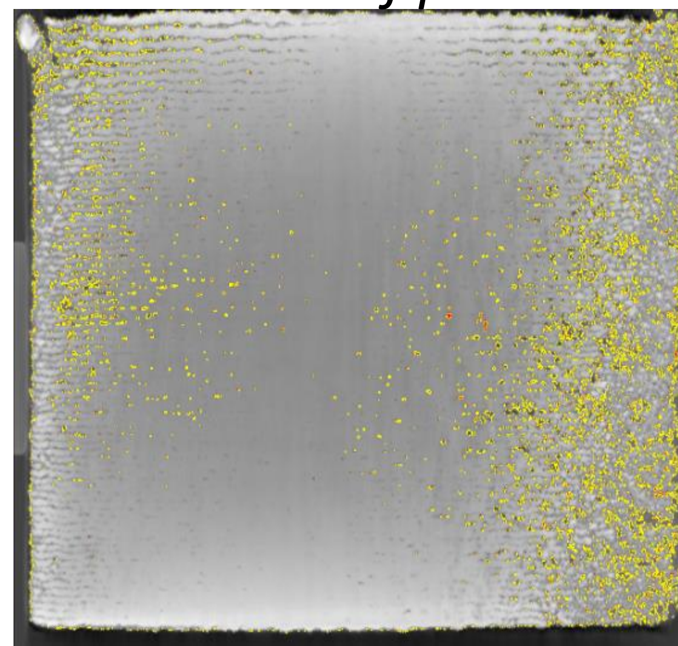

Who Cares?

Fundamental research is needed in AM processes integrating modeling, sensing, and process control.

2014 NSF Additive Manufacturing Workshop Report.

Y. Huang, M. C. Leu, J. Mazumder, and A. Donmez, *Additive Manufacturing: Current State, Future Potential, Gaps and Needs, and Recommendations*, Transactions of the ASME, Journal of Manufacturing Science and Engineering, vol. 137, p. 014001, 2015.

Outline

Motivation & Rationale

Who cares?

Part I: The graph theory approach for thermal modeling in AM

How does it work, and what is different about it?

Verification of the graph theory approach

How does it compare to the known solutions and existing techniques?

Experimental validation

How well does it work in the real-world?

Part II: Application (Digital Twin)

Combining thermal modeling with machine learning to detect defects

Conclusions and future work

Research Goal

Predict the thermal history in AM parts and use the knowledge to prevent defects.

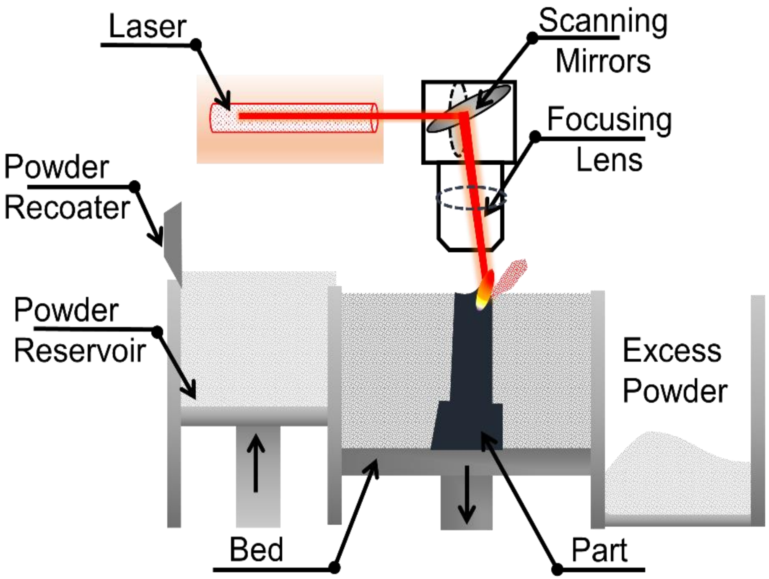

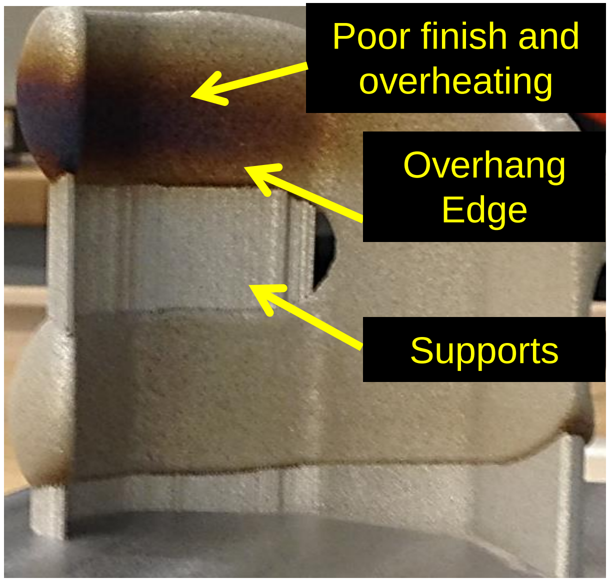

Metal AM Knee Implant

Part quality (geometry, microstructure, surface finish) in AM is governed by the thermal history.

Build-and-test is ineffective in AM

Seven identical parts built simultaneously on a commercial machine. Only 2 out of 7 were built defect free.

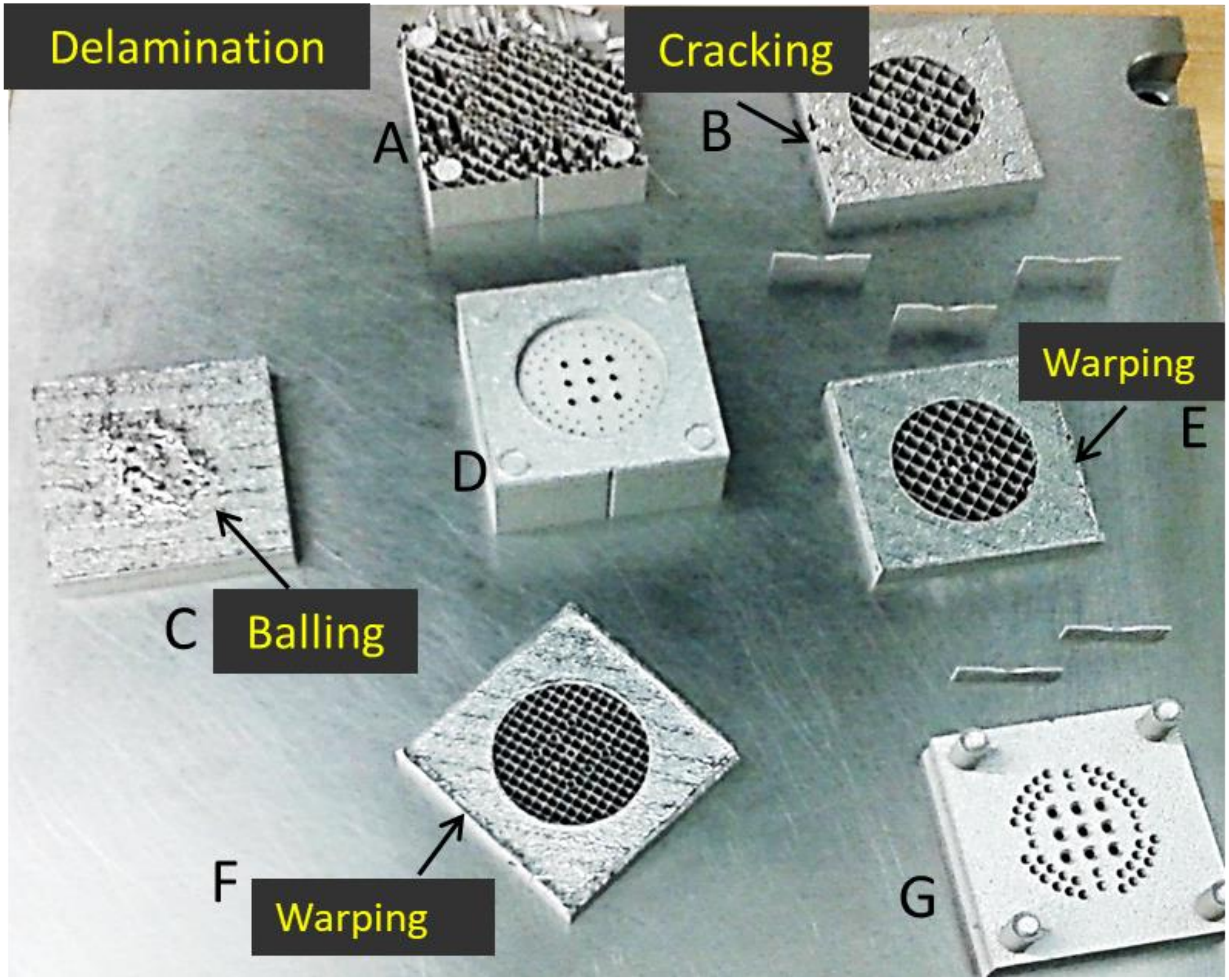

No global optimal parameter set can be defined.

Everything is linked to the thermal history

Experiments may span over several years and cost millions of dollars.

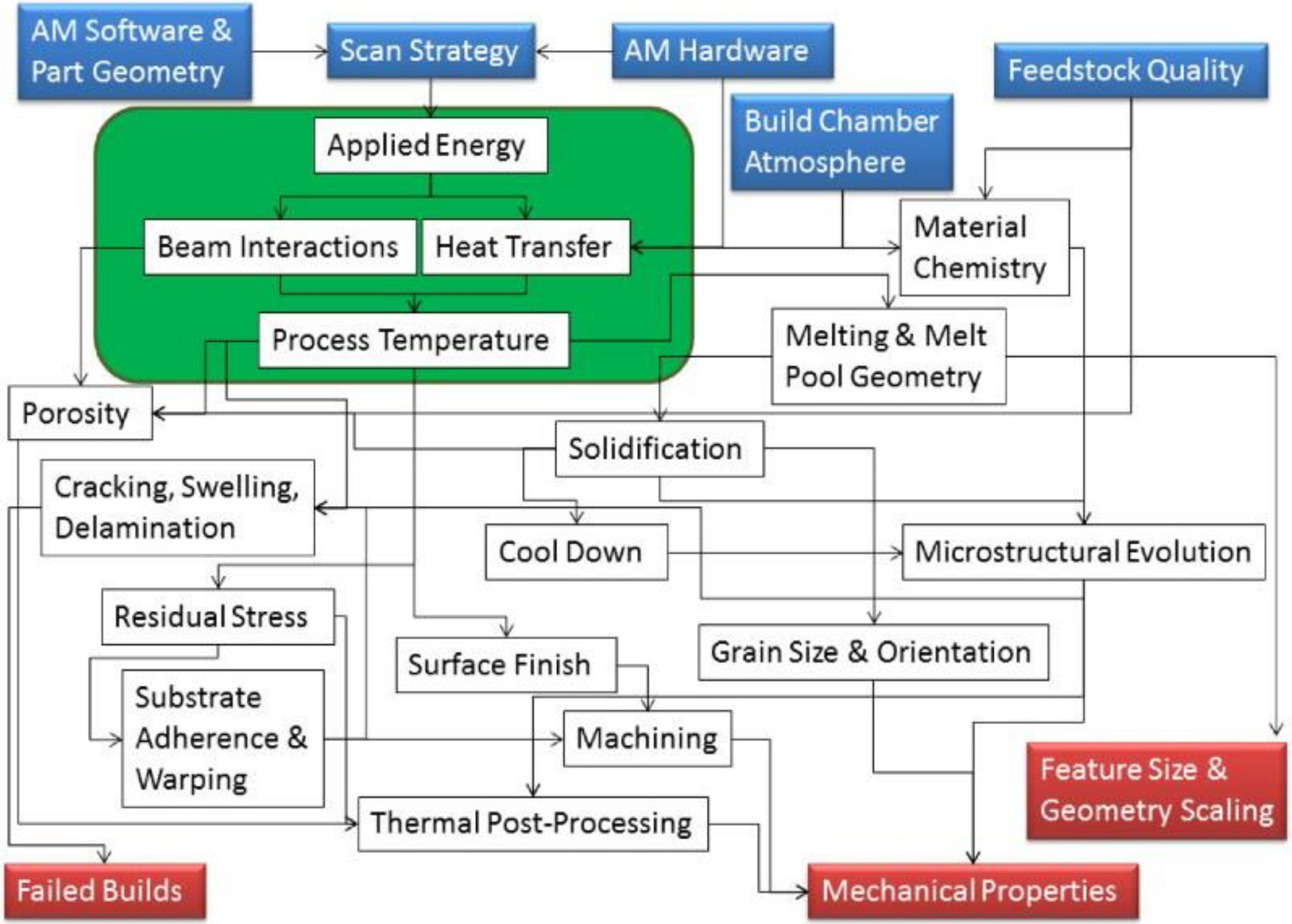

W. J. Sames, F. A. List, S. Pannala, R. R. Dehoff & S. S. Babu (2016) The metallurgy and processing science of metal additive manufacturing, International Materials Reviews, 61:5, 315-360, DOI: 10.1080/09506608.2015.1116649

Rationale

It is important to have a simulation capability and models that can predict part performance, support development of processing and materials strategies, and enable materials design in an integrated fashion.

W. J. Sames, F. A. List, S. Pannala, R. R. Dehoff & S. S. Babu (2016) The metallurgy and processing science of metal additive manufacturing, International Materials Reviews, 61:5, 315-360, DOI: 10.1080/09506608.2015.1116649

Combine process physics with data analytics and sensing to scale AM

Paradigm shift from empirical optimization to physics-driven AM.

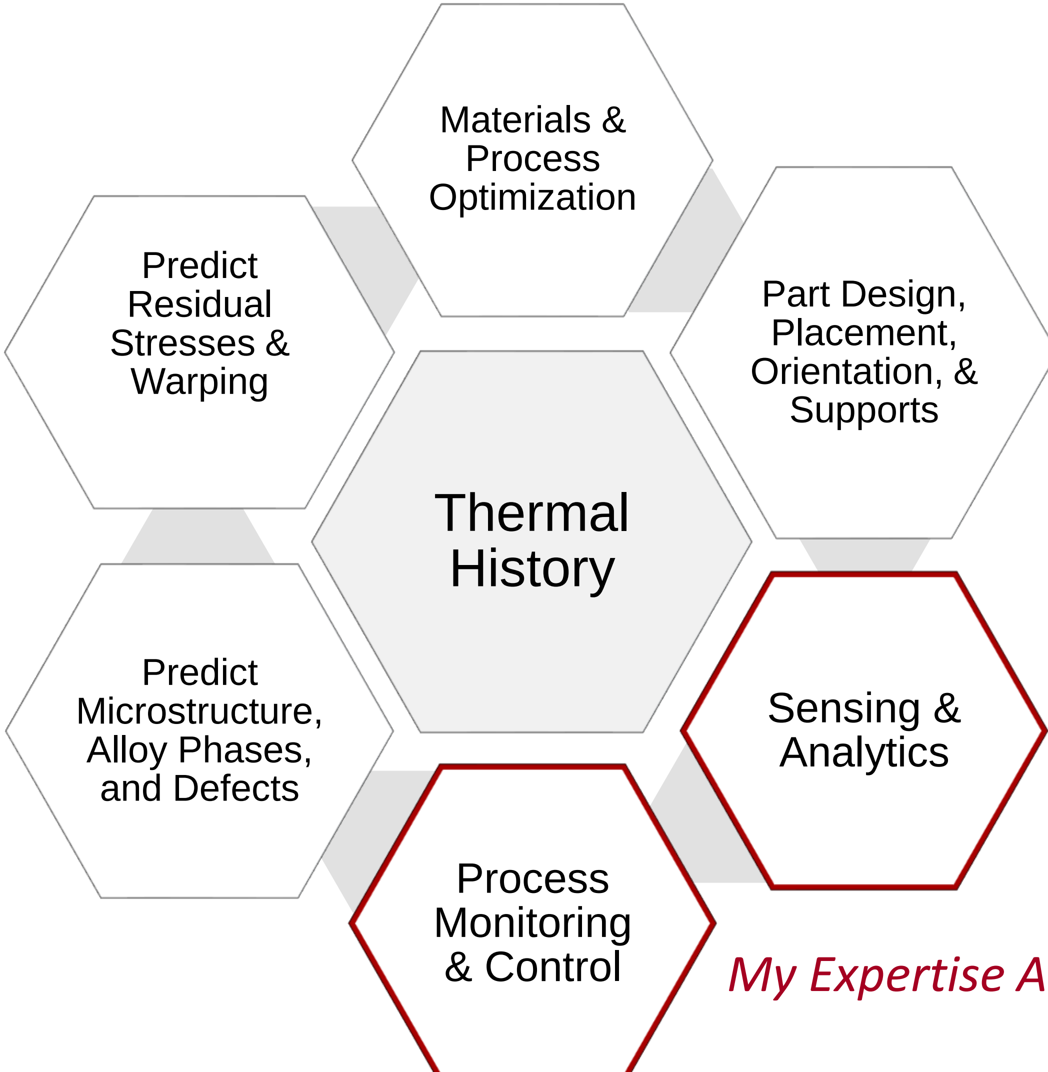

My Expertise Area

My Vision: Correct-as-you-build in AM

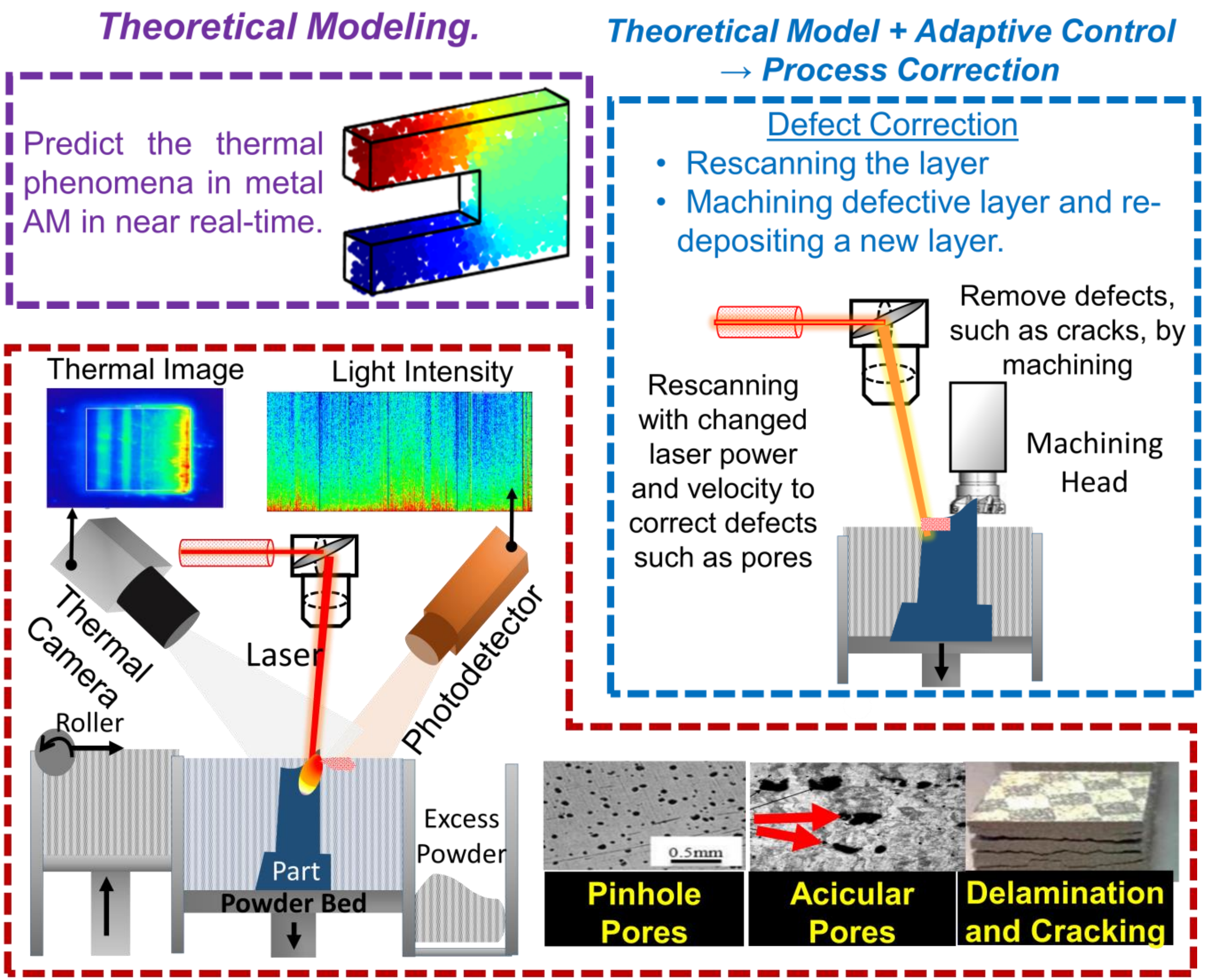

Sensing and Analytics for Real-time Defect Defection.
Sensor Signatures + Theoretical Predictions → Defects

Unique Capabilities for Metal AM in Nebraska

2 X Matsuura Lumex Hybrid LPBF

Optomec LENS 450 Hybrid DED

- Optomec LENS 450 Hybrid Directed Energy Deposition Metal Additive Manufacturing system
- Matsuura Lumex Avance Hybrid Laser Powder Bed Fusion Machine (open atmosphere)
- Matsuura Lumex Avance Hybrid Laser Powder Bed Fusion Machine (inert atmosphere)

Hybrid AM is the key to Correct-as-you-build.

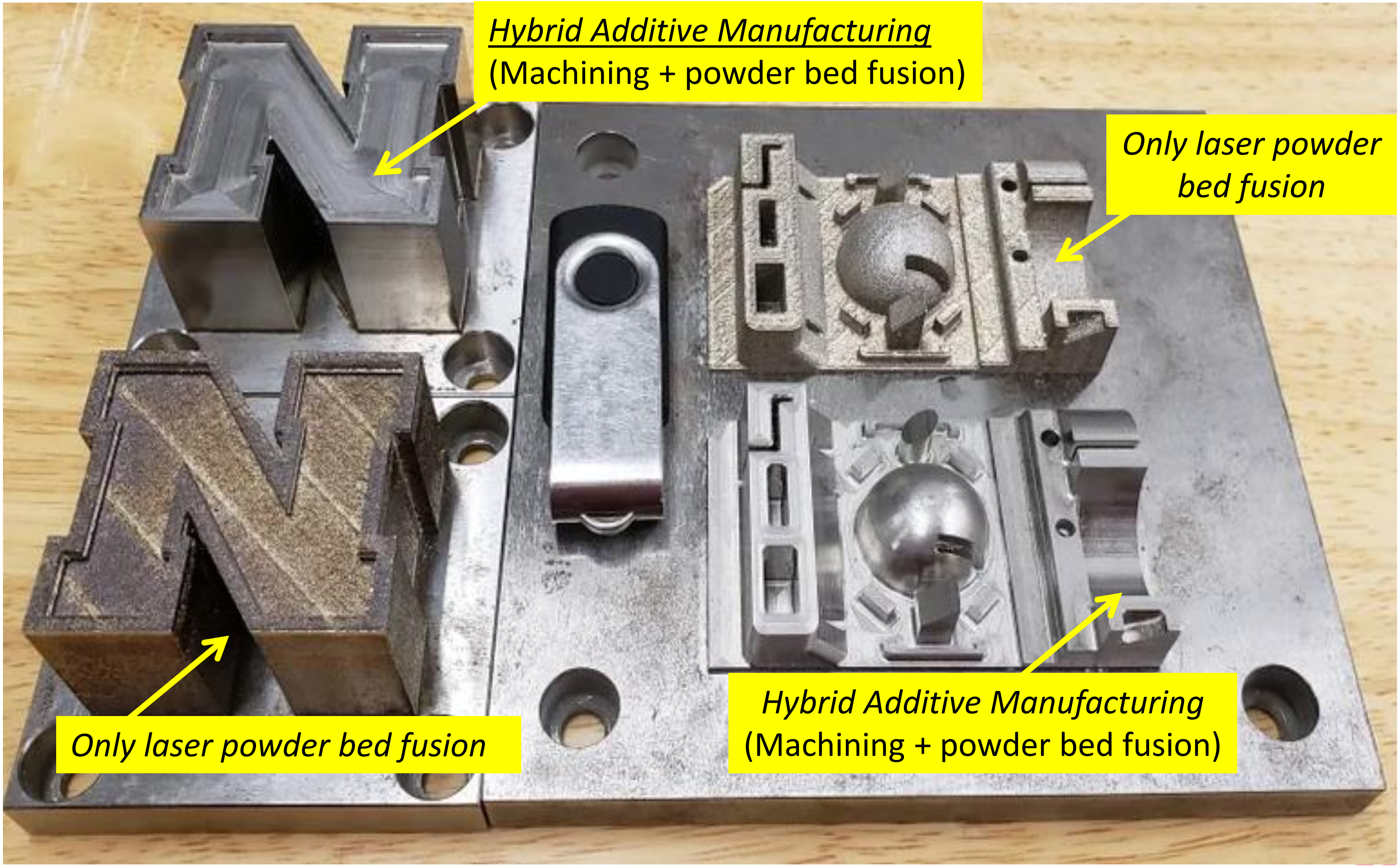

Outline

- Motivation
- Part I: Graph theory approach for thermal modeling in AM

  How does it work, and what is different about the approach?

  - Verification of the graph theory approach
  - Experimental validation
- Part II: Application
- Conclusions and future work

Background to Thermal Modeling in AM

1. Meltpool or small-scale modeling (< 100 µm)
   Focuses on heat source interaction zone (melt-pool)
2. Part-scale modeling (> 100 µm)
   Focus on predicting part-level distortion and residual stresses

Meltpool Scale

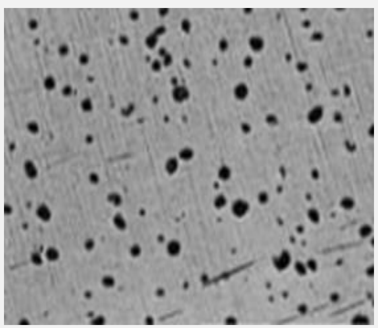

< 10 µm
Vaporization

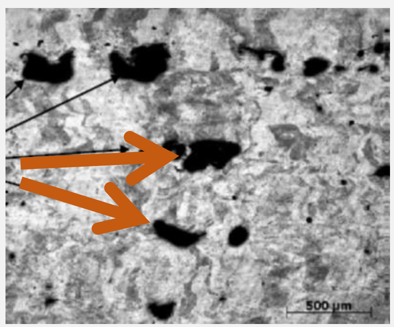

10 µm – 100 µm
Melting/Fusion

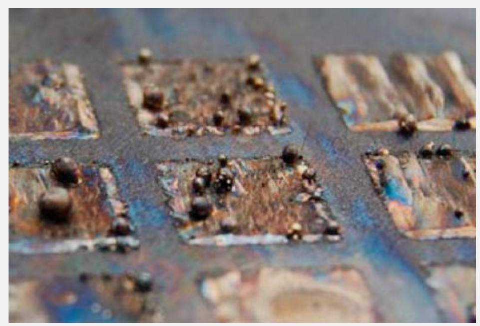

100 µm – 200 µm
Meltpool dynamics

Part- Scale Modeling

> 100 µm
Thermal-induced cracking and distortion

W. J. Sames, F. List, S. Pannala, R. R. Dehoff, and ***S. S. Babu***, "The Metallurgy and Processing Science of Metal Additive Manufacturing," International Materials Reviews, vol. 61, pp. 315-360, 2016.

 27

Part-level thermal modeling in AM is computationally intensive

It takes several hours, if not days to conduct thermal analysis of a simple geometry.

THE CORRECT ANSWER REQUIRES VECTOR-BY-VECTOR COMPUTATION

Without Supports

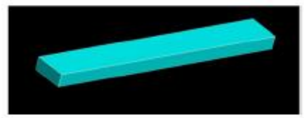

40mm x 5mm x 2mm part

Layers: 66

Hatches Considered: 17,490

Laser Positions: 13,216,038

With pillar supports

Layers: 233

Hatches Considered: 61,745

Laser Positions: 25,766,422

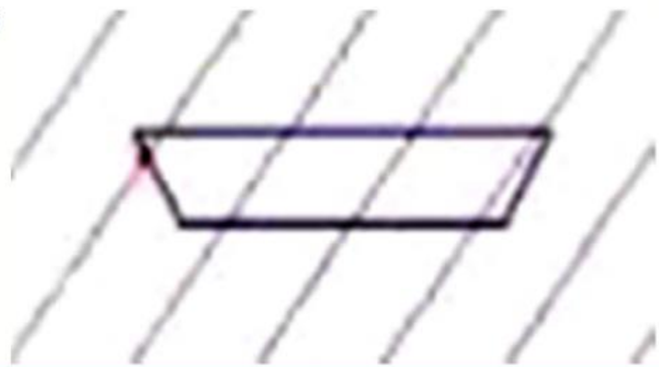

ANSYS Computational Time

~150 years

3DSIM

WWW.3DSIM.COM

Z. Luo and Y. Zhao, "A survey of finite element analysis of temperature and thermal stress fields in powder bed fusion Additive Manufacturing," *Additive Manufacturing,* vol. 21, pp. 318-332, 2018/05/01/ 2018.

Thermal modeling in AM involves multi-scale phenomena

Simplify computation by ignoring meltpool-level and meso-scale phenomena

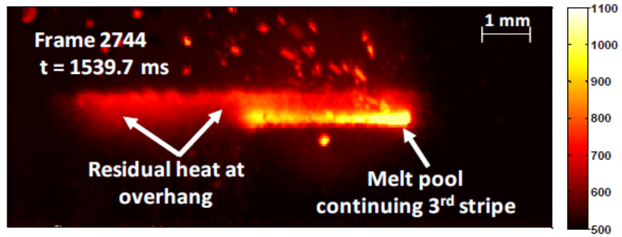

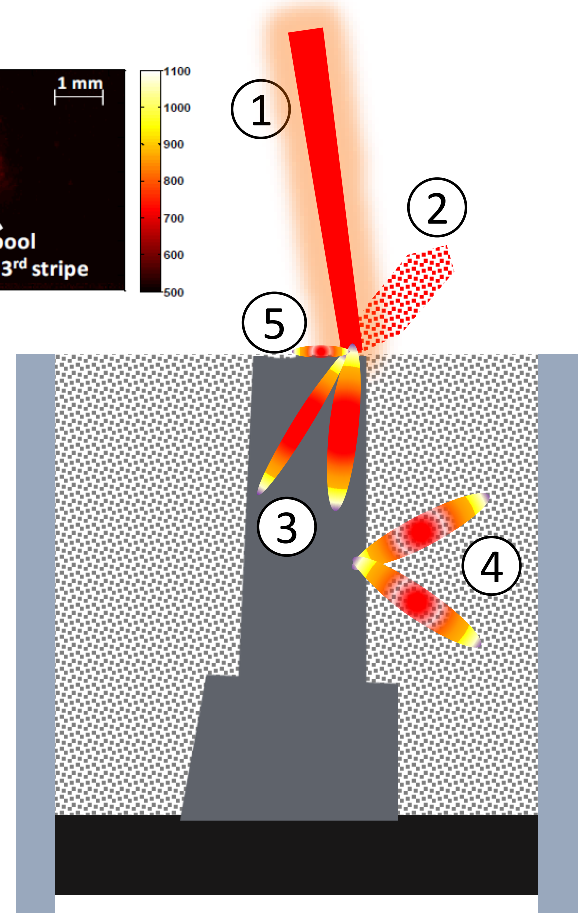

1) Energy supplied by the laser
2) Radiation on the top layer (part to air)
3) Conduction within the part (within part)
4) Convection between part and surrounding area
5) Latent heat at the melt-pool.
6) Temperature dependent properties

King, W., Anderson, A., Ferencz, R., Hodge, N., Kamath, C., Khairallah, S., and Rubenchik, A., 2015, "Laser powder bed fusion additive manufacturing of metals; physics, computational, and materials challenges," Applied Physics Reviews, 2(4), p. 041304.

Khairallah, S. A., Anderson, A. T., Rubenchik, A., and King, W. E., 2016, "Laser powder-bed fusion additive manufacturing: Physics of complex melt flow and formation mechanisms of pores, spatter, and denudation zones," Acta Materialia, 108, pp. 36-45.

Graph Theory Approach for Thermal Modeling in AM

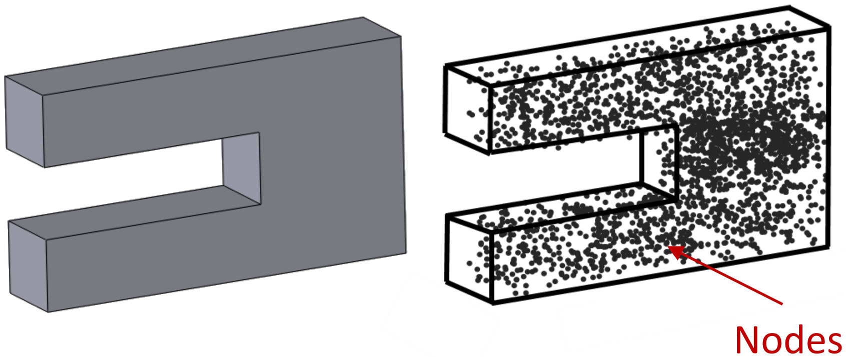

Step 1- Convert the part into a set of discrete nodes

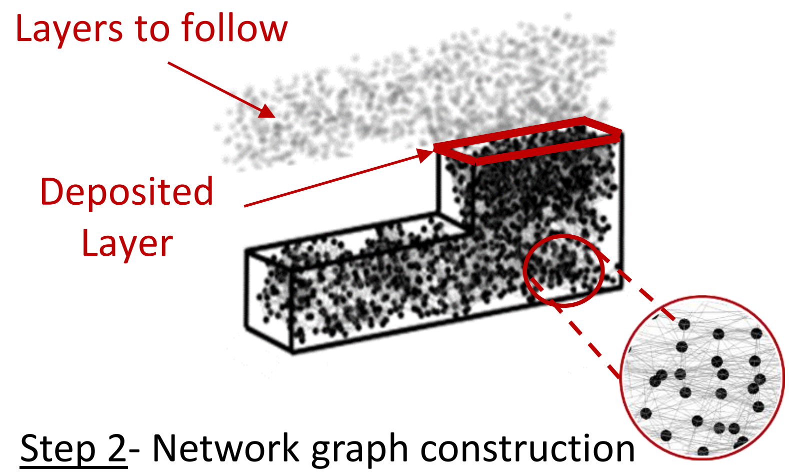

Step 2- Network graph construction

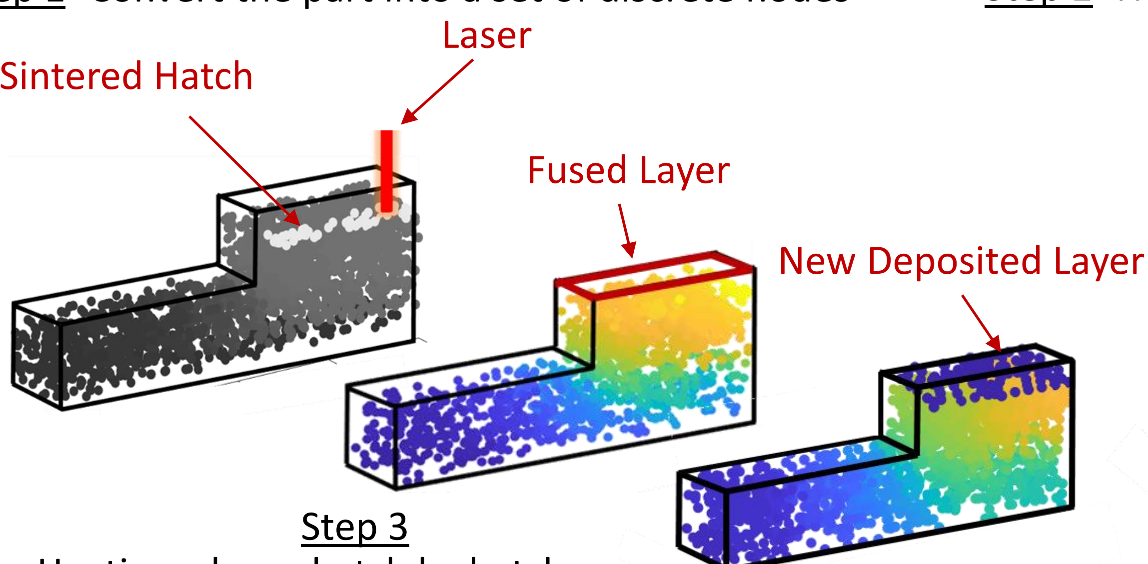

Step 3

- Heating a layer, hatch by hatch,
- Diffusion of the heat through the part
- Deposition of a new layer

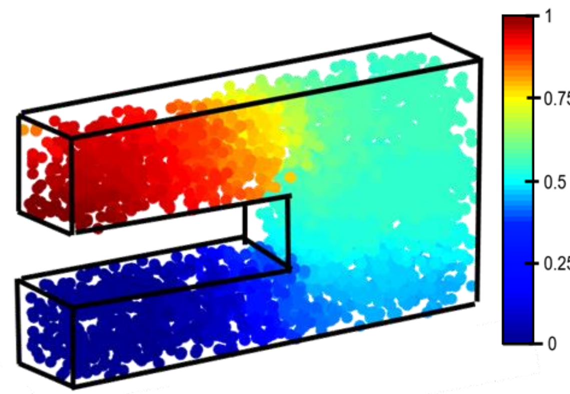

Step 4

Result as temperature matrix which shows the temperature history of the part

The Scientific Problem

Solve the steady-state continuum heat diffusion equation

Temperature (T) is a function of space (x, y, z) and time (t)

The Heat Equation (Fourier's Law of Conduction)

$$\underbrace{\boxed{\rho c_p \frac{\partial T}{\partial t}}}_{\text{Time } (t)} - k \underbrace{\boxed{\left(\frac{\partial^2}{\partial x^2} + \frac{\partial^2}{\partial y^2} + \frac{\partial^2}{\partial z^2}\right)}}_{\text{Space } (x,y,z)} T = E_V$$

K = thermal conductivity ρ = density C_p = specific heat

Solving the Heat Equation with Graph Theory

$$\frac{\partial \mathrm{T}}{\partial t} - \frac{k}{\rho c_p}\left(\frac{\partial^2}{\partial x^2} + \frac{\partial^2}{\partial y^2} + \frac{\partial^2}{\partial z^2}\right)\mathrm{T} = \mathrm{E}_V$$

Laplacian operator

$$\Delta \stackrel{\text{def}}{=} \left(\frac{\partial^2}{\partial x^2} + \frac{\partial^2}{\partial y^2} + \frac{\partial^2}{\partial z^2}\right)$$

$$\boxed{\frac{\partial \mathrm{T}}{\partial t} - \alpha(\Delta)\mathrm{T} = 0}$$

Thermal diffusivity

$$k/\rho\, c_p = \alpha$$

Melting point of the material

$$\mathrm{T}(\mathrm{t} = 0) = \mathrm{T}_0$$

Solving the Heat Equation with Graph Theory

$$\frac{\partial \mathrm{T}}{\partial t} - \alpha(\Delta)\mathrm{T} = 0$$

The Key Idea

Replace the continuous Laplacian operator Δ
with a discrete matrix called the Graph Laplacian $\mathcal{L}$.

$$\boxed{\Delta \approx -\mathcal{L}}$$

$$\frac{\partial \mathrm{T}}{\partial t} + \alpha(\mathcal{L})\mathrm{T} = 0$$

Why do it this way?
The second derivative term does not have to be solved.

Solving the Heat Equation with Graph Theory

$$\frac{\partial \mathrm{T}}{\partial t} + \alpha(\mathcal{L}\ )\mathrm{T} = 0$$

First Order differential equation → separate variables and integrate.

$$\frac{\partial \mathrm{T}}{-\alpha(\mathcal{L}\ )\mathrm{T}} = \partial t$$

$$\int \frac{\partial \mathrm{T}}{-\alpha(\mathcal{L}\ )\mathrm{T}} = \int \partial t$$

$$-\alpha\mathcal{L}(\ln \mathrm{T}) = \mathrm{t} + \mathrm{K}$$

$$\boxed{\mathrm{T}\ = e^{-\alpha\mathcal{L}(\mathrm{T})}\ \mathrm{T}_o}$$

Solving the Heat Equation with Graph Theory

$$\mathrm{T} = e^{-\alpha(\mathcal{L})t}\ \mathrm{T}_o$$

Decompose $\mathcal{L}$ into eigenvalues and eigenvectors

$$\mathcal{L}\phi = \phi\Lambda$$

$$\mathcal{L} = \phi\Lambda\phi^{-1}$$

Eigenvectors of $\mathcal{L}$ are orthogonal

$$\phi^{-1} = \phi'$$

$$\mathcal{L} = \phi\Lambda\phi'$$

$$\boxed{\mathrm{T} = e^{-\alpha(\phi\Lambda\phi')t}\ \mathrm{T}_o}$$

The Heat Equation is solved as a function of the
Eigenvalues (Λ) and Eigenvectors (ϕ) of the Discrete Laplacian Matrix ($\mathcal{L}$)

Simplify $e^{-\alpha(\phi\Lambda\phi')t} = \phi e^{-\alpha(\Lambda)t}\phi'$

Taylor Series Expansion

$$e^{-\alpha(\phi\Lambda\phi')t} = 1 + \frac{(-\alpha(\phi\Lambda\phi')t)}{1!} + \frac{(-\alpha(\phi\Lambda\phi')t)^2}{2!} + \frac{(-\alpha(\phi\Lambda\phi')t)^3}{3!} + \cdots$$

$$e^{-\alpha(\phi\Lambda\phi')t} = 1 - \alpha t\frac{\phi\Lambda\phi'}{1!} + \alpha^2 t^2\frac{(\phi\Lambda\underbrace{\phi')(\phi}_{=1}\Lambda\phi')}{2!} - \alpha^3 t^3\frac{(\phi\Lambda\underbrace{\phi')(\phi}_{=1}\Lambda\underbrace{\phi')(\phi}_{=1}\Lambda\phi')}{3!} + \cdots$$

Eigenvectors are Orthogonal $\quad \phi\,\phi' = 1$

$$e^{-\alpha(\phi\Lambda\phi')t} = 1 - \frac{\phi\Lambda\alpha t\phi'}{1!} + \frac{\phi(\Lambda\alpha t)^2\phi'}{2!} - \frac{\phi(\Lambda\alpha t)^3\phi'}{3!} + \cdots = \phi e^{-\alpha(\Lambda t)}\phi'$$

$$\boxed{T = \phi e^{-\alpha(\Lambda)t}\phi' T_o}$$

Solving the Heat Equation with Graph Theory

The Heat Equation is solved as a function of the Eigenvalues (Λ) and Eigenvectors (ϕ) of $\mathcal{L}$

$$\boxed{\mathrm{T} = \phi e^{-\alpha g(\Lambda) t} \phi' \mathrm{T}_o}$$

g is called the *gain factor*

Even Einstein was allowed a fudge factor…

Cosmological Constant

$$R_{\mu\nu} - \frac{1}{2}Rg_{\mu\nu} + \boxed{\Lambda}g_{\mu\nu} = \frac{8\pi G}{c^4}T_{\mu\nu},$$

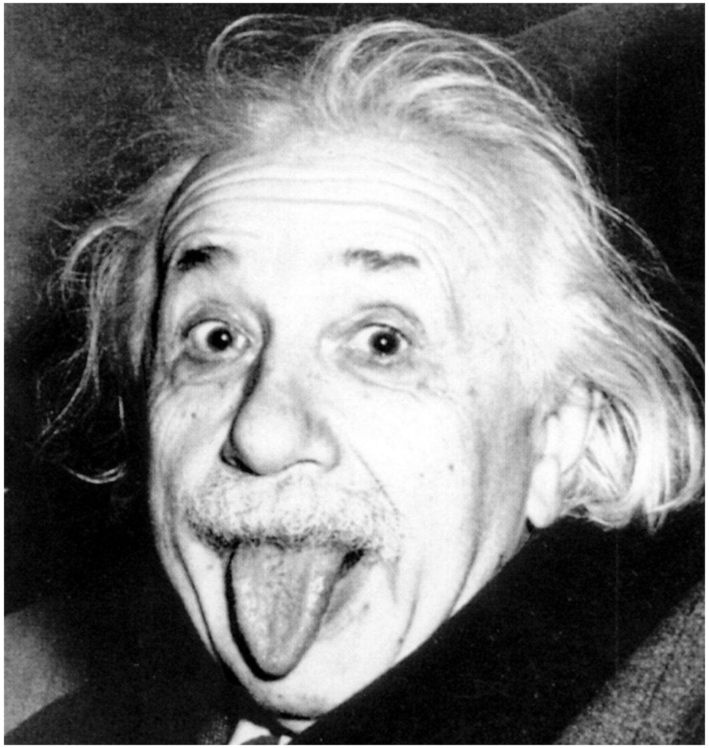

Advantages of the graph theory approach

$$\boxed{\mathrm{T} = \phi e^{-\alpha \mathrm{g}(\Lambda)t} \phi' \mathrm{T}_o}$$

1. No meshing steps.
2. Freedom to discretize time t into any desired length.
3. Does not require matrix inversion; only matrix multiplication.

How to obtain ϕ and Λ?

ϕ and Λ are obtained in Step 2

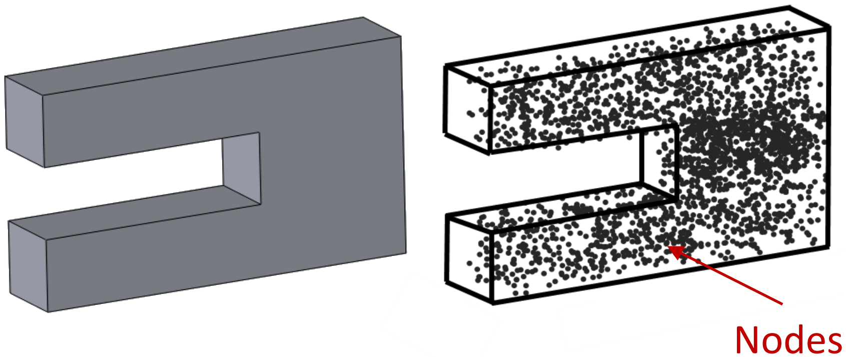

Step 1- Convert the part into a set of discrete nodes

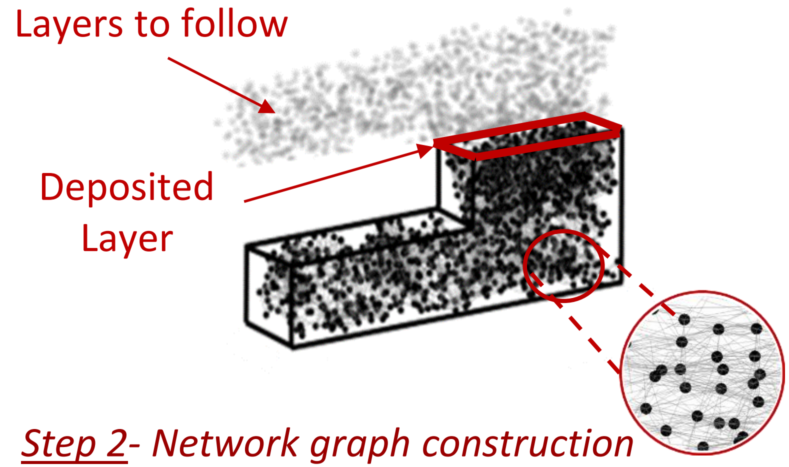

Step 2- Network graph construction

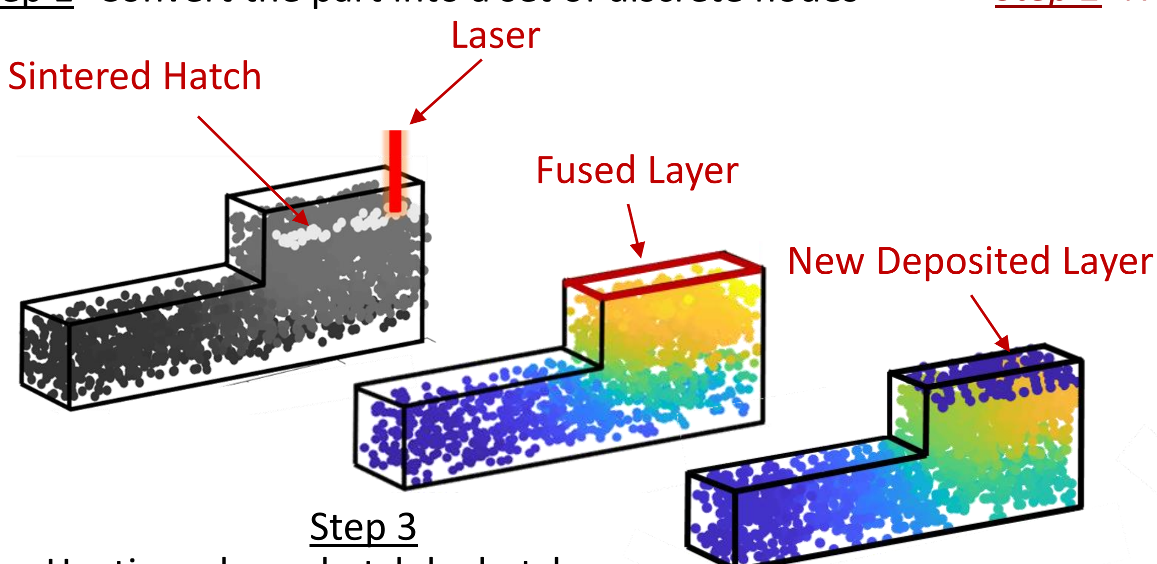

Step 3

- Heating a layer, hatch by hatch,
- Diffusion of the heat through the part
- Deposition of a new layer

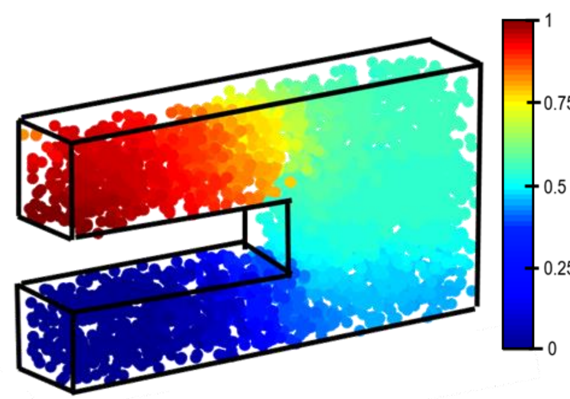

Step 4

Result as temperature matrix which shows the temperature history of the part

Obtaining the Laplacian Matrix ($\mathcal{L}$)

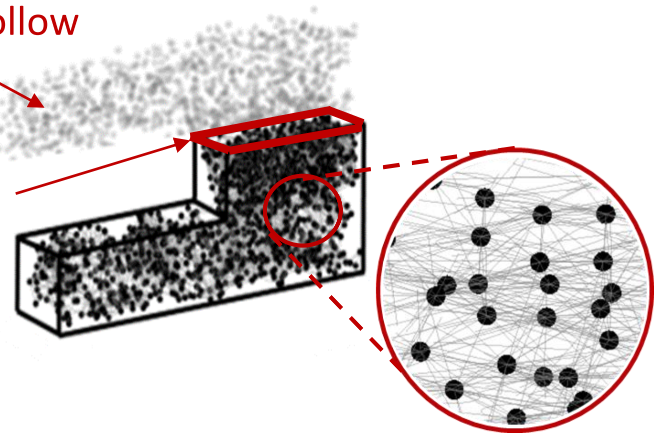

Step 2- Network graph construction

Connect nodes with a radius of ε mm

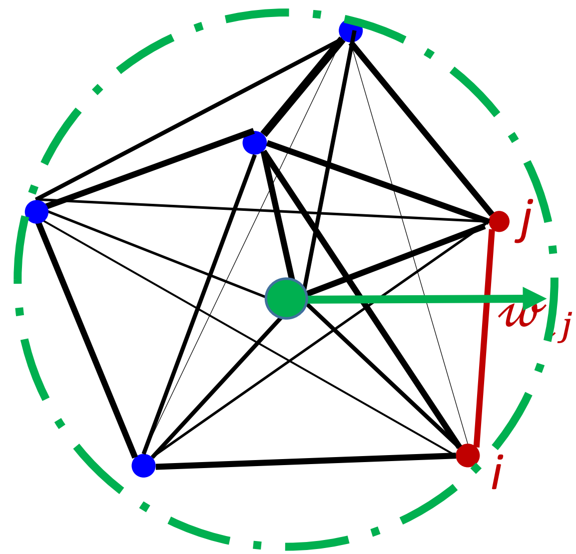

Find the Gaussian distance between nodes
(Closer nodes have higher edge weights)

$$w_{ij} = e^{-\frac{(\vec{x_i}-\vec{x_j})(\vec{x_i}-\vec{x_j})^{\mathrm{T}}}{\sigma^2}} \qquad w_{ij} = w_{ji}$$

Similarity matrix

$$S^{M\times M} \stackrel{\text{def}}{=} [w_{ij}]$$

Obtaining Eigenvectors (ϕ) and Eigenvalues (Λ)

Similarity matrix $S \stackrel{\text{def}}{=} [w_{ij}]$

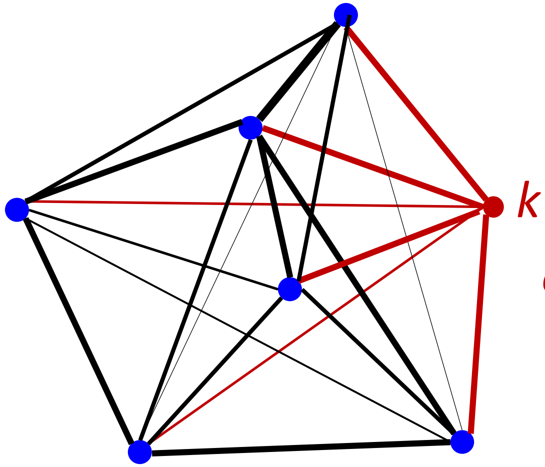

$$d_k = \sum_{j=1}^{j=M} w_{kj}$$

Degree matrix

$$\mathcal{D} \stackrel{\text{def}}{=} \begin{bmatrix} d_1 & 0 & 0 \\ 0 & d_k & 0 \\ 0 & 0 & d_M \end{bmatrix}$$

Sum each row of the Similarity matrix, and put it on the diagonal

Laplacian matrix

$$\mathcal{L} \stackrel{\text{def}}{=} (\mathcal{D} - S)$$

Obtaining Eigenvectors (ϕ) and Eigenvalues (Λ)

Laplacian matrix

$$\mathcal{L} \stackrel{\text{def}}{=} (\mathcal{D} - S)$$

$\mathcal{L}$, $\mathcal{D}$ and S are Matrices of real positive numbers

$$\mathcal{L} = \begin{bmatrix} d_1 & 0 & 0 \\ 0 & d_k & 0 \\ 0 & 0 & d_M \end{bmatrix} - \begin{bmatrix} 1 & w_{12} \cdots & w_{1\mathrm{M}} \\ w_{21} = w_{12} & \cdots 1 \cdots & w_{2M} \\ \vdots & \vdots & \vdots \\ w_{M1} & \cdots & 1 \end{bmatrix}$$

$$\boxed{\mathcal{L}\phi = \Lambda\phi}$$

Outline

- Introduction
- Graph theory approach in AM
- Part I: Verification of the graph theory approach

  How does it compare to the known solutions and existing techniques?

  - Graph Theory vs. exact analytical solution (Green's Function)
  - Graph Theory vs. finite element for AM
- Experimental validation of the graph theory approach

Part II: Application (Digital Twin)

- Conclusions and future work

Green’s Functions Analysis

Exact Analytics solution to the heat equation in simple shaped bodies.

Cole, K. D., Beck, J. V., Haji-Sheikh, A., and Litkouhi, B., 2010,
Heat Conduction Using Green’s Functions, CRC Press, Boca Raton, FL.

Cole, K. D.,2018, “Parallelepiped with Insulated Boundaries and Piecewise Initial Condition” EXACT Analytical Conduction Toolbox, Oct. 18. Link

Exact Analytical Conduction Toolbox (EXACT) at UNL
www. exact.unl.edu

Comparison with Exact Analytical Solution

Quantify the accuracy of graph theory diffusion with Green's Function analytical solution

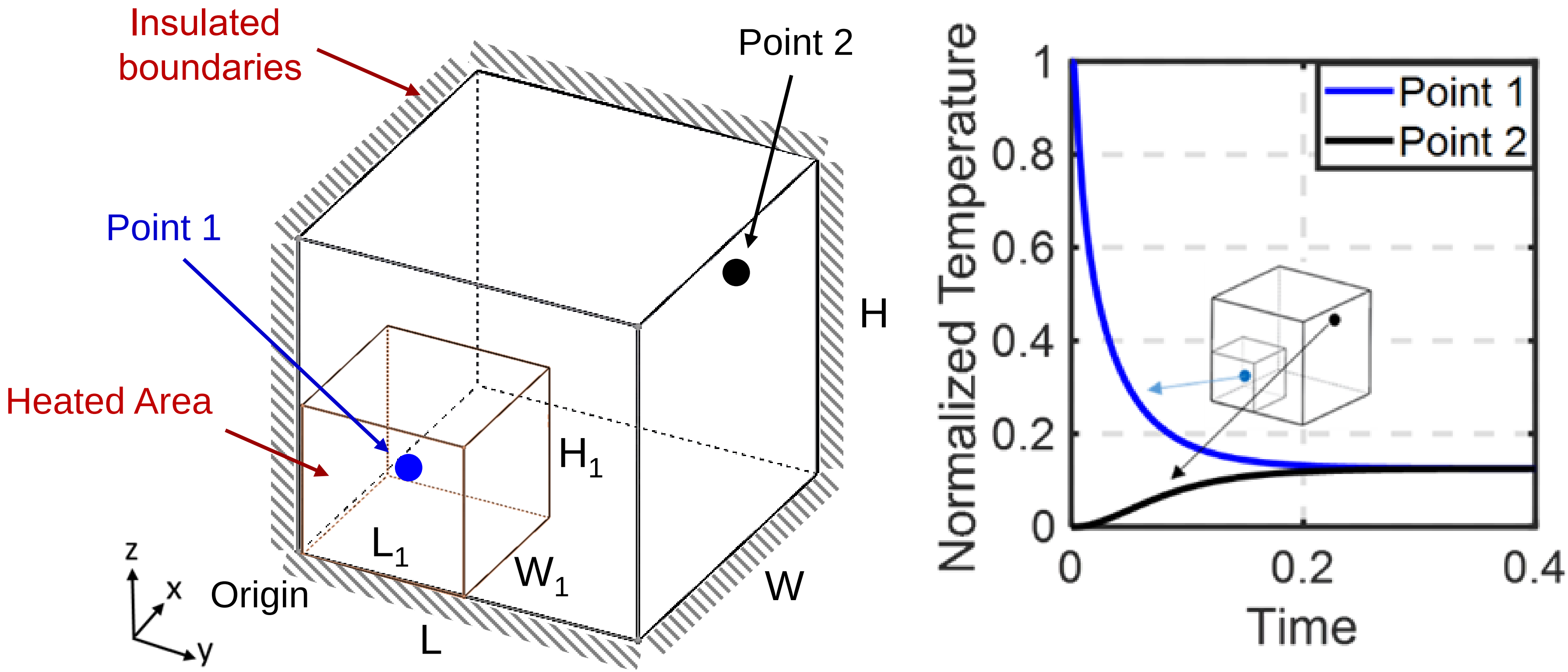

Graph Theory vs. Green's Function Solution

Graph theory captures the physics of heat transfer in an insulated cuboid

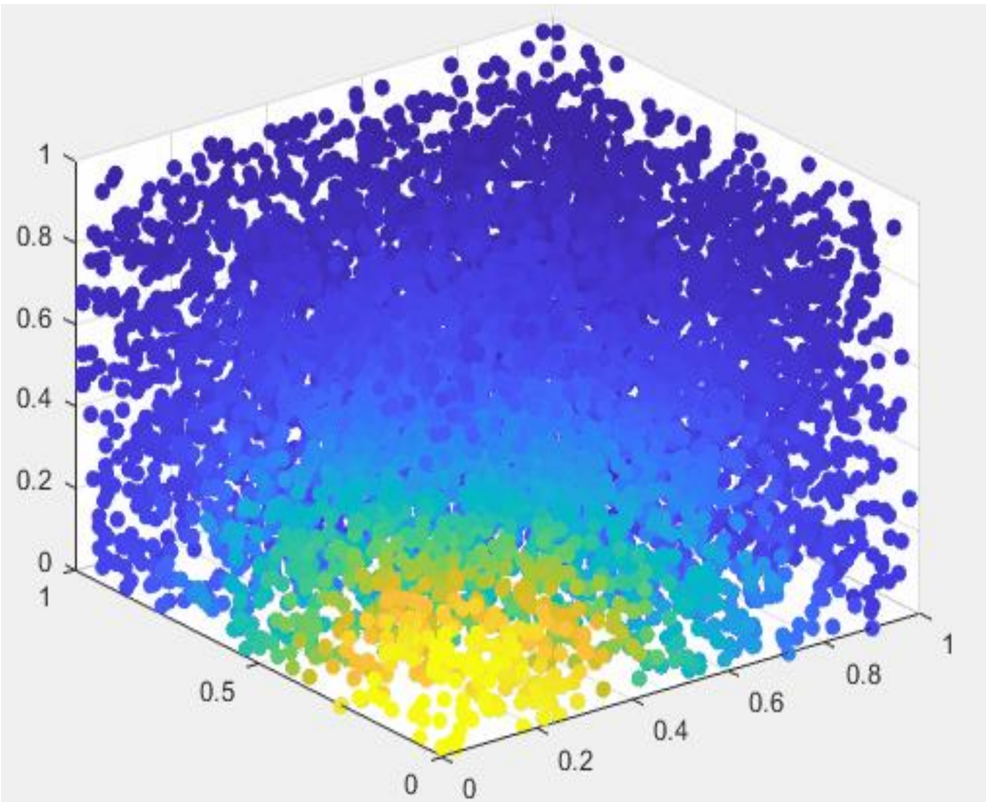

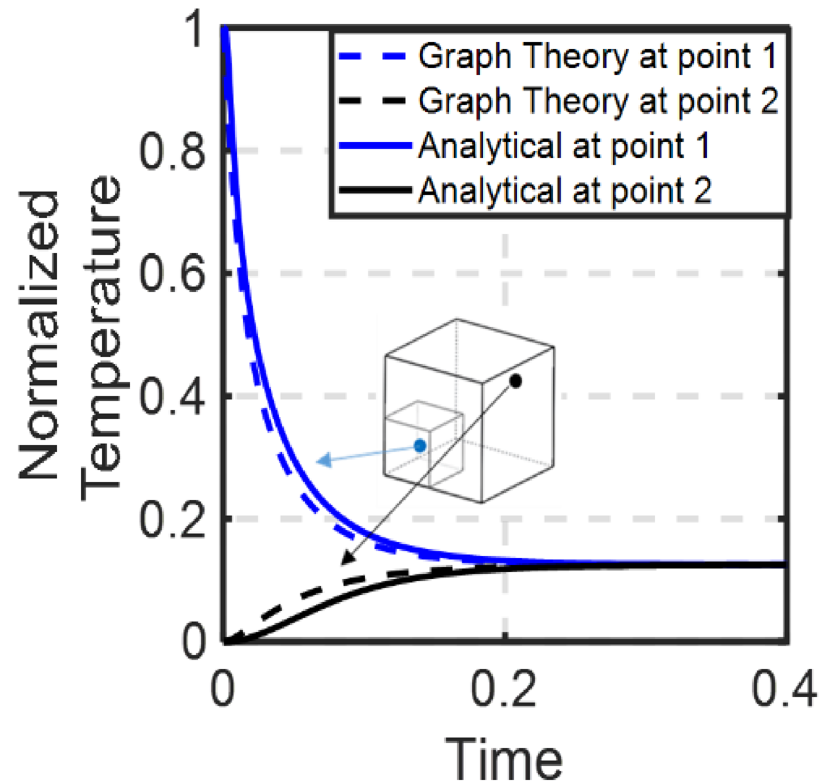

Number of nodes	computational time [seconds]	Mean Absolute Error
80	0.97	10%
800	1.55	7%
4,000	38.14	5%
8,000	236.64	3%

Graph Theory Comparison with Finite Element Analysis

Graph theory solution converges much faster than FE analysis for a fixed error level

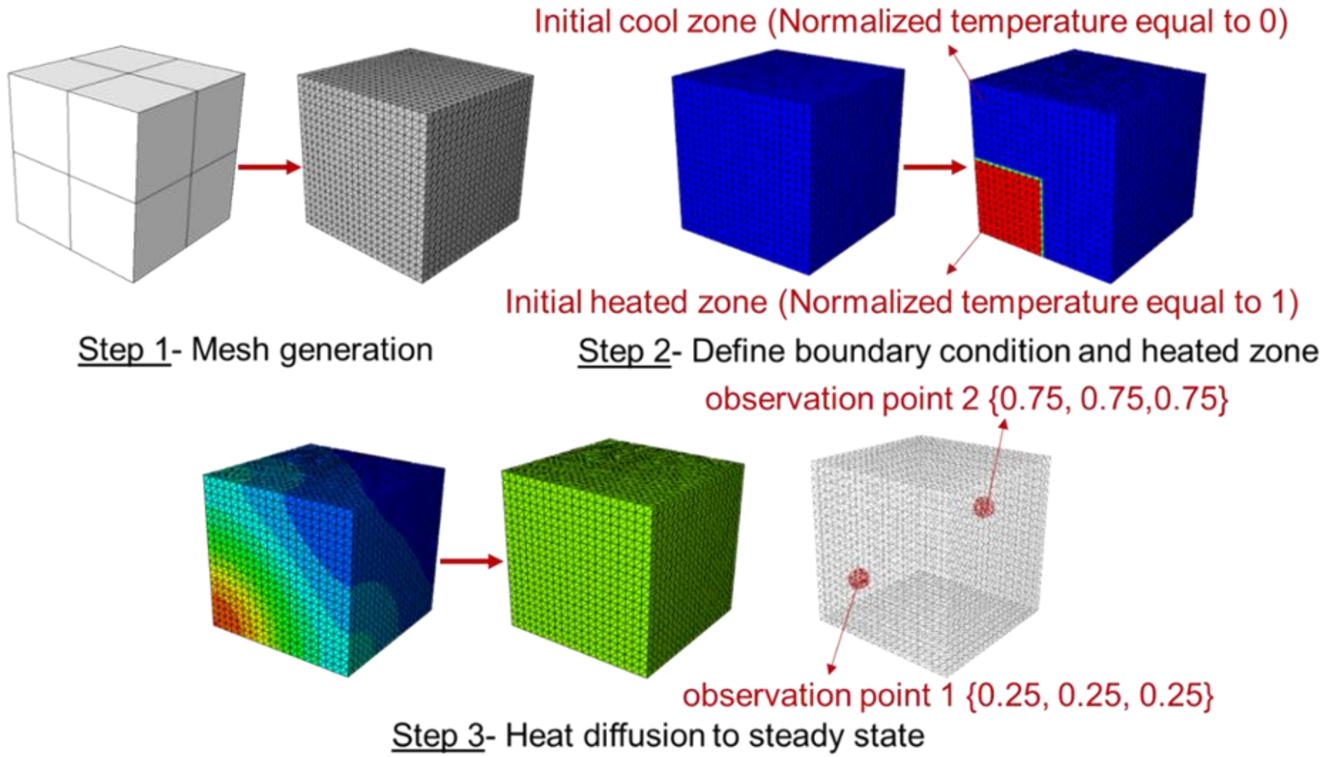

Error	Graph theoretic approach time (sec.)	FE analysis time (sec.)
~ 5%	237	3,540
	4 mins	59 mins

Outline

- Motivation
- Part 1: Graph theory approach for thermal modeling in AM

  How does it compare to the commercial solution?

  - Graph Theory vs. exact analytical solution (Green's Function)
  - Graph Theory vs. finite element vs. Netfabb for AM
- Experimental validation
- Part 2: Digital Twin Application
- Conclusions and future work

Effect of Part Geometry on Heat Flux

Two different part geometry studied in the context of LPBF.

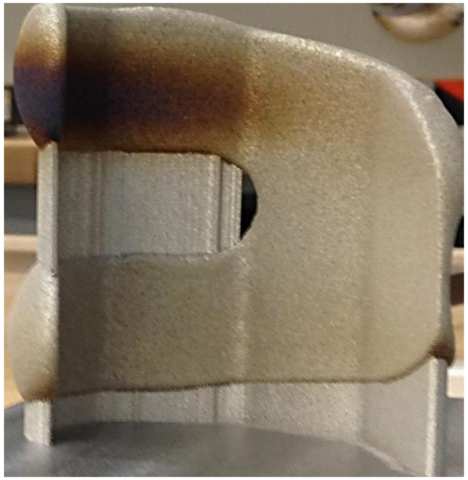

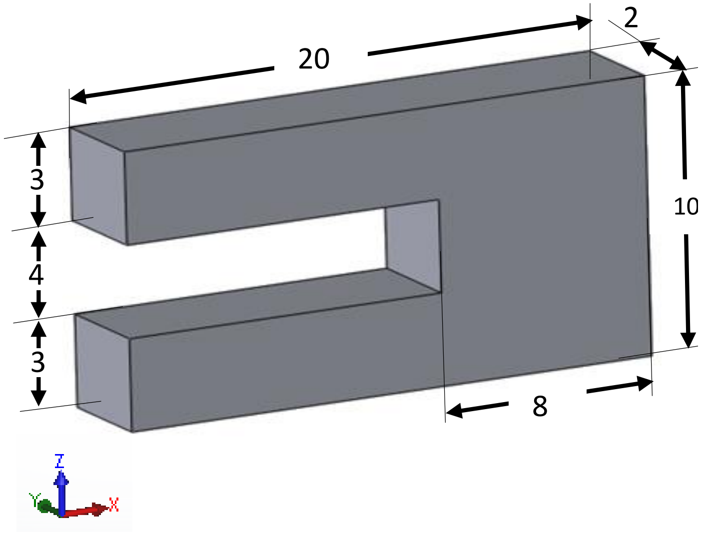

C-Shaped Part

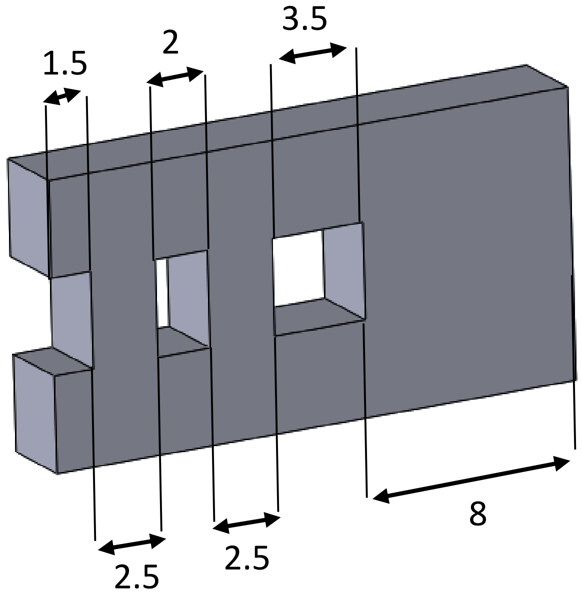

Modified C-Shaped part

Graph theory converges to similar trends as FE.

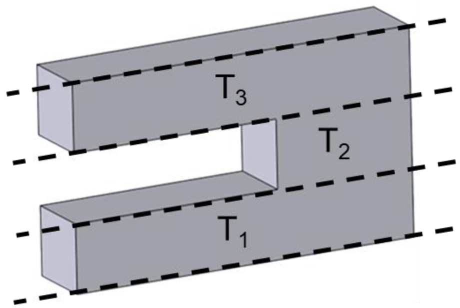

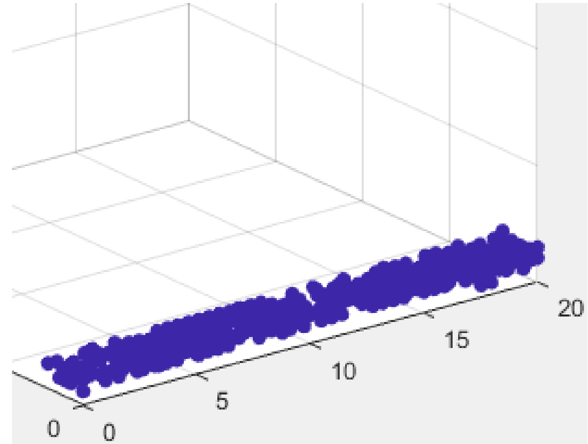

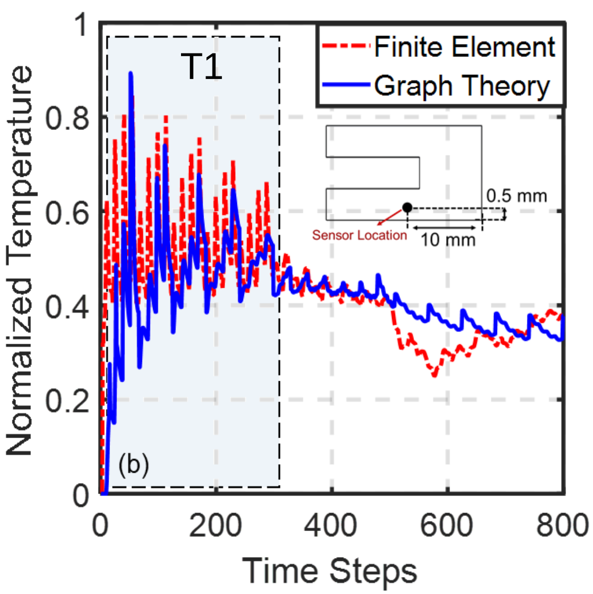

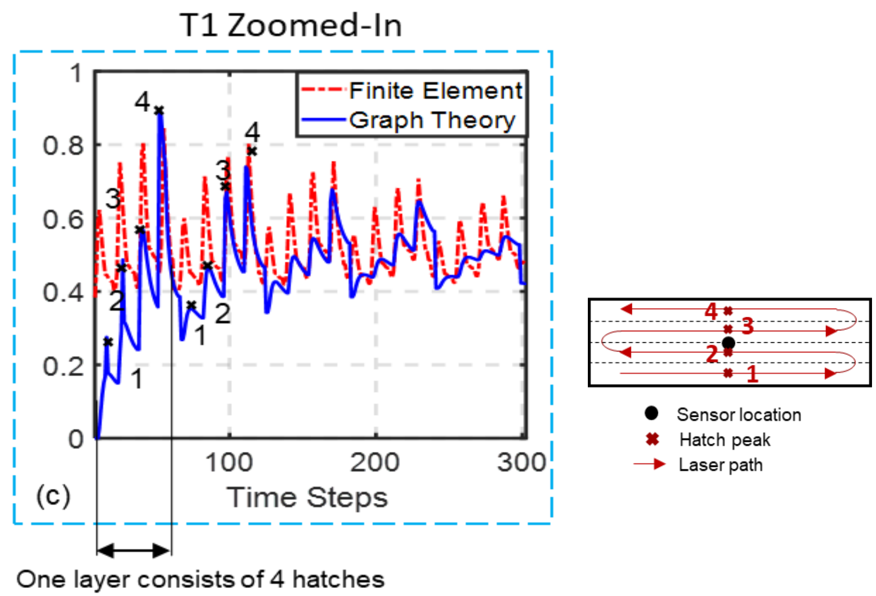

Graph theory captures heat accumulation in the overhang region of the C-shaped part.

Graph theory captures the effect of change in geometry.

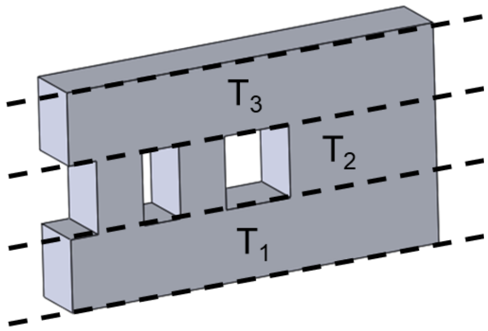

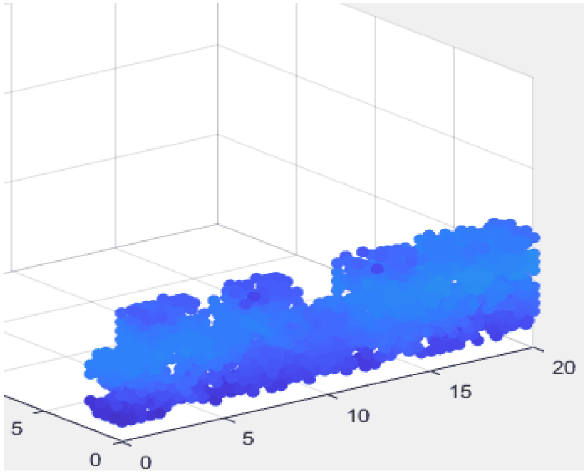

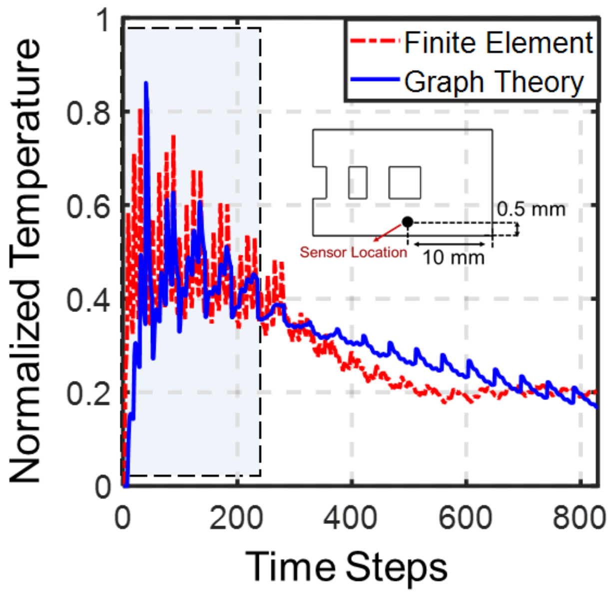

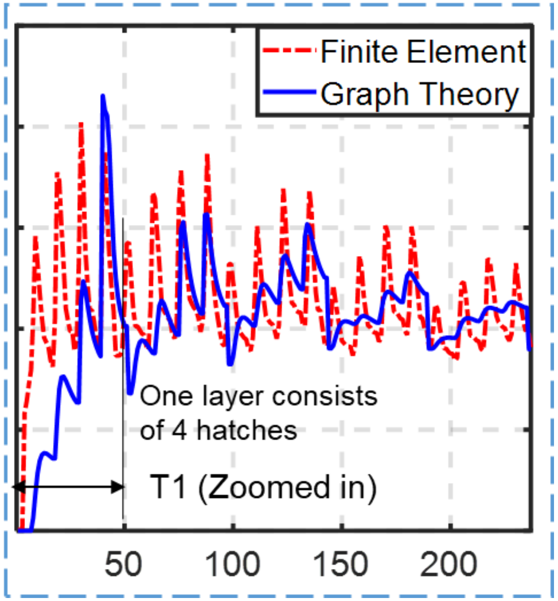

Graph theory predicts the heat diffusion facilitated by supports.

Graph theory converges to similar trends as commercial software.

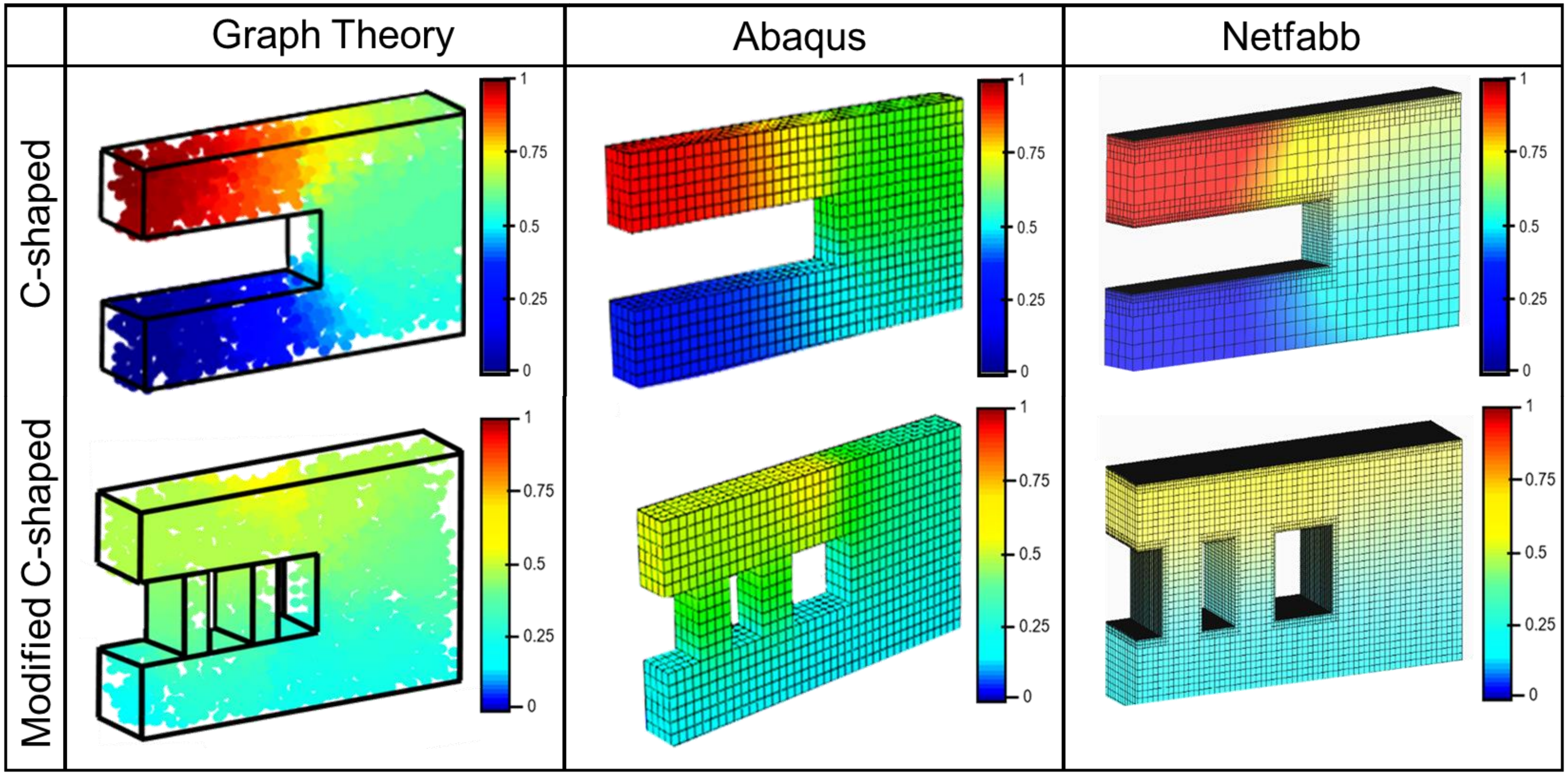

Error (SMAPE)	Total number of nodes	Graph theory approach time	FE analysis time
16%	1,000	0.5 min	200 min (2,000 elemnts)
10%	5,000	18 min	
8%	8,000	41 min	

Conclusion from Verification with FE

Graph theory simulates the thermal field with error less-than 10% and within 1/10th of time of FE.

Outline

- Introduction
- Graph theory approach in AM
- Verification of the graph theory approach

  How does it compare to the known solutions and existing techniques?

  – Graph Theory vs. exact analytical solution (Green's Function)
  – Graph Theory vs. finite element for AM

- *Experimental validation of the graph theory approach*

How does it stand up to the "real world"

Part II: Application (Digital Twin)

- Conclusions and future work

The experimental data of this study are provided by
Dr. Paul Hooper at Imperial College, London

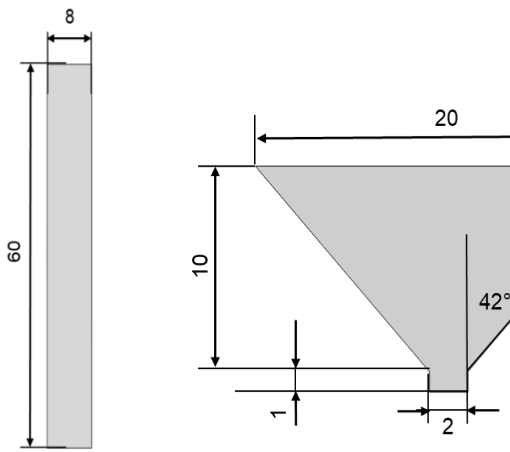

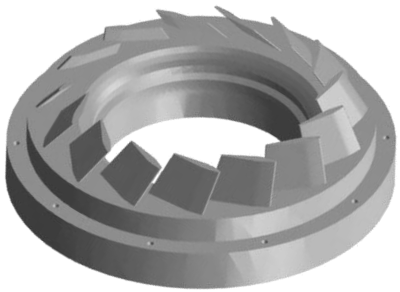
Φ200 mm × 125 mm

Williams, R., Piglione, A. , Ronneberg, T. , Pham, M. S., Davis, C. M. and **Hooper, P. A.** , 2019, "In-situ thermography for laser powder bed fusion: effects of layer temperature on porosity, microstructure and mechanical properties", *Additive Manufacturing*, In Press

Experimental Setup

A thermal camera is used to measure the surface temperature on the top surface.

Thermal camera is calibrated offline using a black-body cavity method.

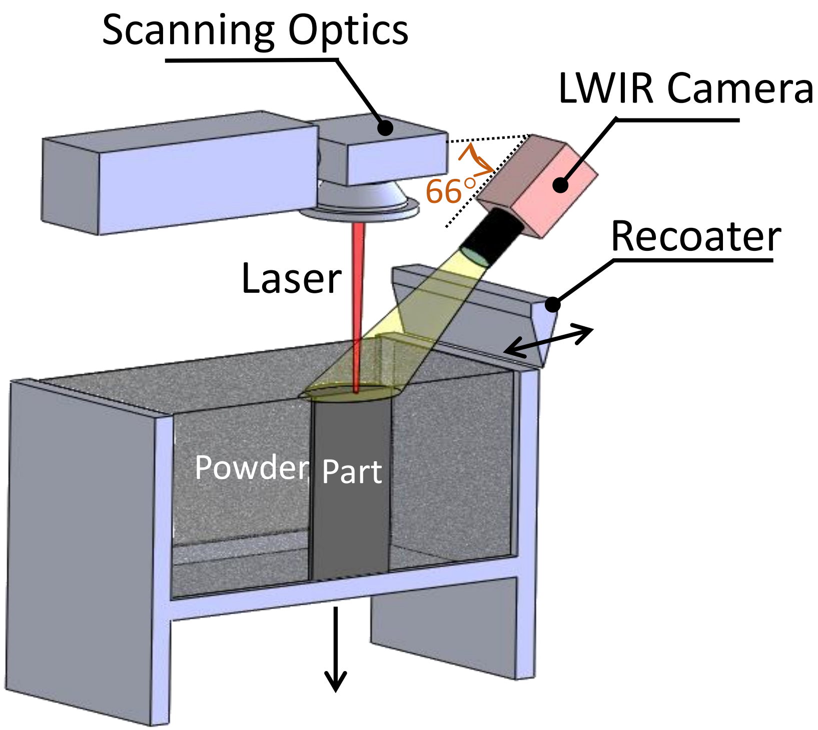

Laser Powder Bed Fusion (LPBF)

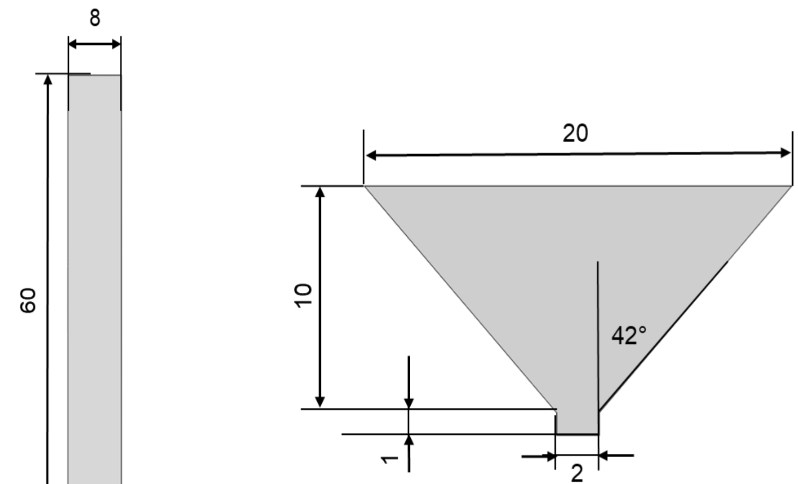

Build 1 (Cylinder)

Build 2 (Inverted Cone)

316L Stainless Steel Material
Laser power: 200 W
Layer thickness: 50 µm
point distance: 40 µm, exposure time: 50 µs

The first two test parts have a simple geometry
Even coarse FE analysis will perform well.

Cylinder is built in three phases to induce change in the surface temperature.

Phase 1: Print 9 cylinders (dia. 8 mm, L = 60 mm).
Phase 2: Print only the middle cylinder.
Phase 3: Print all 9 cylinders again.

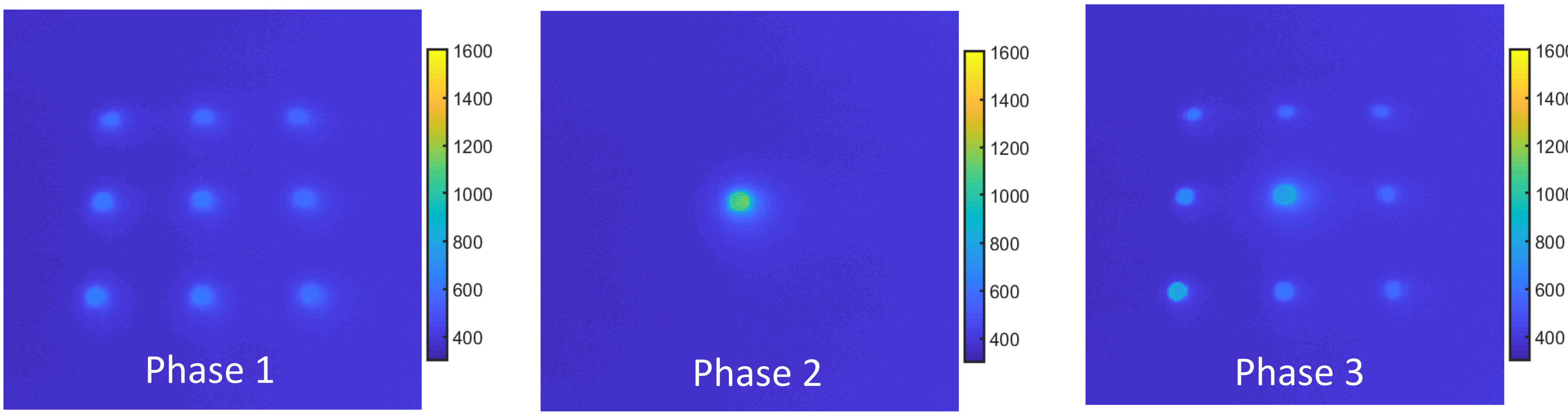

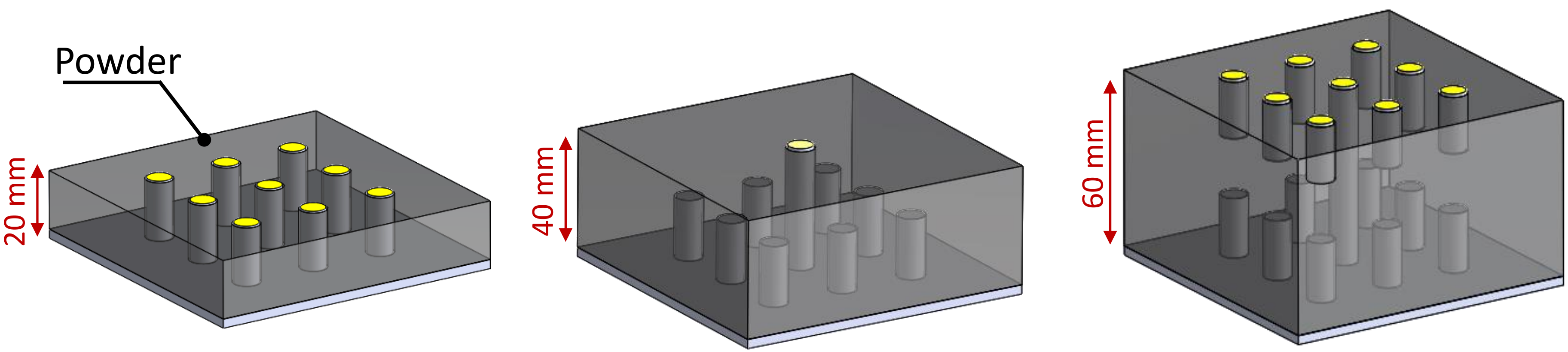

Change in the build plan causes variation in the inter-layer cooling time (ILCT).

Surface temperature is a function of interlayer cooling time (ILCT).

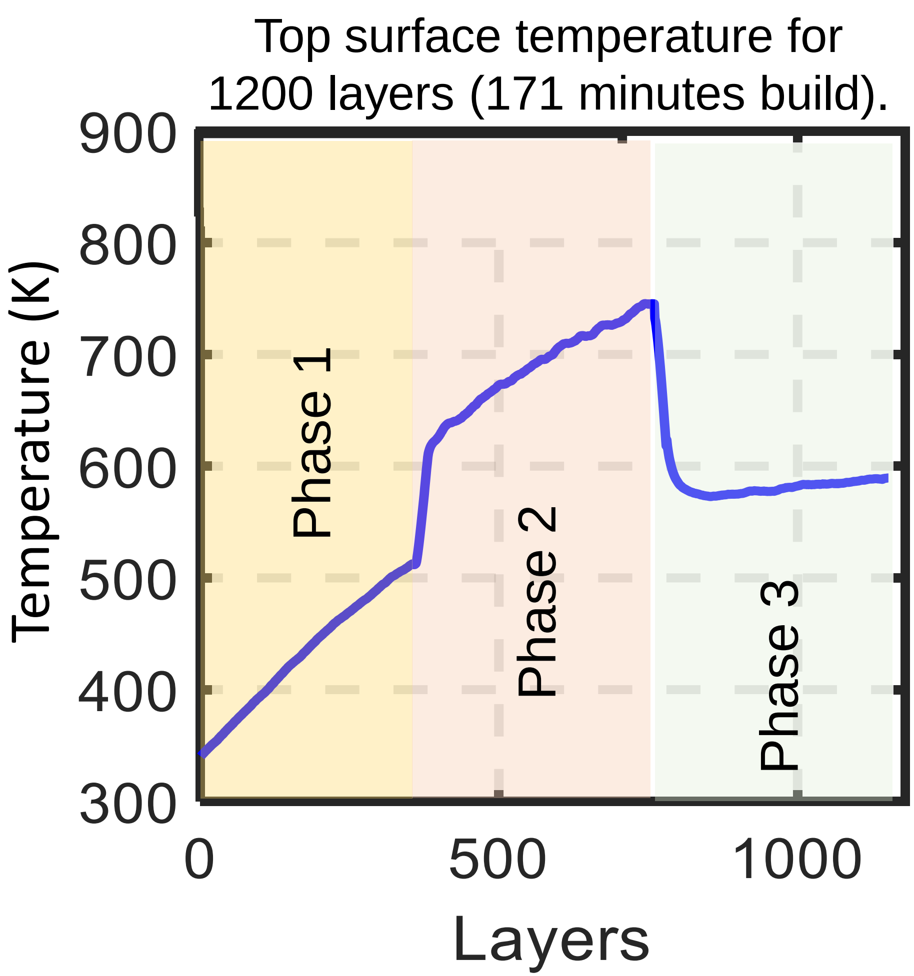

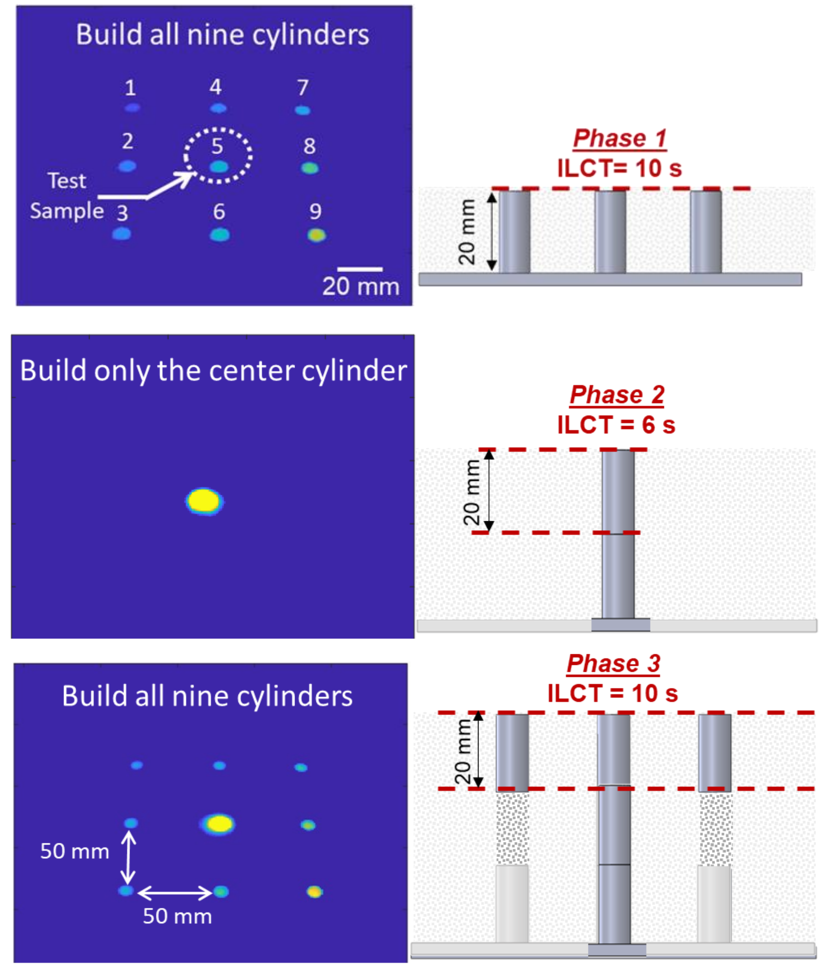

Increase in ILCT linked to decrease in surface temperature

Graph Theoretic Thermal Modeling in AM

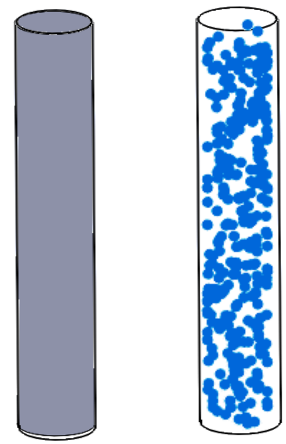

Step 1- Convert the part into a set of discrete nodes

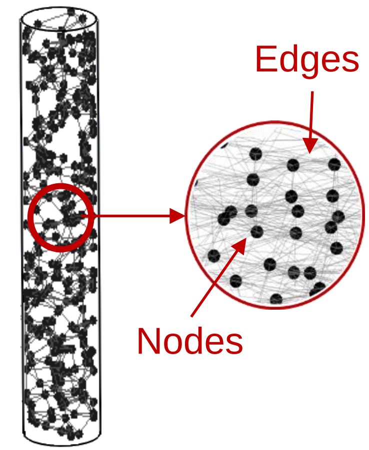

Step 2- Network graph construction

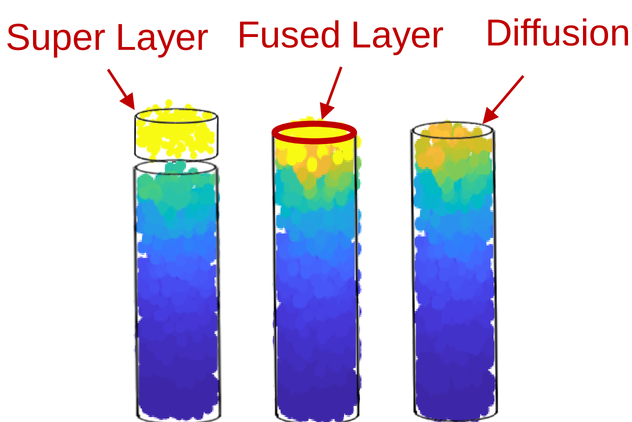

Step 3
- Deposition of **super layers**
- Diffusion of the heat through the part

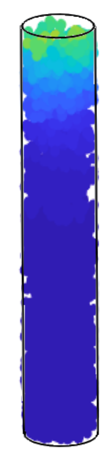

Step 4- Obtaining the result

Simulating the deposition of multiple layers (metalayers/superlayers) favors FE analysis.

Close match of graph theory and FE predictions.

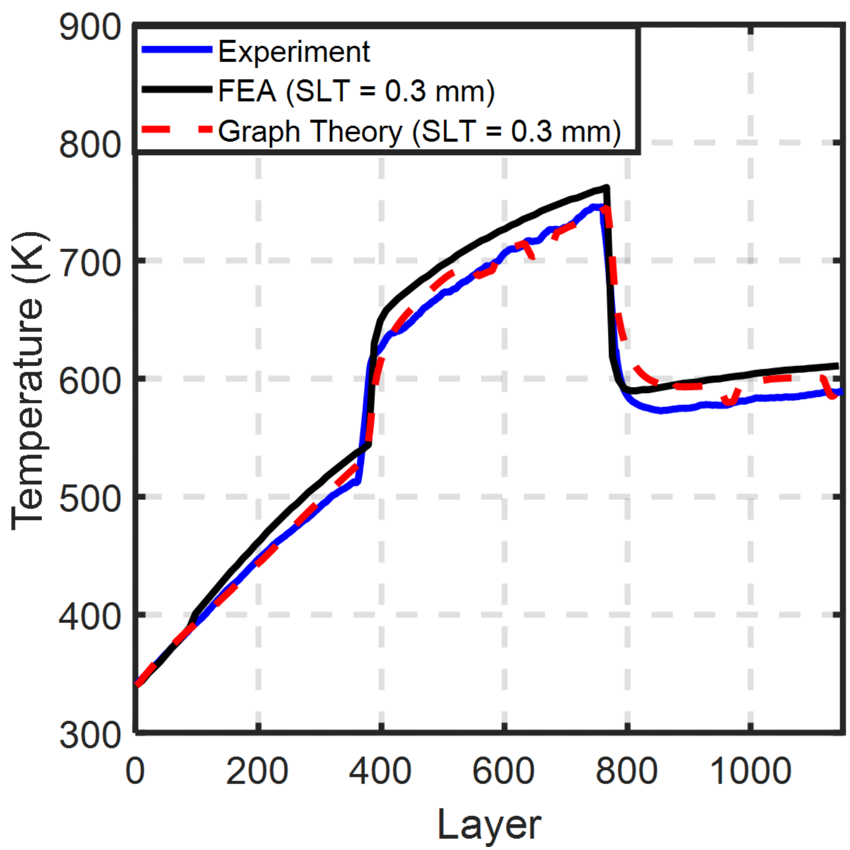

Actual Build Time 171 minutes	Finite Element		Graph Theory	
Super Layer Thickness	0.3 mm	0.5 mm	0.3 mm	0.5 mm
Computation Time	34 minutes	22 minutes	27 minutes	15 minutes
MAPE	8 %	18 %	6 %	14 %
RMSE (Kelvin, K)	33.8	48.1	14.5	33.8

Graph theory converges faster than FE, and has slightly smaller error.

Build 2 (Inverted Cone)

Both surface temperature interlayer cooling time increase during the build.

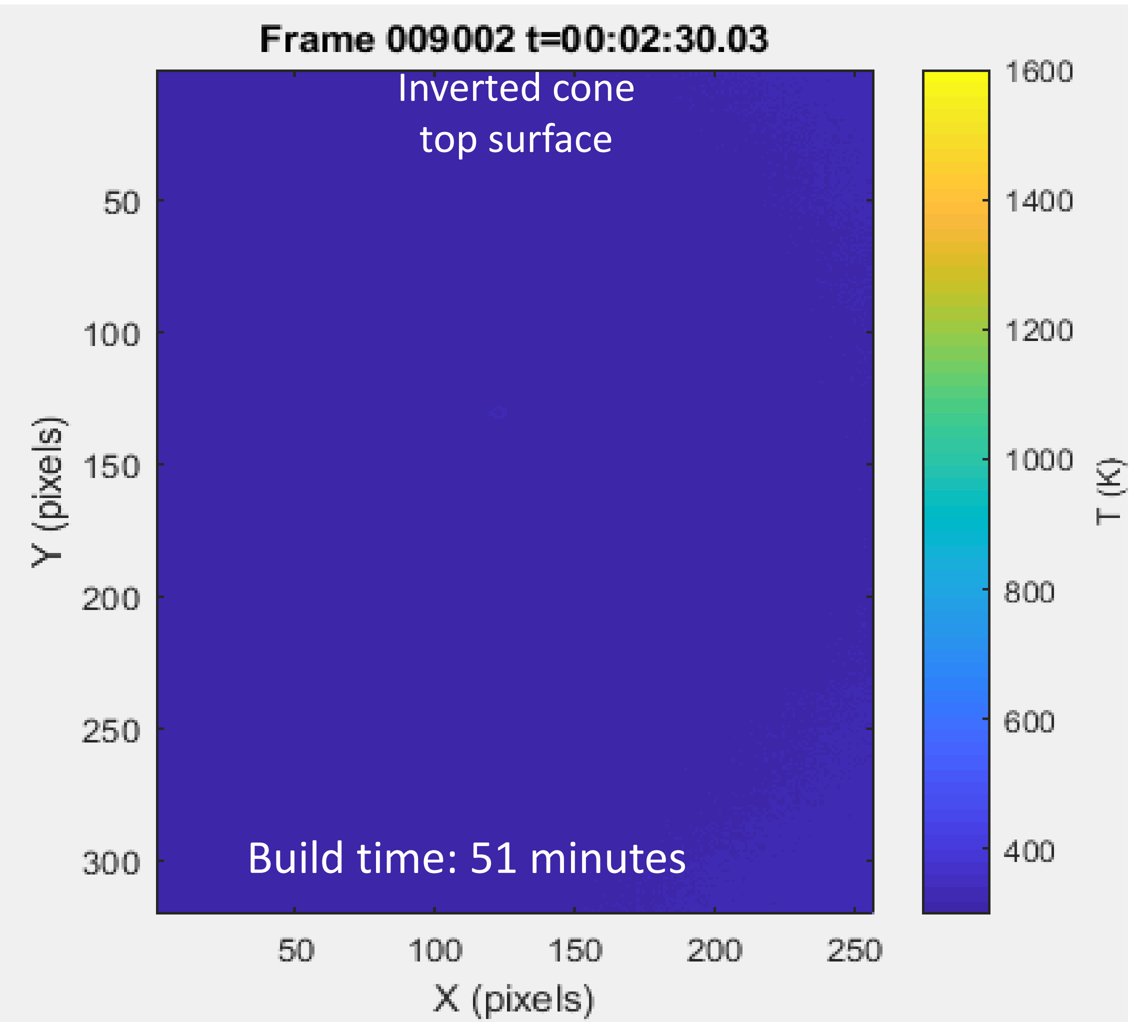

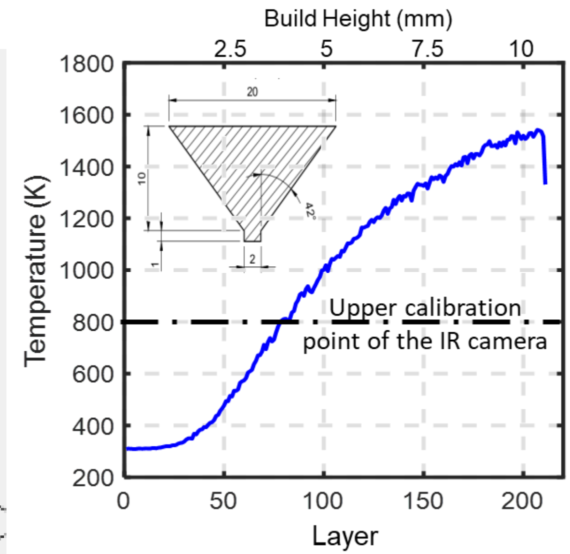

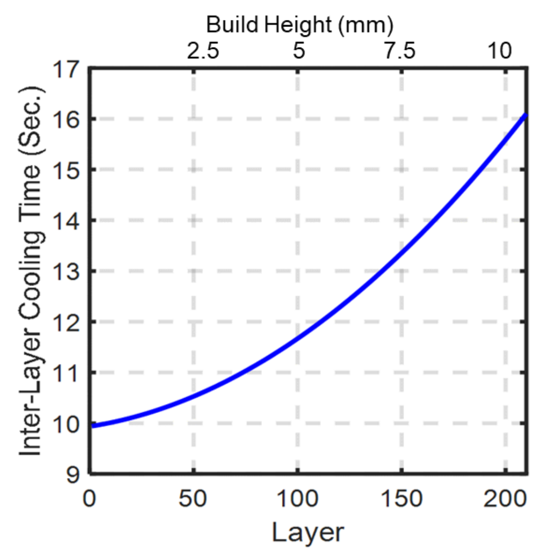

Change in surface temperature leads to microstructural heterogeneity and flaws.

Need to adapt ILCT and processing conditions to avoid flaws.

Close match of graph theory and FE predictions.

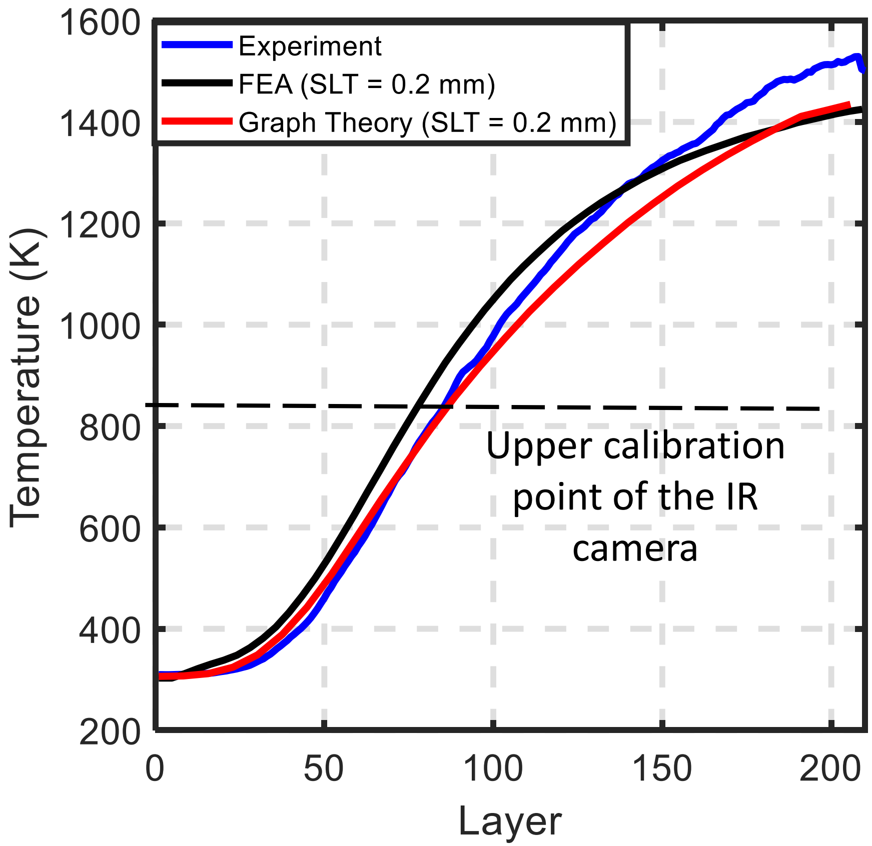

Actual Build Time 53 minutes	Finite Element		Graph Theory	
Super Layer Thickness	0.2 mm	0.3 mm	0.2 mm	0.3 mm
Computation Time	54 minutes	48 minutes	41 minutes	35 minutes
MAPE	9 %	14 %	8 %	9 %
RMSE (Kelvin, K)	37.7	73.0	26.0	35.4

Outcome

Graph theory simulates the thermal heat field within error less than 10% of experimental data, and is about 25% faster than coarse FEA.

Experimental Validation with a Large Part

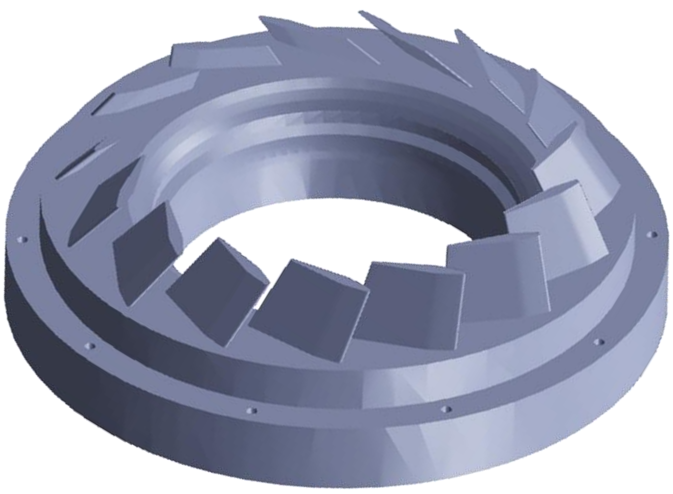

8 inch-wide, 1.5-inch high
316L Stainless steel part
16-hour build time.

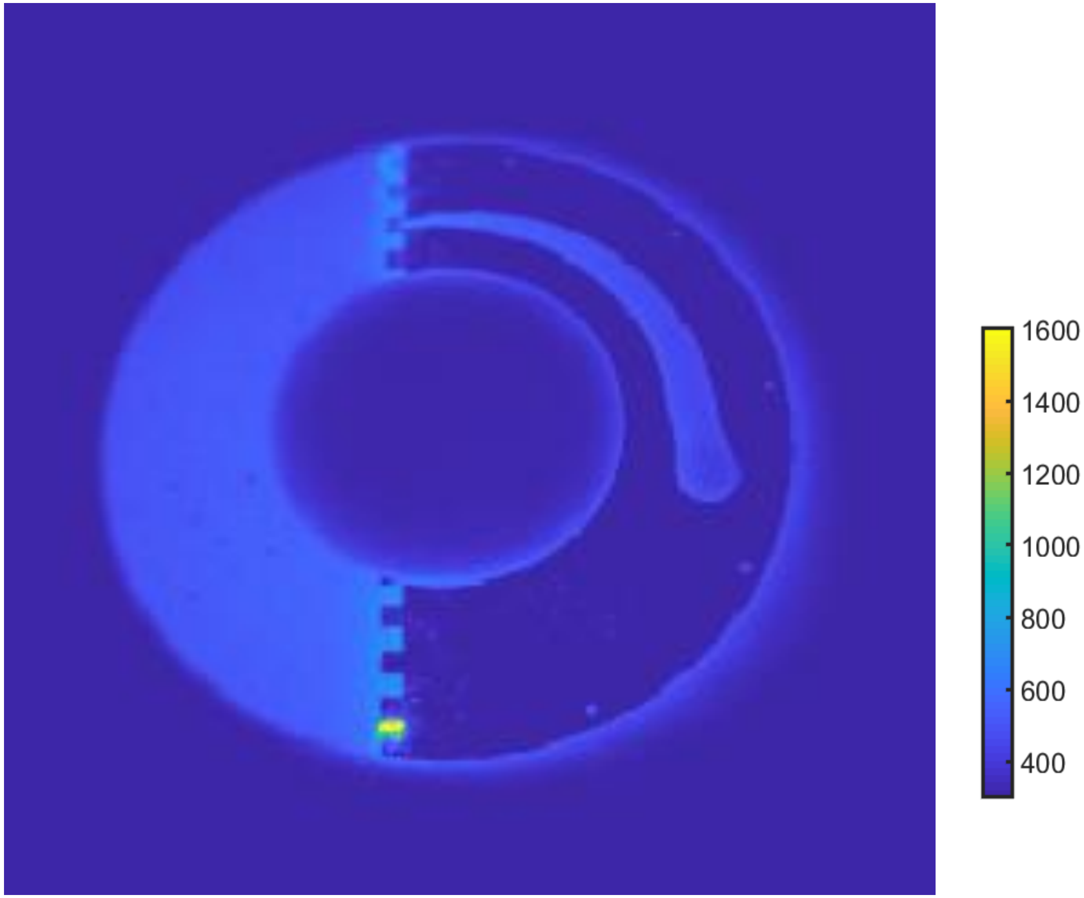

Video of Infrared Thermal Images

Surface temperature varies due to change in cooling time and surface area.

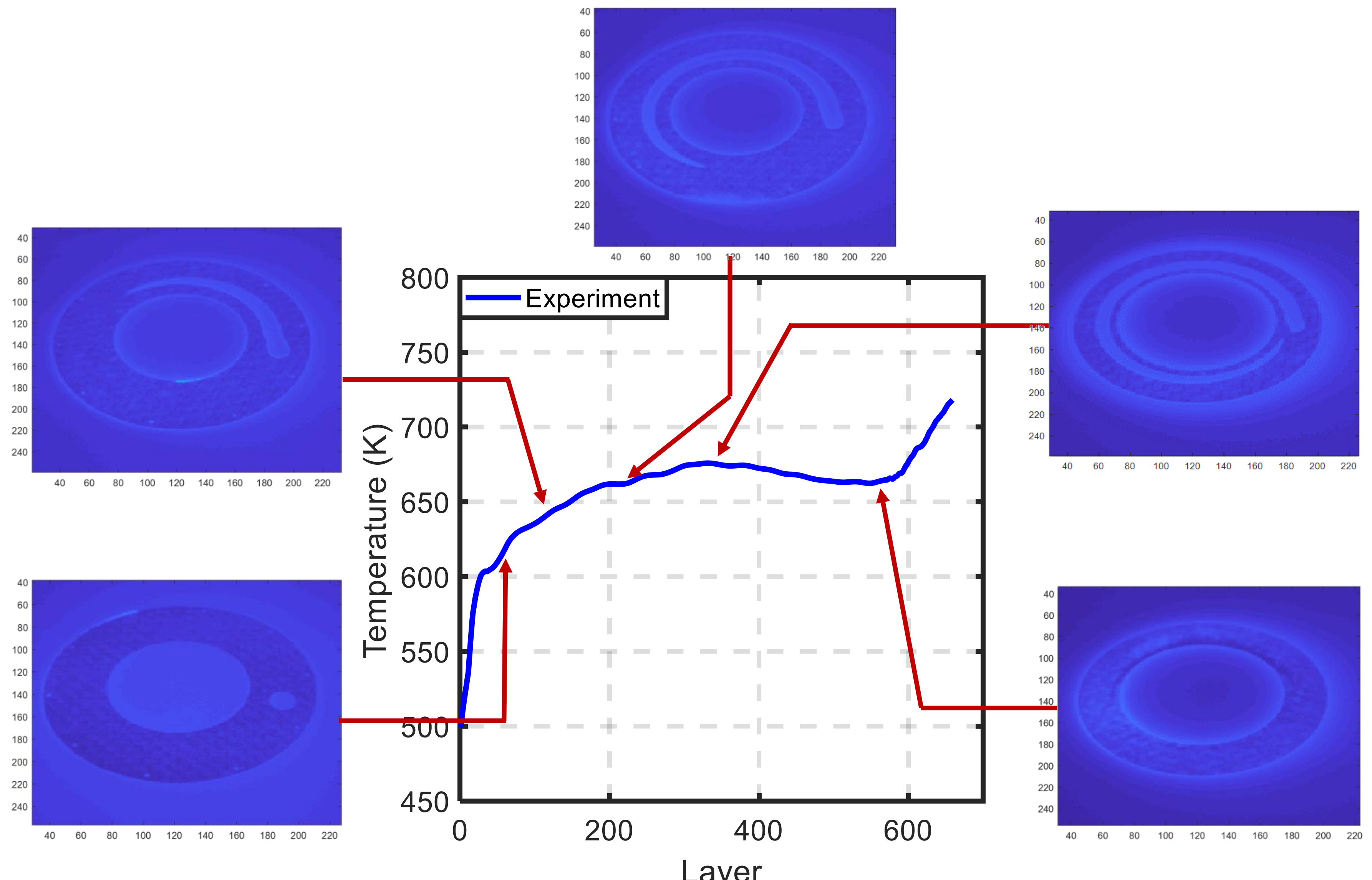

Two simulation strategies to reduce computation burden

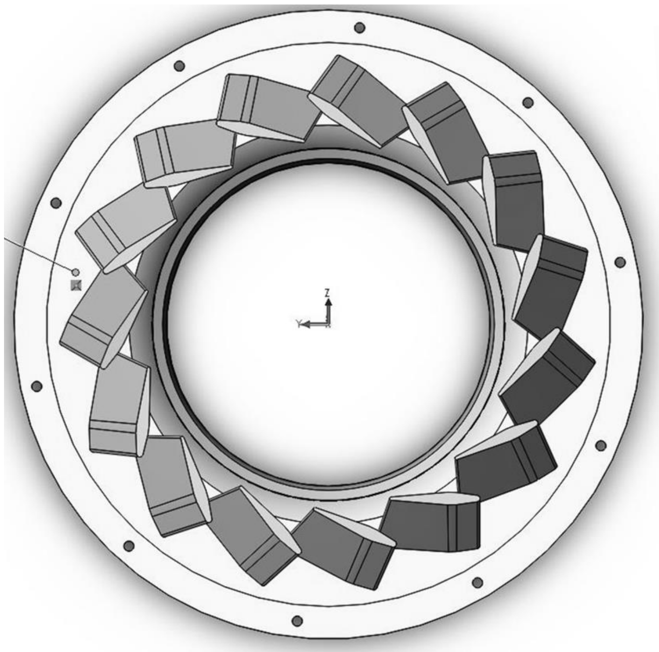

Strategy 1
Radial slice

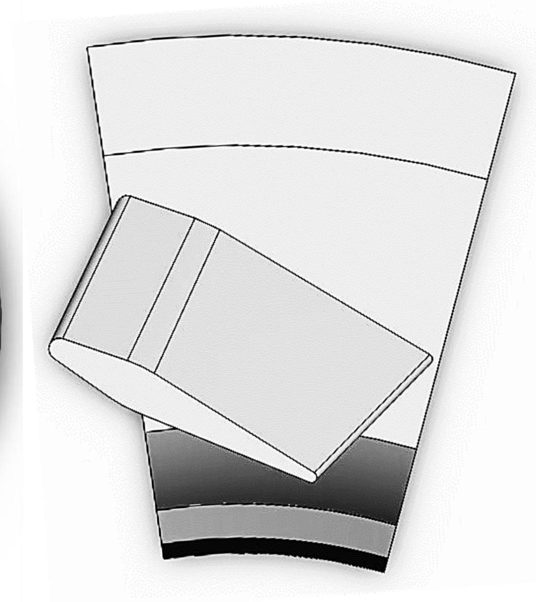

Strategy 2
Horizontal Slice

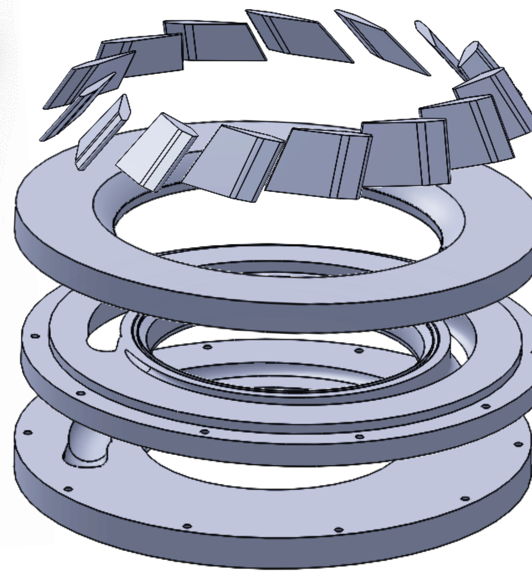

Graph theory scales to large part geometries

Graph theory converges with error less than 10% and within 10% of the build time

Computation Time: 35 min.
Part build Time: 16 hours
Mean Absolute Error: 7%
RMS error < 30K

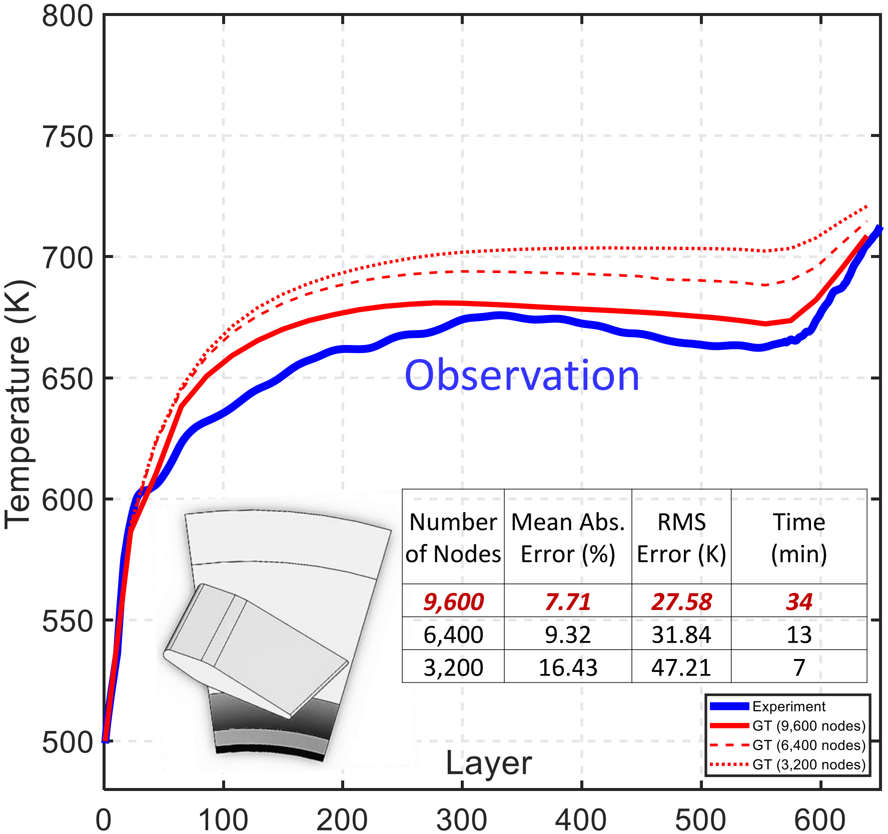

Number of Nodes	Mean Abs. Error (%)	RMS Error (K)	Time (min)
9,600	***7.71***	***27.58***	***34***
6,400	9.32	31.84	13
3,200	16.43	47.21	7

Computation Time: 80 min.
Part build Time: 16 hours
Mean Absolute Error: 8%
RMS error < 30K

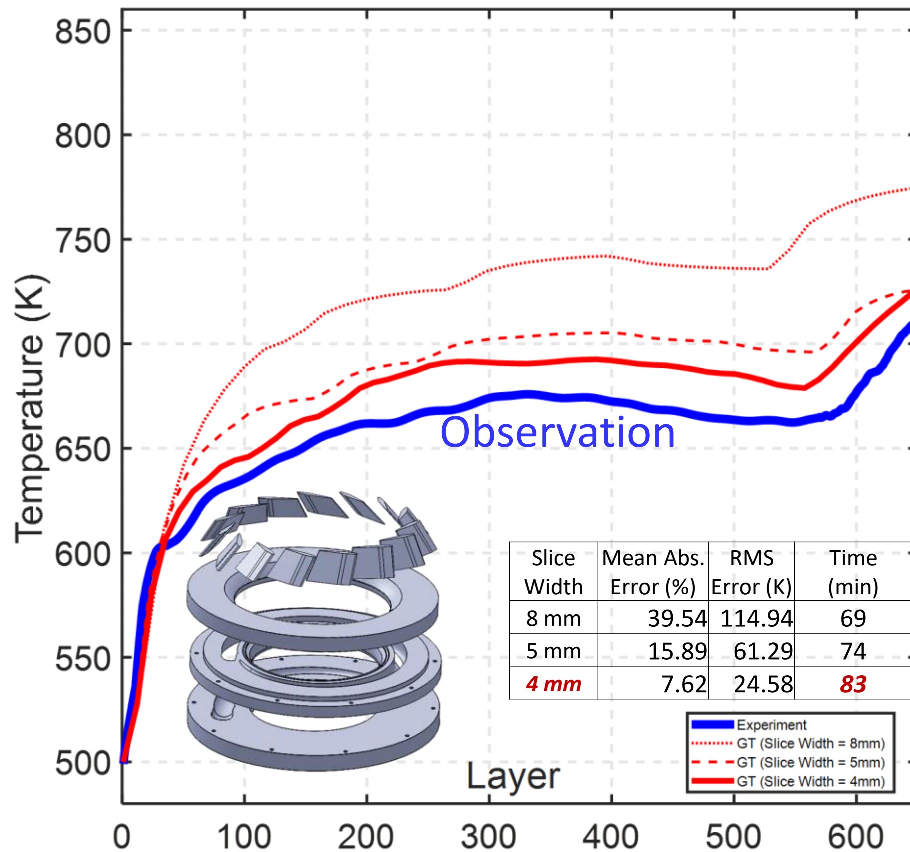

Slice Width	Mean Abs. Error (%)	RMS Error (K)	Time (min)
8 mm	39.54	114.94	69
5 mm	15.89	61.29	74
4 mm	7.62	24.58	***83***

Outline

- Introduction
- Graph theory approach in AM
- Part 1: Verification of the graph theory approach

How does it compare to the known solutions and existing techniques?

  - Graph Theory vs. exact analytical solution (Green's Function)
  - Graph Theory vs. finite element for AM
- Experimental validation of the graph theory approach

Part II: Application (Digital Twin)

So what – who cares about thermal simulations?

- Conclusions and future work

Experimental data was generated at
NIST by Dr. Brandon Lane, and
Mississippi State University by Dr. Linkan Bian

A.C. Gaikwad, R. Yavari, M. Montazeri, K. Cole, L. Bian, P. Rao,

Toward the Digital Twin in Metal Additive Manufacturing – Integrating Thermal Simulations, Sensing, and Analytics to Detect Process Faults, IISE Transactions (Accepted)
10.1080/24725854.2019.1701753

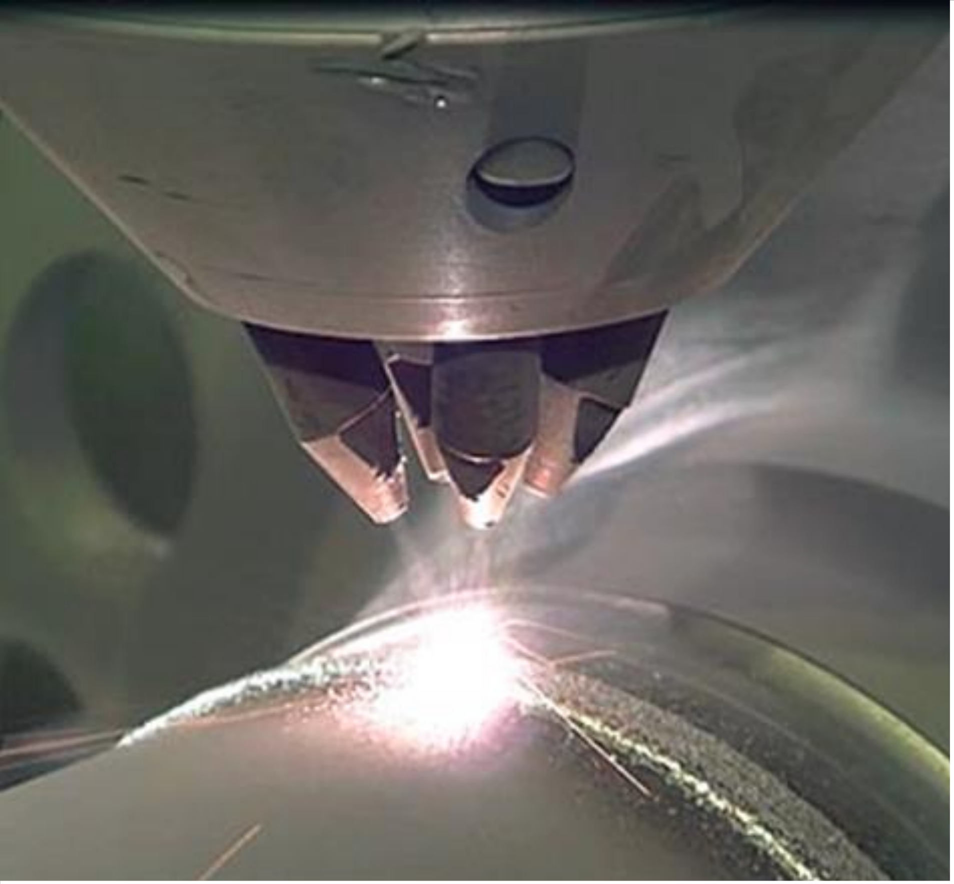 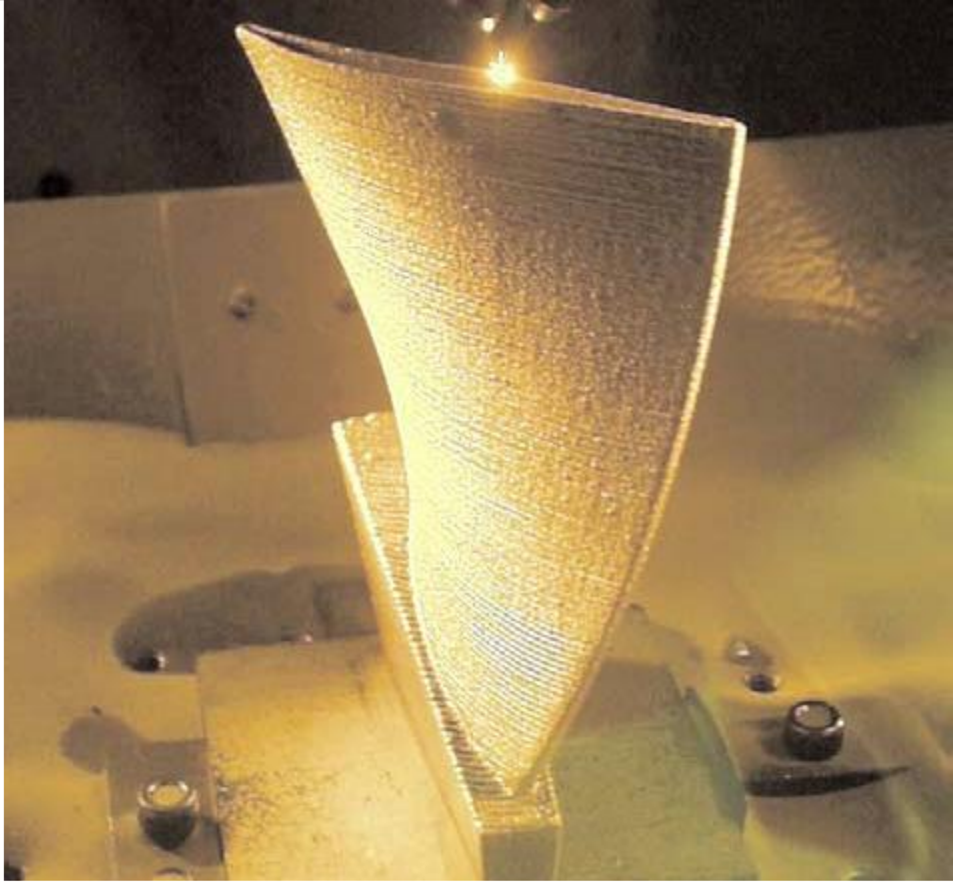

Directed Energy Deposition (DED)
Direct Material Deposition (DMD)
Laser Engineered Net Shaping (LENS)

ISO/ASTM 52900:2015

Source: Optomec

Previous work in the Digital Twin

G.L. Knapp, T. Mukherjee, J.S. Zuback, H.L. Wei, T.A. Palmer, A. De, ***T. DebRoy***, Building blocks for a digital twin of additive manufacturing, Acta Materialia, Volume 135, 2017.

T. DebRoy, W. Zhang, J. Turner, S.S. Babu, Building digital twins of 3D printing machines, Scripta Materialia, Volume 135, 2017.

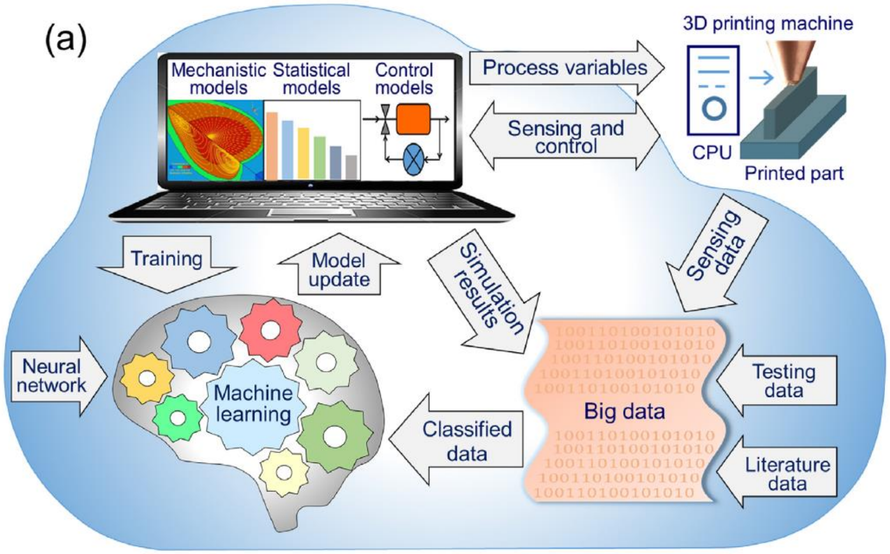

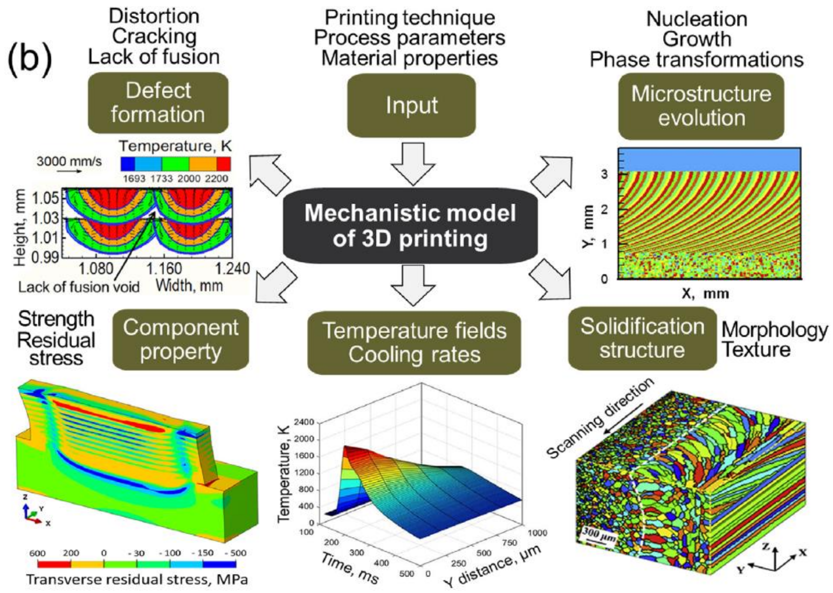

Objective and Hypothesis

- Predict the instantaneous spatiotemporal temperature distribution with graph-theory
- Combine with in-process sensor data to monitor the process condition.

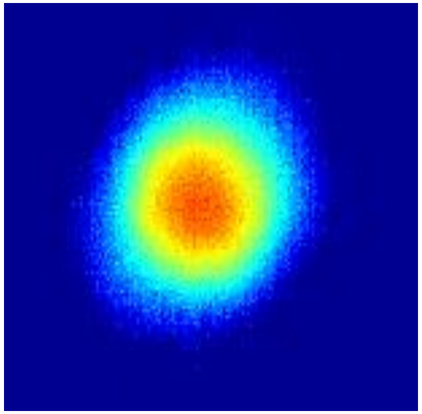

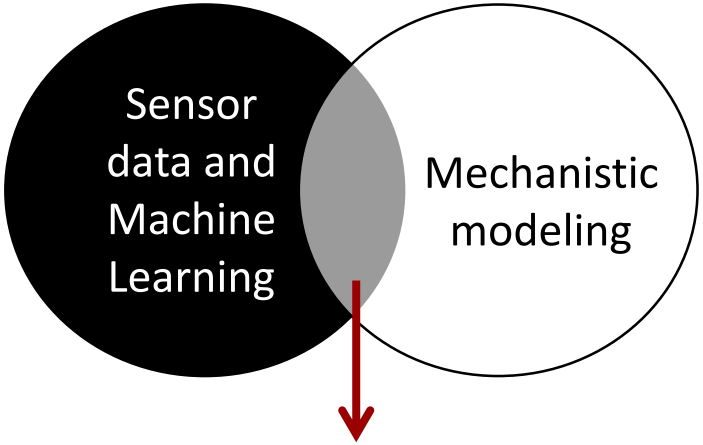

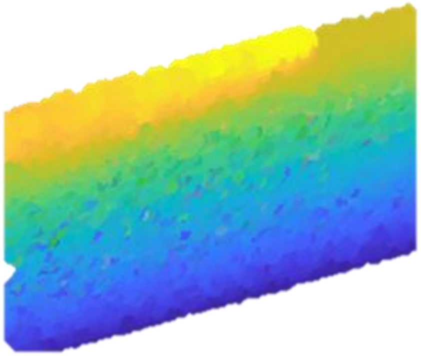

Hypothesis: Improved defect prediction accuracy

Digital Twin – A Gray-Box Model

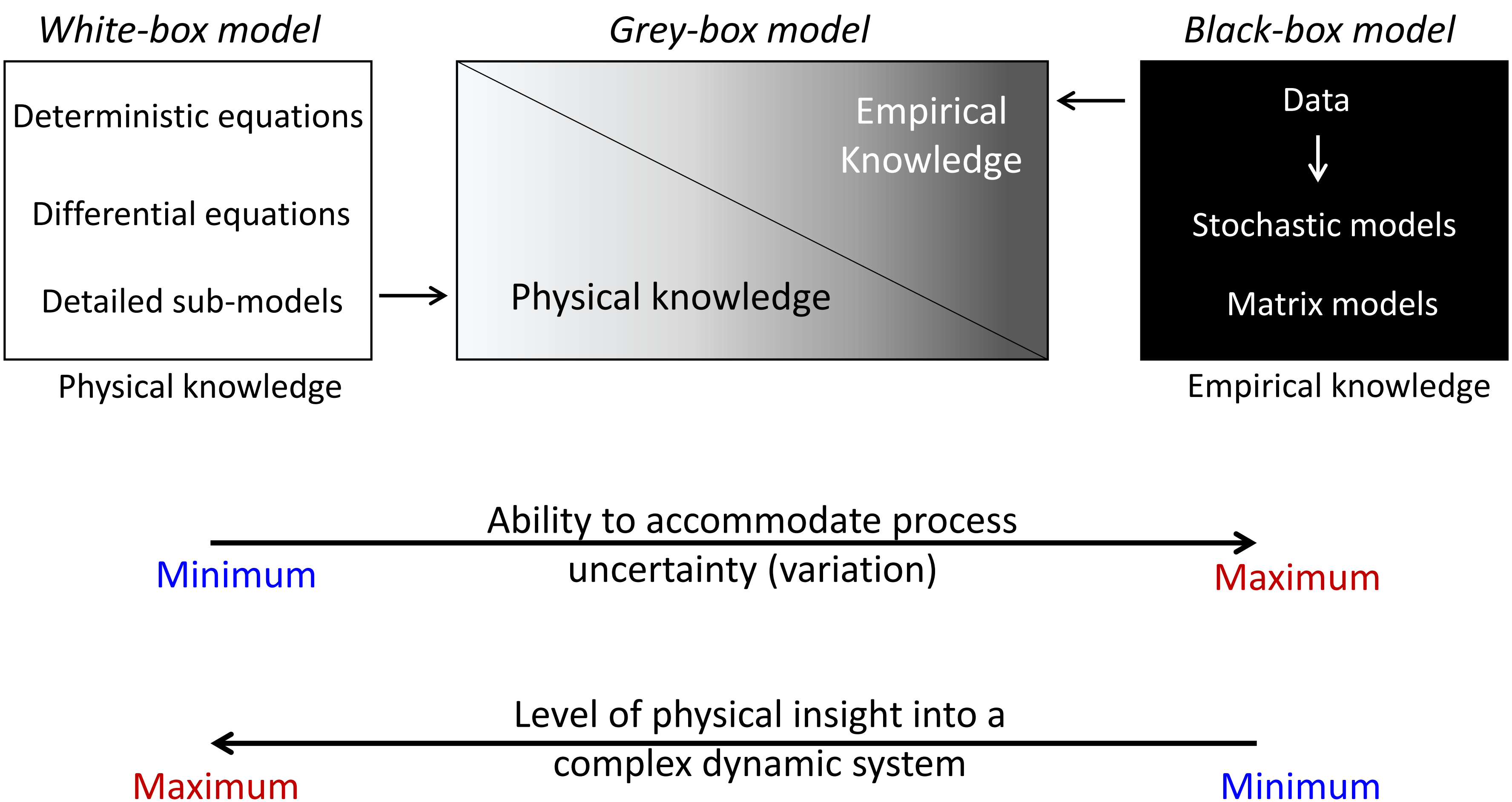

Test Artifact

Single track thin wall part with Ti6Al4VOptomec LENS 750

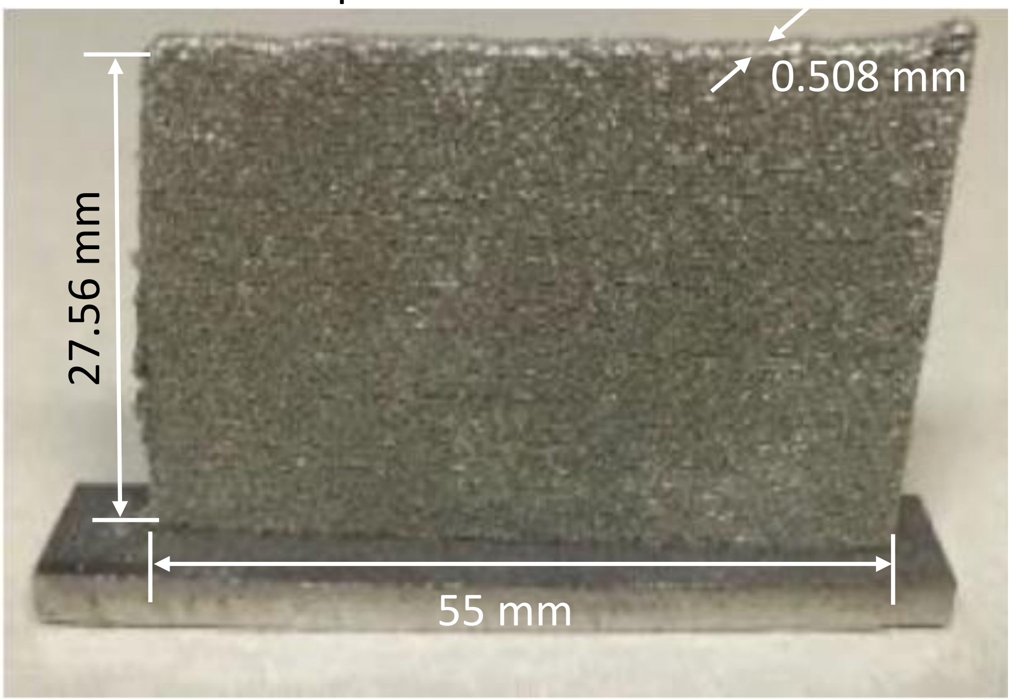

Post-process characterization with X-ray computed tomography

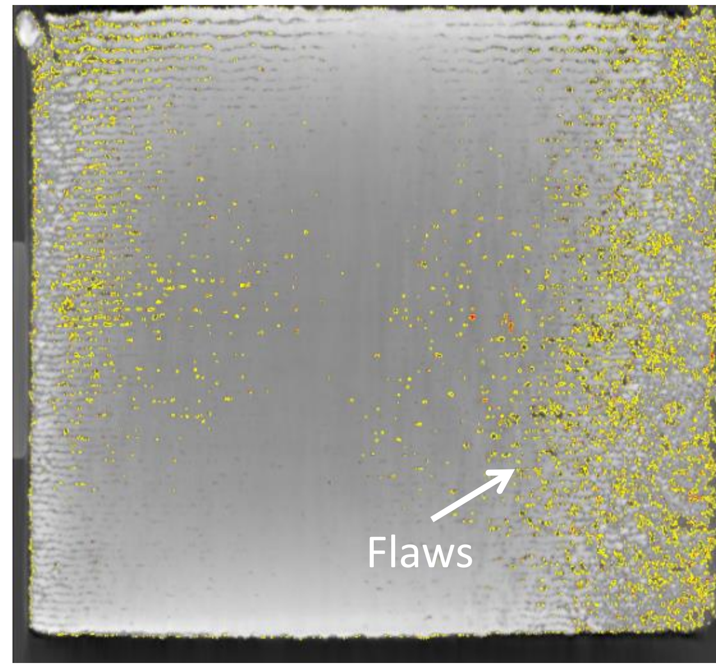

Power: 300 W

Scan Speed: 12.7 mm/s

Layer Thickness: 0.508 mm

A pyrometer and IR camera is integrated into the DED machine.

- Co-axial dual-wavelength pyrometer
- Short-wave infrared (SWIR) camera

  Oriented at approximately 45° to the table

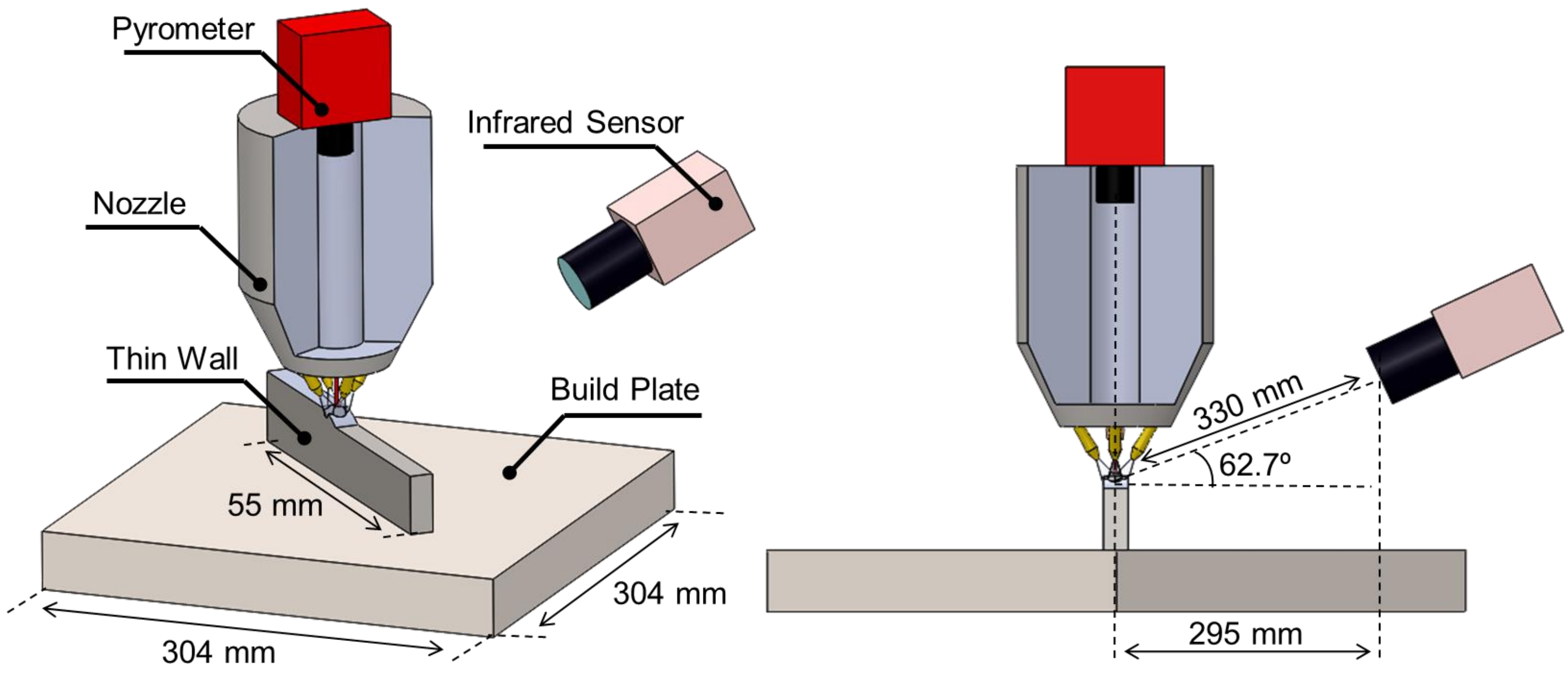

a) Isometric View

b) Side View

Change in the melt pool characteristics is related to the quality of the part.

Two-color pyrometer measurements of the meltpool temperature distribution.

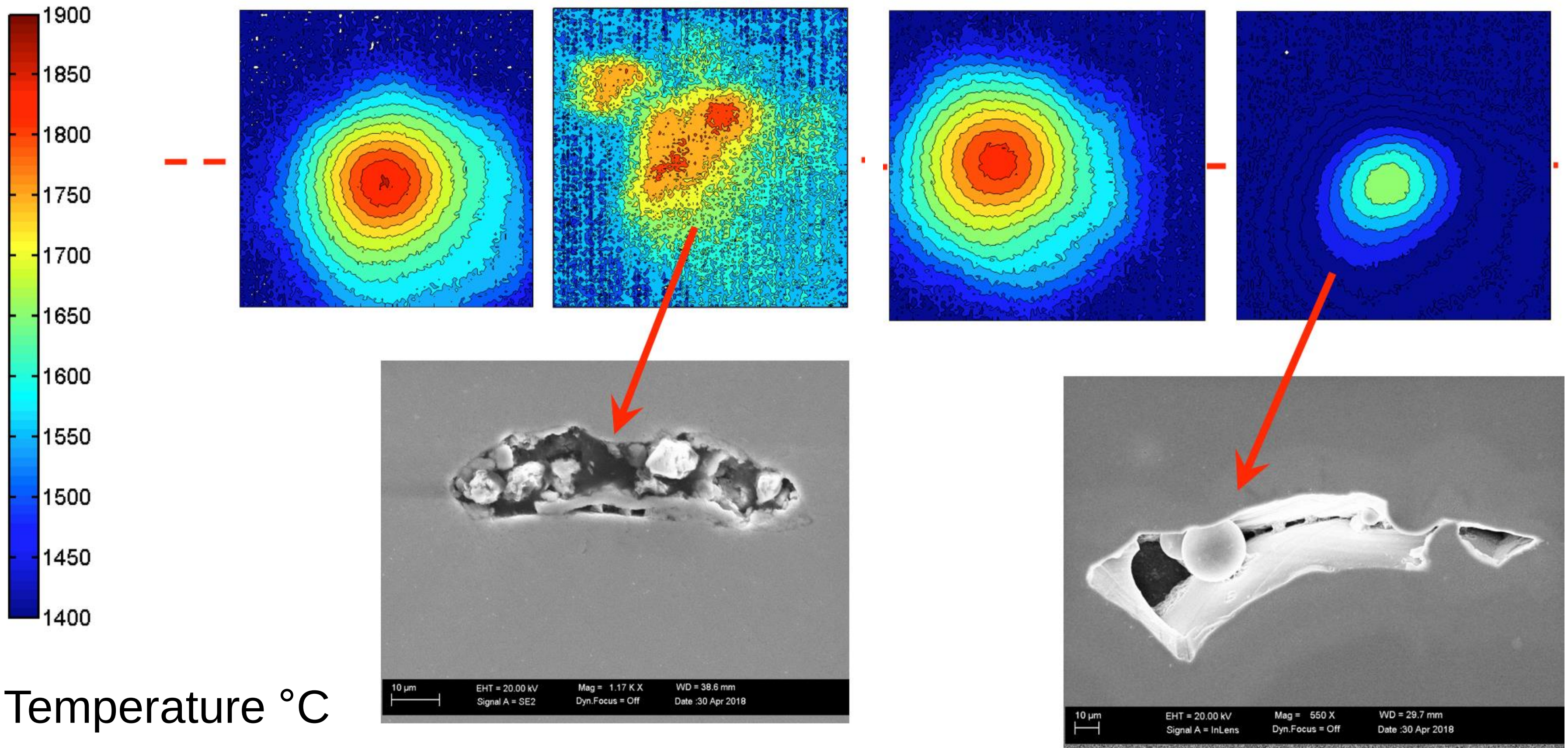

SEM Measurements

Block-by-block regime is adopted to simulate the thin-wall

Same strategy can be used to simulate Wire-DED at Oak Ridge.

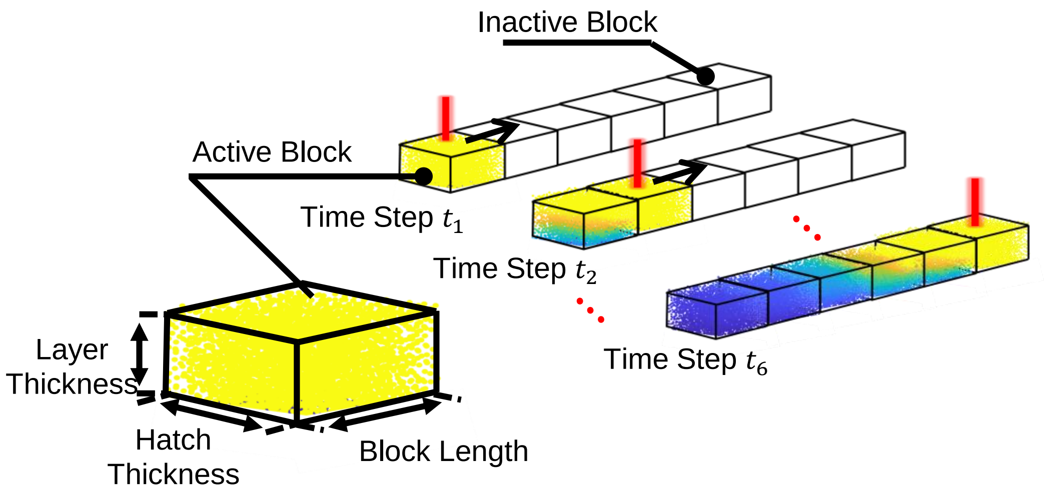

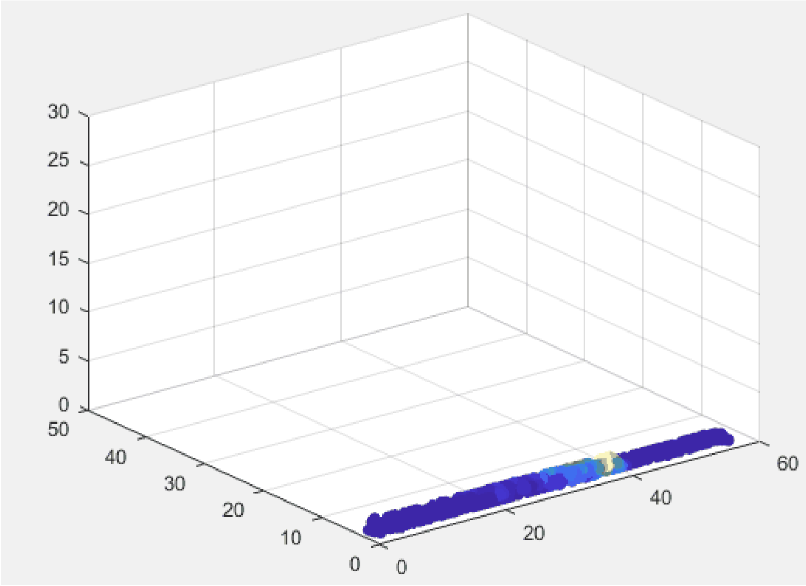

Comparison of Experimental and Simulation Data

There is a high correlation between simulated part-level temperature and experimental meltpool temperature data.

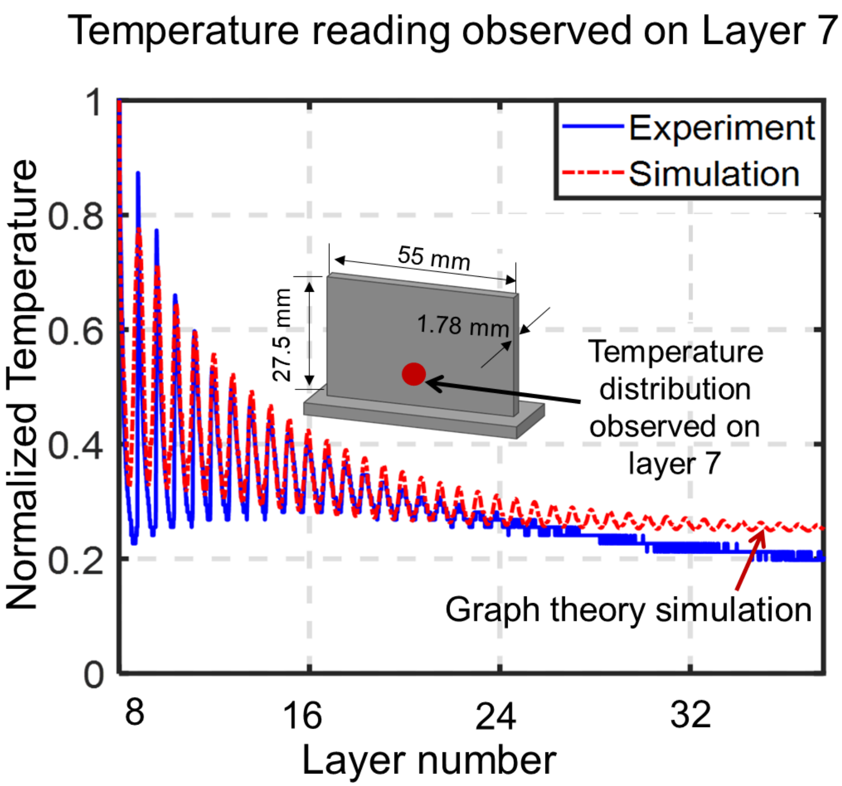

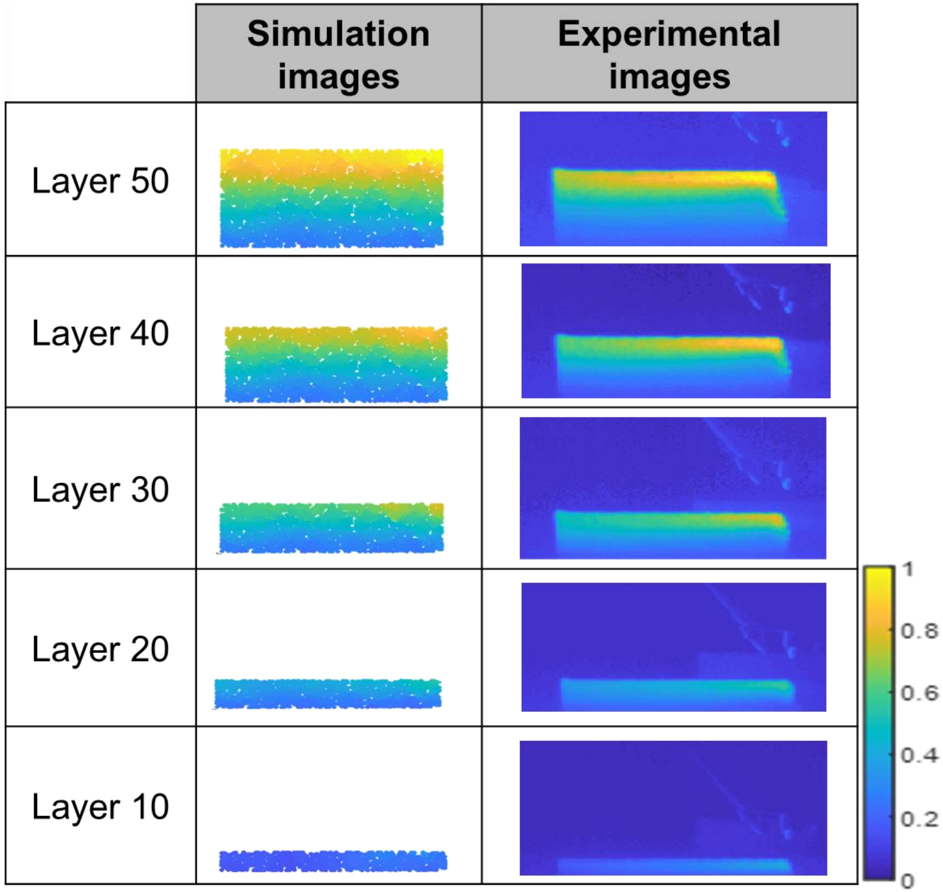

Combining Simulation and Sensor Data

Experimental Data
Meltpool Images

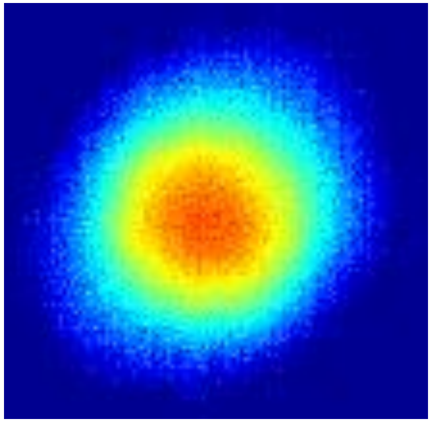

Part-level Simulation

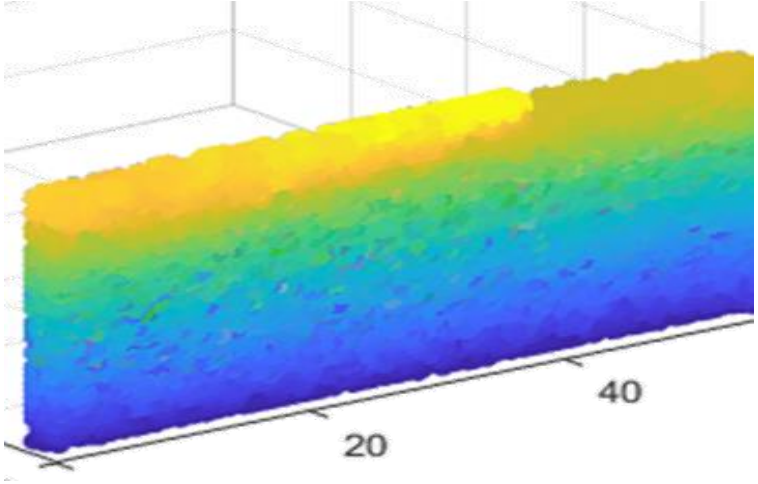

Ground Truth: XCT

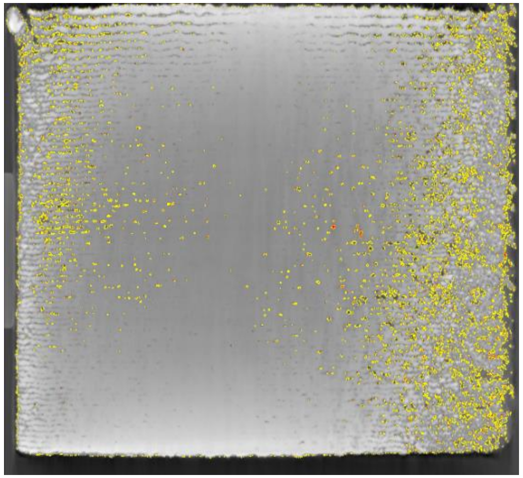

- Extract the mean, standard deviation of area of each melt pool image where pixel values are above 1600 ^{o}C.
- Extract the mean, standard deviation of the simulated temperature in the corresponding area of the part.
- Use X-ray CT data to label locations with flaw size larger than 100 μm.

Prediction of Porosity

The digital twin predicts the occurrence of porosity with higher accuracy in comparison to individual sensor and simulation data.

Data	**Input features**	**F-Score**
Pyrometer data	mean, standard deviation of meltpool area.	81.6% (3.2%)
Simulation data	mean, standard deviation of temperature readings.	82.9% (2.7%)
Digital Twin: Pyrometer + Simulation data	mean, standard deviation of pyrometer readings. + mean, standard deviation of temperature readings.	**91.0% (1.2%)**

Outline

- Introduction
- Graph theory approach in AM
- Part 1: Verification of the graph theory approach

How does it compare to the known solutions and existing techniques?

  - Graph Theory vs. exact analytical solution (Green's Function)
  - Graph Theory vs. finite element for AM
- Experimental validation of the graph theory approach

Part II: Application (Digital Twin)

So what – who cares about thermal simulations?

- *Conclusions and future work*

Graph theory is shown to be faster than high-resolution FE analysis

Graph theory simulates the thermal field with error within 10% and in 1/10th of time of FE.

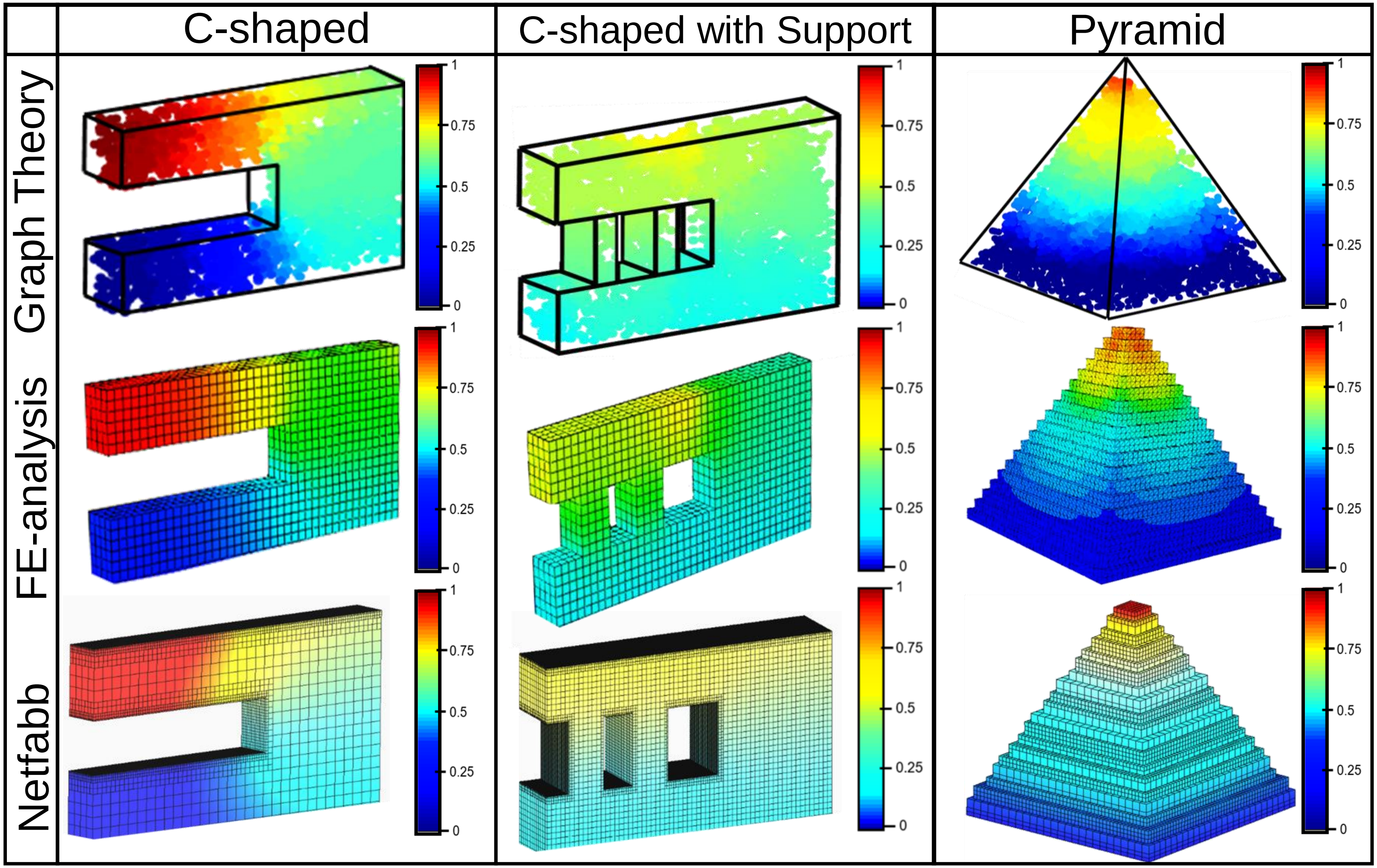

Graph theory is faster than coarse-resolution FE analysis.

Graph theory simulates the thermal heat field with error less than 10% of experimental data, and about 25% faster than FEA Test parts have a simple geometry.

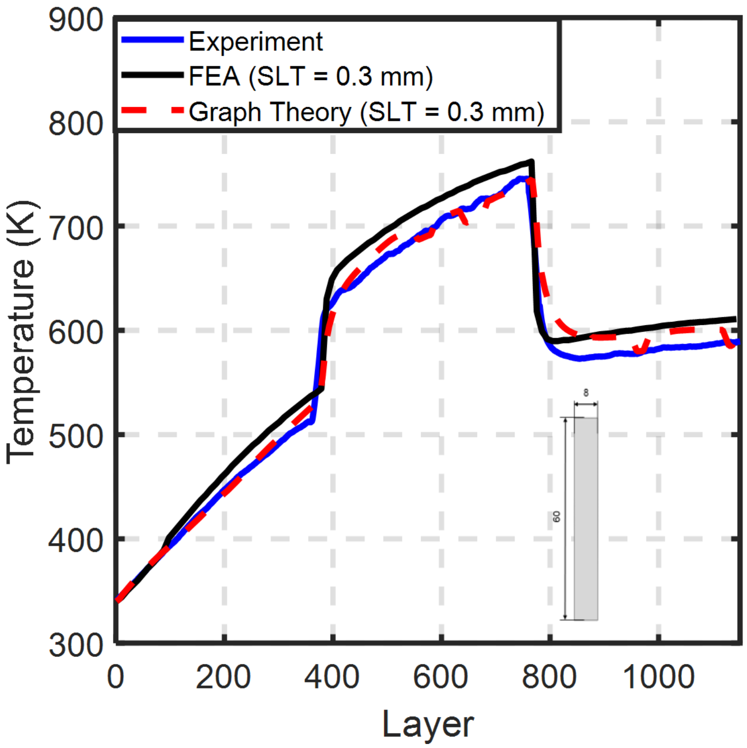

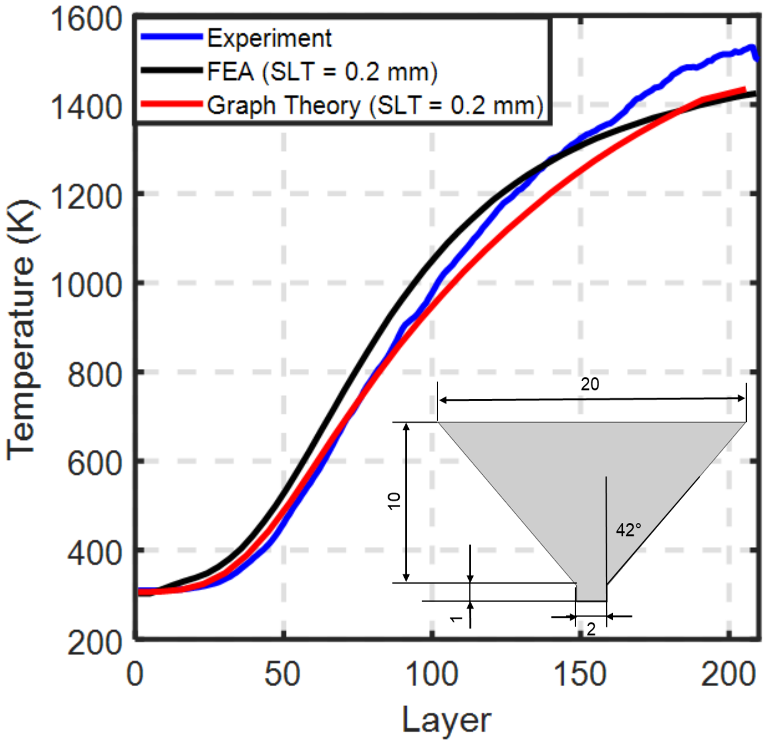

Graph theory scales to large part geometry.

Error ≈10% to 15% of experimental data, and within 1/20th of the build time for a large part.

Computation Time: 37 min.
MAPE: 10.8%

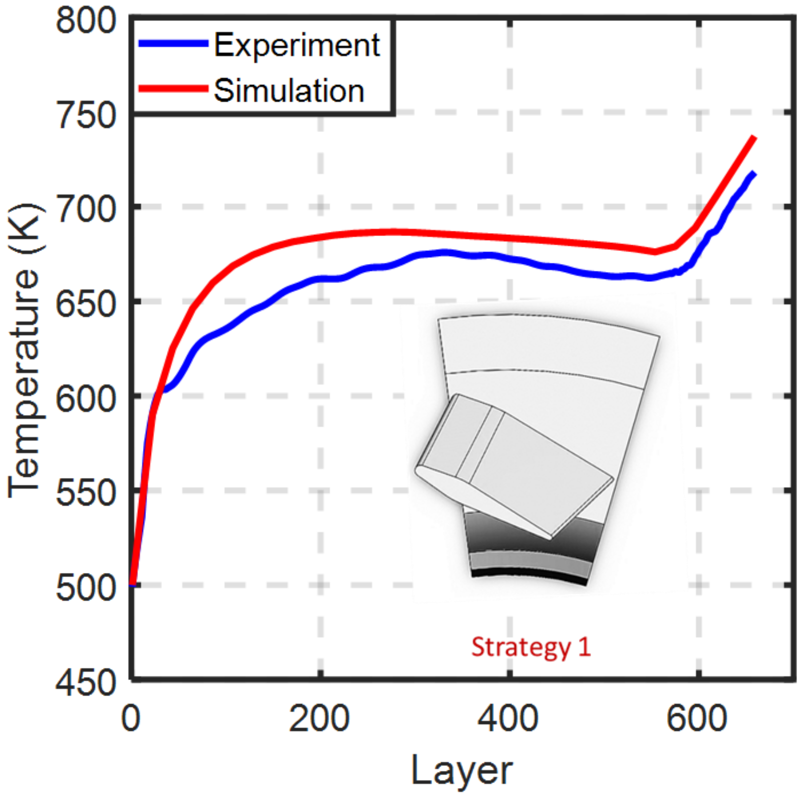

Computation Time: 11 min.
MAPE: 14.2%

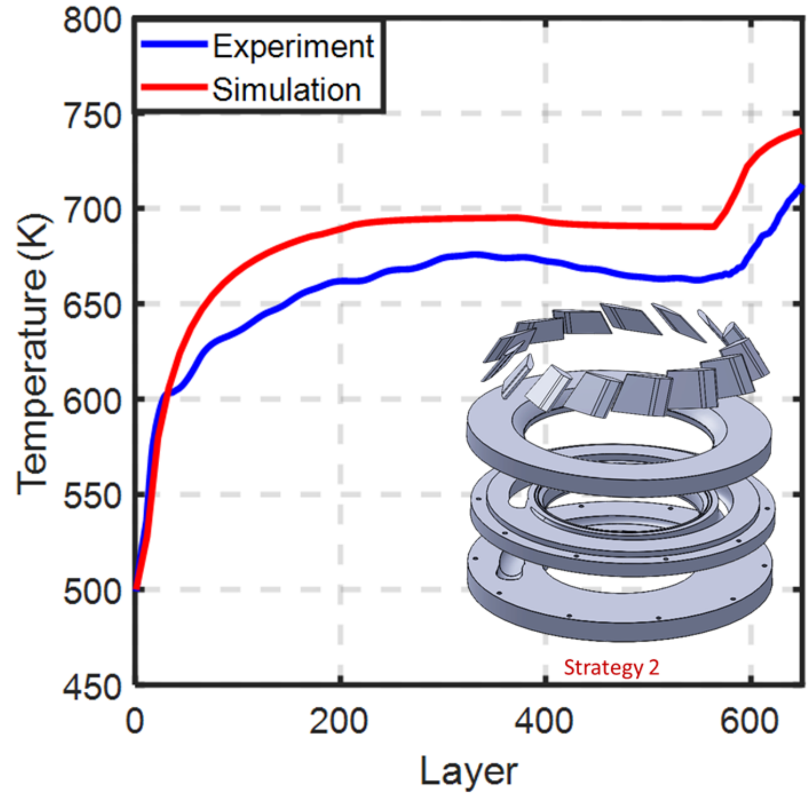

Thermal simulations combined with sensor data leads to fast prediction

The digital twin predicts the occurrence of porosity with higher accuracy in comparison to individual sensor and simulation data.

Data	**Input features**	**F-Score**
Pyrometer data	mean, standard deviation of meltpool area.	81.6% (3.2%)
Simulation data	mean, standard deviation of temperature readings.	82.9% (2.7%)
Digital Twin: Pyrometer + Simulation data	mean, standard deviation of pyrometer readings. + mean, standard deviation of temperature readings.	**91.0% (1.2%)**

Outline

- Goal and Motivation
- Graph theory approach in AM
- Part 1: Verification of the graph theory approach
- Part 2: Experimental validation of the graph theory approach
- Oak Ridge + UNL $\longrightarrow$ ∞ Opportunities

Collaboration Opportunities with Oakridge → ∞

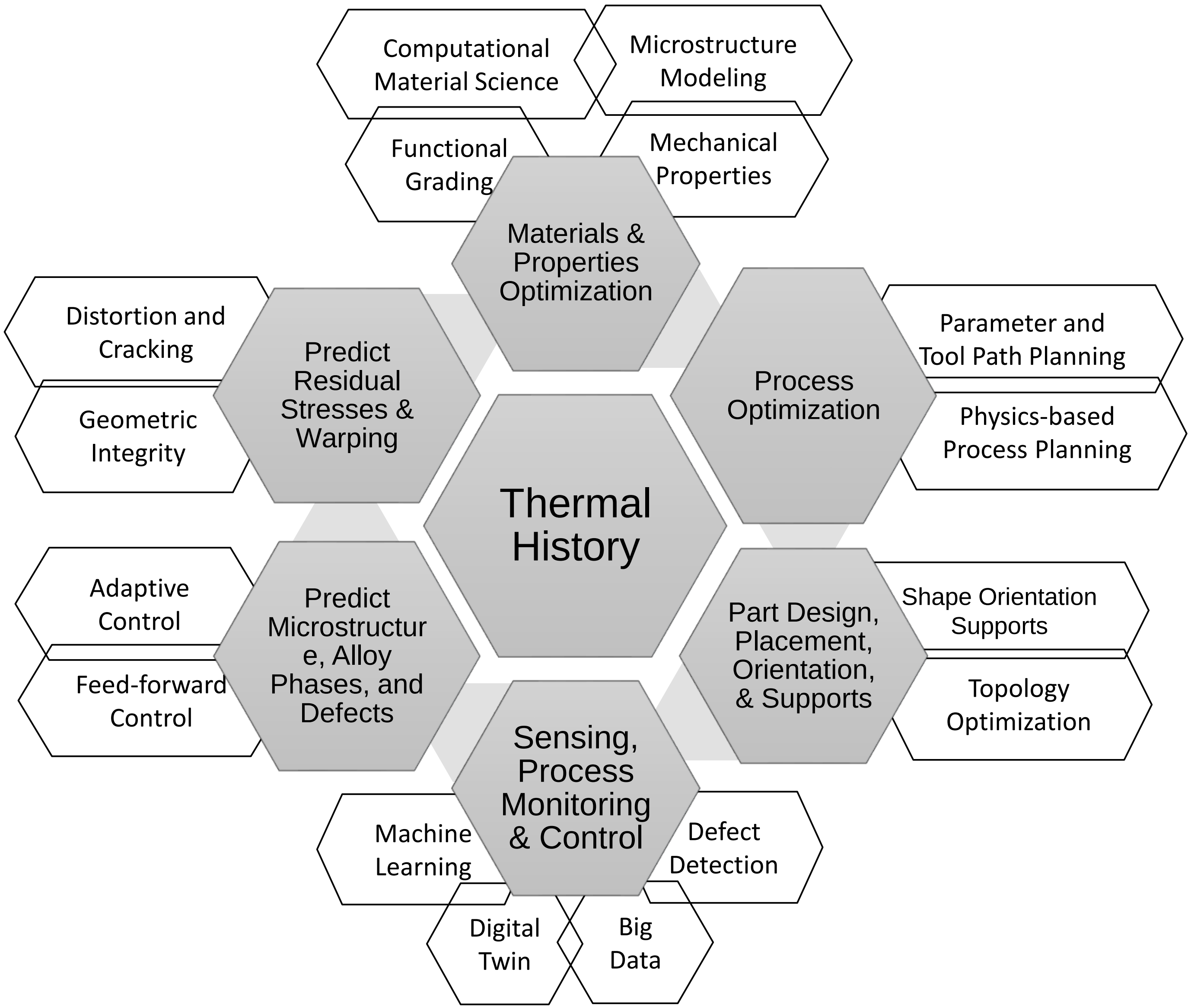

Three “right now” areas for Collaboration with Oakridge

- Commercialization of the graph theory approach
- Thermal Modeling of Wire DED: Dr. Andrzej Nycz.
- Monitoring, Analytics, and Defect Detection in AM and Manufacturing.

Opportunities for Commercialization

- Optimize graph theory approach for parallel computation
- Algorithm is currently implemented in Matlab (single core processing)

Validation with Directed Energy Deposition Experiments

"Under construction; beware graduate students at work"

Total of 62 layers of titanium deposited.

Build Time 26 minutes Computation time 7 minutes

Side View

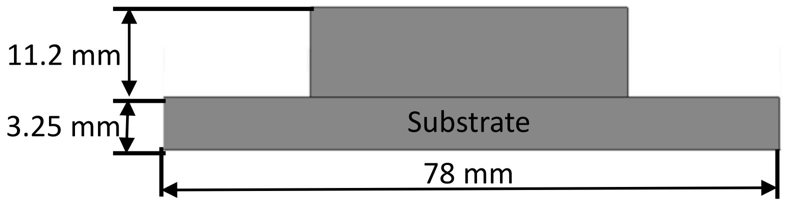

Top View

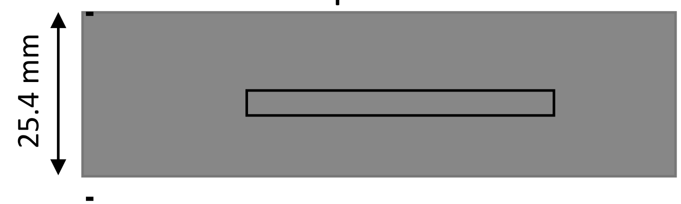

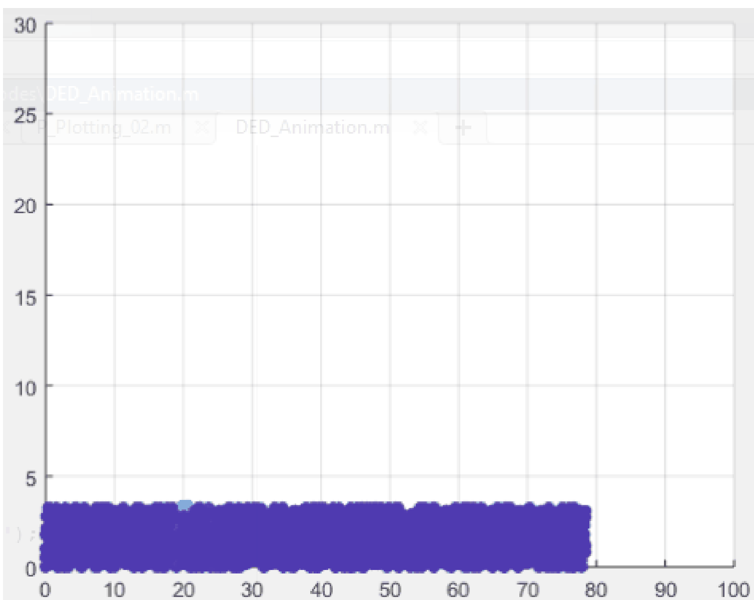

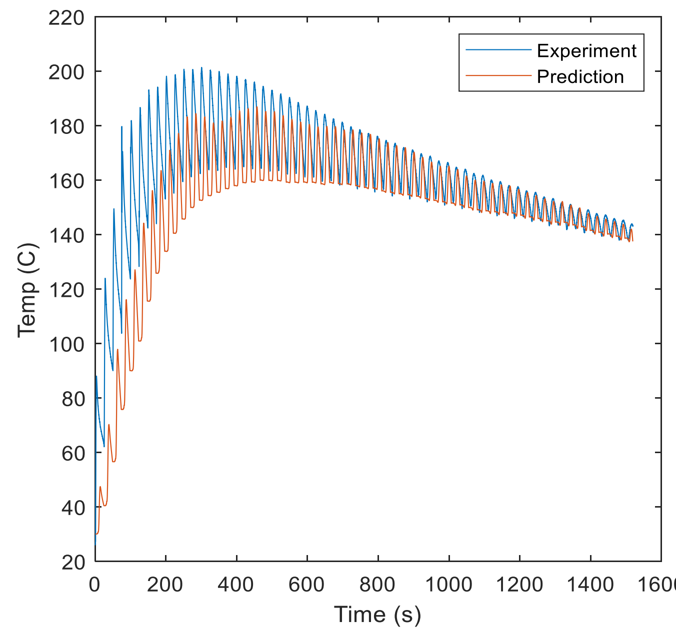

Data from: Heigel, J., Michaleris, P, and Reutzel, T. *Thermo-mechanical model development and validation of directed energy deposition additive manufacturing of Ti–6Al–4V, Additive Manufacturing Volume 5, January 2015, Pages 9-19*

Sensing and Machine Learning for Defect Detection in AM

25+ Publications in AM Monitoring (LPBF, DED, AJP, Binder Jetting, FFF),

https://engineering.unl.edu/mme/faculty/prahalada-rao/

- M. Montazeri, A. Nassar. C. Stutzman, P. Rao, Heterogeneous Sensor-based Condition Monitoring in Directed Energy Deposition, Additive Manufacturing, (Accepted, In-press). doi.org/10.1016/j.addma.2019.100916
- M. Montazeri, A. Nassar, A. Dunbar, P. Rao, *In-Process Monitoring of Porosity in Additive Manufacturing Using Optical Emission Spectroscopy Signals*, IISE Transactions (Manufacturing and Design), 2019, Accepted, In-Press (Published Online). doi: 0.1080/24725854.2019.1659525
- M. Montazeri, R. Yavari, P. Rao, P. Boulware. *In-process Monitoring of Material Cross-Contamination Defects in Laser Powder Bed Fusion*. ASME Transactions, Journal of Manufacturing Science and Engineering, 140(11), 111001-20, 2018. doi: 10.1115/1.4040543
- J. Williams, P. Dryburgh, A. Clare, P. Rao, A. Samal, *Defect Detection and Monitoring in Metal Additive Manufactured Parts through Deep Learning of Spatially Resolved Acoustic Spectroscopy Signals.* ASTM Journal of Smart and Sustainable Manufacturing, Vol. 2(1), 204-226, 2018. doi/10.1520/SSMS20180035
- F. Imani, A. Gaikwad[2], M. Montazeri[3], P. Rao, H. Yang, E. Reutzel. *Process Mapping and In-Process Monitoring of Porosity in Laser Powder Bed Fusion Using Layerwise Optical Imaging.* ASME Transactions, Journal of Manufacturing Science and Engineering, 140(10), 101009-23, 2018. doi: 10.1115/1.4040615
- J. Liu, C. Liu, Y. Bai, Z. Kong, P. Rao, and C. Williams. *Layer-wise Spatial Modeling of Porosity in Additive Manufacturing.* IISE Transactions, (Additive Manufacturing Special Issue), Accepted, In-Press, 2018. Article Highlighted in January 2019 issue of the Industrial and Systems Engineer Magazine.doi:/10.1080/24725854.2018.1478169
- F. Imani, B. Yao, R. Chen, P. Rao, H. Yang, *Joint Multifractal and Lacunarity Analysis of Image Profiles for Manufacturing Quality Control* (Technical Brief), ASME Transactions, Journal of Manufacturing Science and Engineering, 141(4), 044501-08, 2018.doi: 10.1115/1.4042579.
- J. Lombardi, R. Salary, D. Weerawarne, P. Rao, M. Poliks, *Image-Based Closed-Loop Control of Aerosol Jet Printing Using Classical Control Methods*, ASME Transactions, Journal of Manufacturing Science and Engineering, 141(7), 071011-20, 2019. doi: 10.1115/1.4043659

Have Data will Crunch

Detecting Porosity from In-Situ Sensor Data in Directed Energy Deposition (DED)

M. Montazeri[1], C. B. Stutzman[2], A. R. Nassar[2], P. Rao[1*]

[1] Laboratory for Advanced Manufacturing Processes and Sensing, Mechanical and Materials Engineering (M²E), University of Nebraska-Lincoln.
[2] Applied Research Laboratory, Pennsylvania State University
* Contact: rao@unl.edu, Assistant Professor, M²E.

Objectives and Motivation

- **Objective**: Detect the onset of defects, such as porosity, in additively manufactured metal parts using data acquired from two sensors, namely, a spectrometer and a visible spectrum optical camera.
- **Hypothesis**: The process signatures derived from our graph theoretic analysis of sensor data predicts lack-of-fusion porosity with high accuracy
- **Motivation**: Defects in metal AM processes, such as DED, can occur despite offline empirical optimization

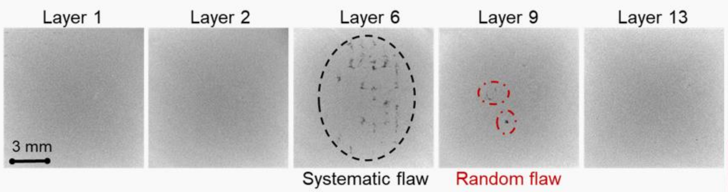

Occurrence of Systematic and random flaws in different layers of one part under the same printing conditions

Experimental Test Coupons

- Test Coupon Dimension: 15 mm × 15 mm × 10 mm (L×W×H).
- Metal Powder: titanium alloy Ti-6Al-4V.
- Fixed Printing Parameters: print speed (10.6 mm/sec), layer height (0.254 mm), hatch spacing (1 mm).

		Laser Power (P, Watt)					
		300		425		475	
Hatch Pattern (H)		Parallel	Cross	Parallel	Cross	Parallel	Cross
Powder Flow Rate (F, g/min)	2						
	3						
	4						

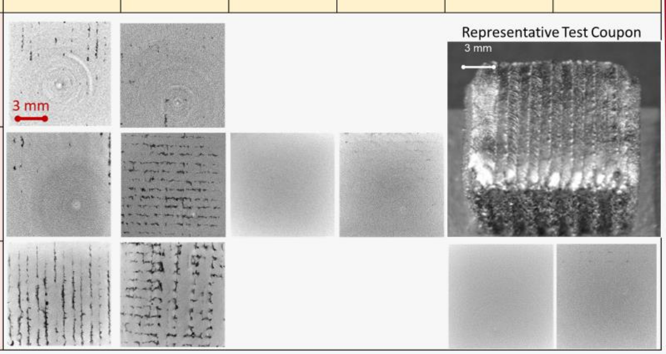

Sensor Setup in DED

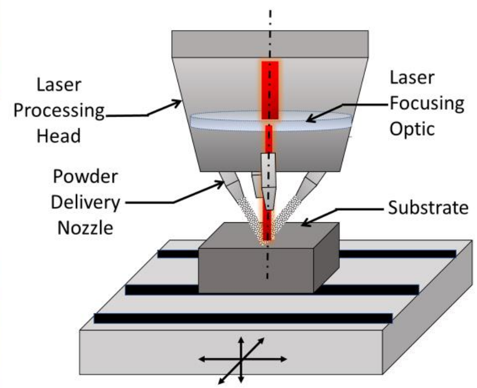

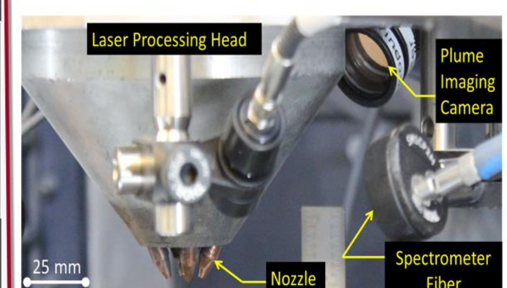

Offline Analysis of Porosity from X-ray Images

Image processing steps for extraction of pores from X-ray Computed Tomography (XCT) images.

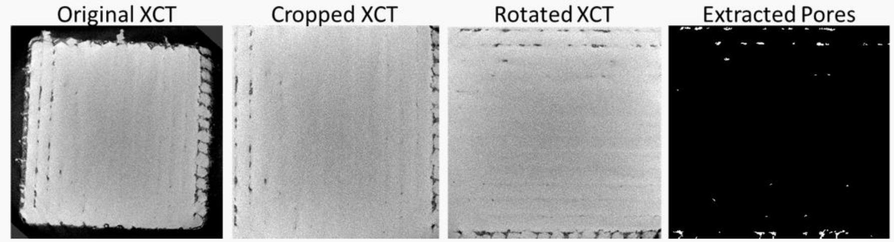

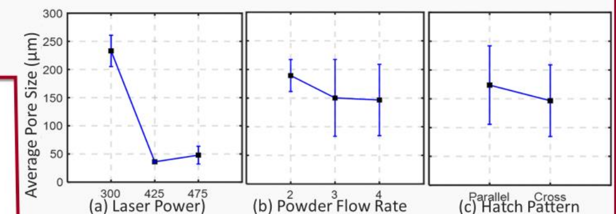

Online Prediction of Porosity from Sensor Data

Our graph theory approach predicts the severity level of pores from in-process sensor data with 85% accuracy.

Confusion Matrix for two-Level Classification of Pore Severity

True Level of Pore Severity ↓	Predicted Size of the Pore	
	Low Severity (Pores Size < 50 µm)	*High Severity* (Pores Size > 50 µm)
Low	20 (out of 26)	6 (False Alarm)
High	12 (Failing to detect)	62 (out of 74)

Confusion Matrix for Three-Level Classification of Pore Severity

True Level of Pore Severity ↓	Predicted Size of the Pore		
	Low Severity (Pore Size < 50 µm)	*Medium Severity* (50 µm < Pore Size < 200 µm)	*High Severity* (Pore Size > 200 µm)
Low	20 (out of 26)	0	6
Medium	4	21 (out of 37)	12
High	6	9	22 (out of 37)

Detecting Pore Formation in Laser Powder Bed Fusion Using In-Process Optical Emission Spectroscopy

M. Montazeri[1], A. J. Dunbar[2], A. R. Nassar[2], P. Rao[1*]

[1] Mechanical and Materials Engineering, University of Nebraska-Lincoln.
[2] Applied Research Laboratory, Pennsylvania State University

Objectives and Motivation

Identification and isolation of defects in terms of porosity level or severity in laser powder bed fusion (L-PBF) using in-process multispectral sensor data.

Schematic of the L-PBF process

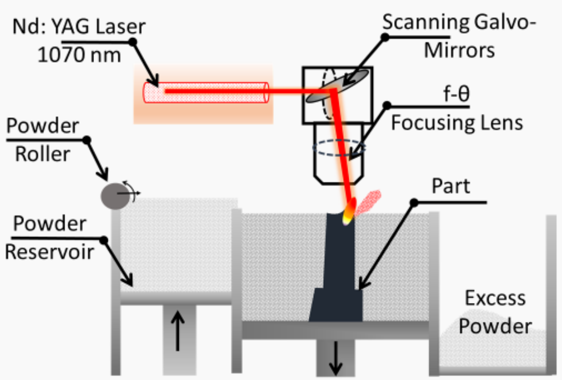

Build Conditions

Inconel 718 cylindrical parts that are 12 mm in diameter and 6.6 mm in height are printed on a 3D Systems ProX DMP 200 L-PBF machine under four conditions.

Nominal Conditions:
laser power (P) = 300 W, hatch spacing (H)= 50 µm,
laser scan velocity (V) = 2.5 m/s

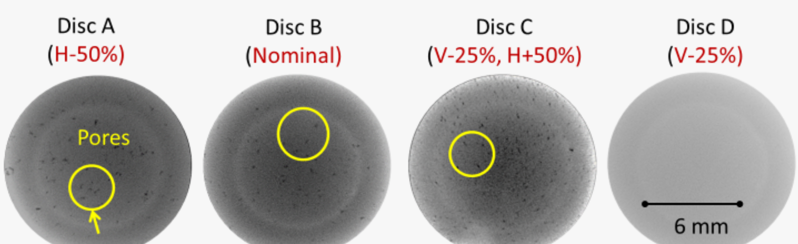

Schematic of the Multispectral Sensor

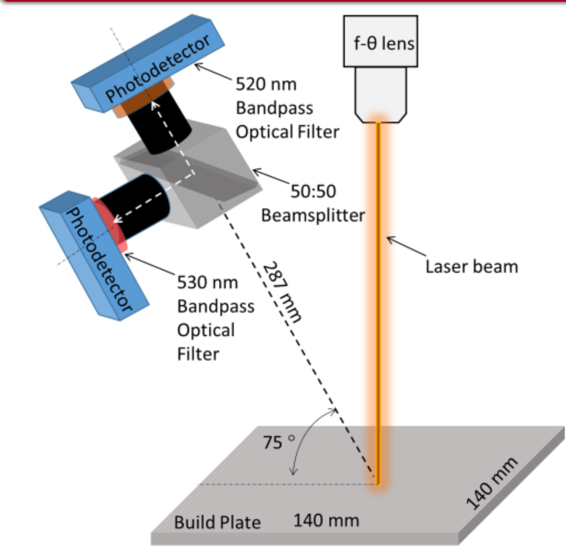

Quantification of Porosity

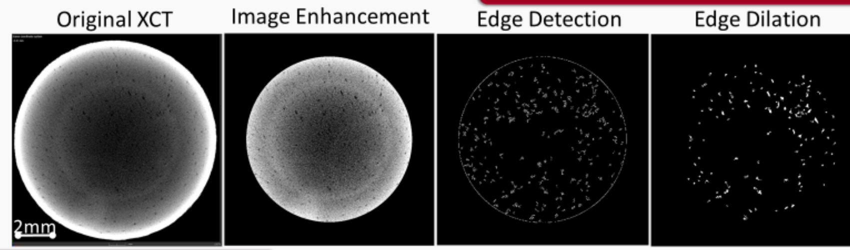

Using the extracted porosity, a dimensionless number (μ) is calculated between 0 and 1, representative of three porosity characteristics namely size, number and distribution along the cylinder surface.

Data Analysis and Results

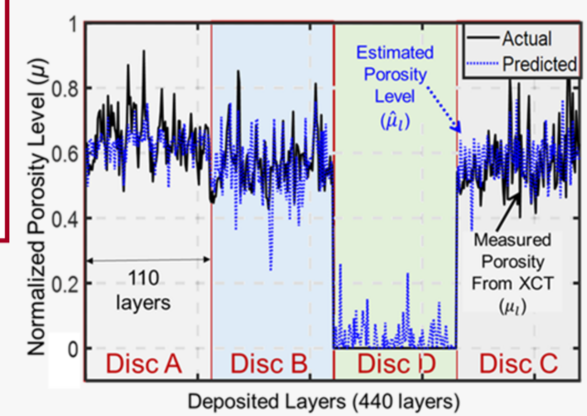

Our graph theoretic machine learning approach predicts the exact level of porosity with 90% accuracy using optical emission data.

In-Process Detection of Material Contamination Defects in Laser Powder Bed Fusion

M.Montazeri[1], R.Yavari[1], P.Rao[1*], and P. Boulware[2]

[1] Mechanical and Materials Engineering, University of Nebraska-Lincoln. [2]Edison Welding Institute (EWI).

Publication: In-process Monitoring of Material Cross-Contamination Defects in Laser Powder Bed Fusion . *ASME Transactions*, 2018.

Funding: National Science Foundation (NSF), CMMI-1752069 (CAREER)

Objective and Motivation

- Material contamination originates from poor quality control of the feedstock and residue from previous builds (Fig. 1)
- Contamination leads to decreased fatigue life and crack initiation.

Objective. Develop and apply a spectral graph theoretic approach to detect material contamination in real-time in LPBF using in-process sensor data.

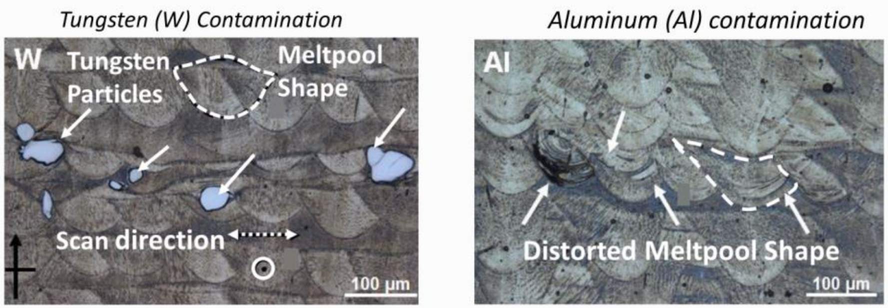

Fig. 1 Micrograph of Inconel 625 sample contaminated with W and Al.

Sensor Data Acquisition

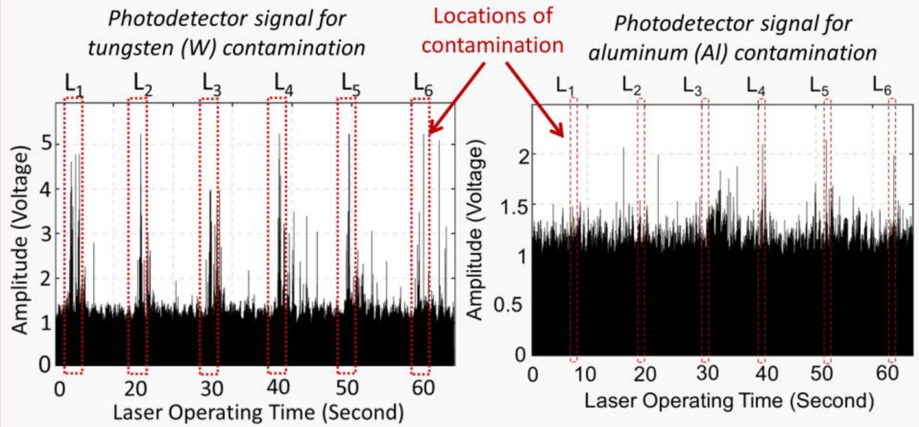

Fig. 4 photodetector signal associated with tungsten and aluminum contamination. Photodetector signals were acquired at 10 KHz during scanning (1 data point/10 μm).

Experimental Setup

- Six levels of tungsten and aluminum contamination ($L_1 - L_6$) were introduced in separate Inconel 625 samples (10 × 10 × 15 mm) . X-ray CT analyses indicates (Fig. 3) that contaminants spread to both subsequent and previously layers.
- Photodetector signals were acquired during the build (Fig. 2).

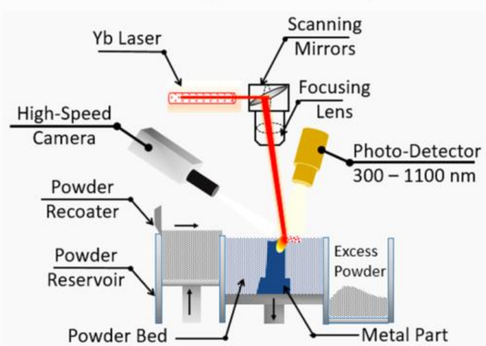

Fig. 2 Experimental Setup integrated with a coaxial photodetector sensor.

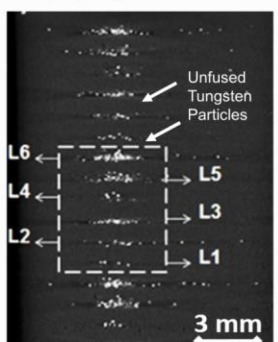

Fig. 3 X-Ray CT scan of Inconel 625 sample contaminated with W particles.

Data Analysis and Results

- Convert the signal into its network graph equivalent, and extract spectral graph Fourier coefficients to track contamination (Fig. 5).
- Spectral graph Fourier coefficients correctly locate the contaminated layer with statistical accuracy greater than 95%, and within 0.8 milliseconds (Fig. 6).

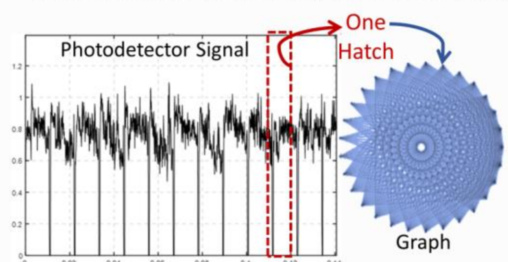

Fig. 5. Convert the photodetector signal hatch-by-hatch into graph. Use the eigenvalues of the graph as features for detecting defects.

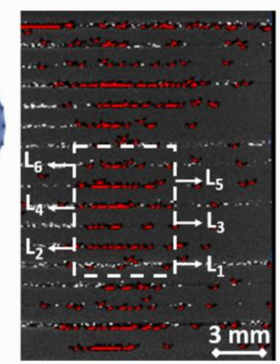

Fig.6 Spectral graph coefficients (red dots) overlaid on the X-Ray CT scan match with contamination (white dots).

The AM pie is Big.

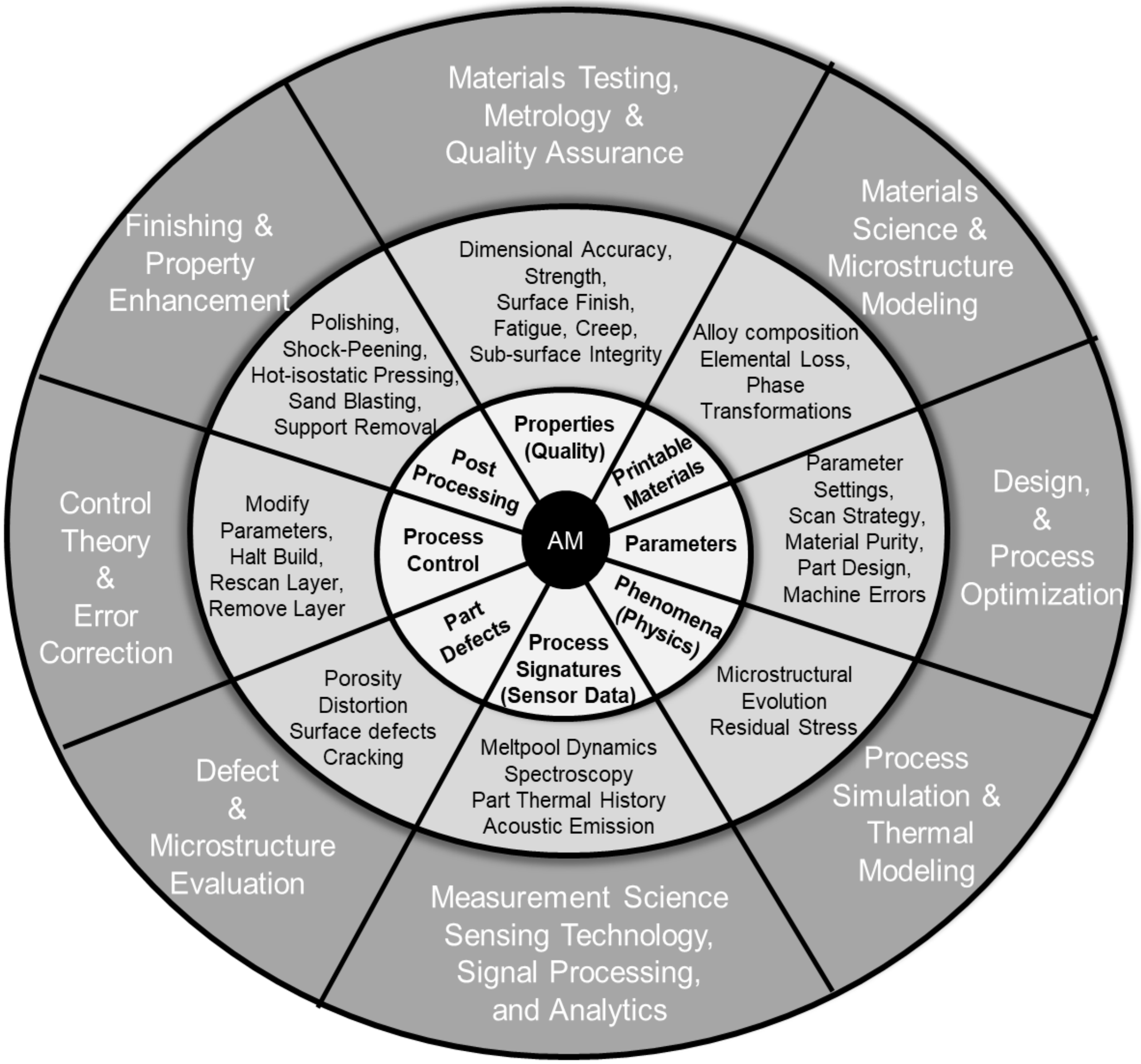

Speaker Information

Prahalada Rao
Assistant Professor
Mechanical and Materials Engineering

University of Nebraska-Lincoln
rao@unl.edu
Cell: 814-384-9676

https://engineering.unl.edu/lamps/

Appendix III

Procedure used to filter transients from IR Data.

Build 1 (Cylinder) Thermal Data

Raw IR camera measurements includes of several high and low peaks.

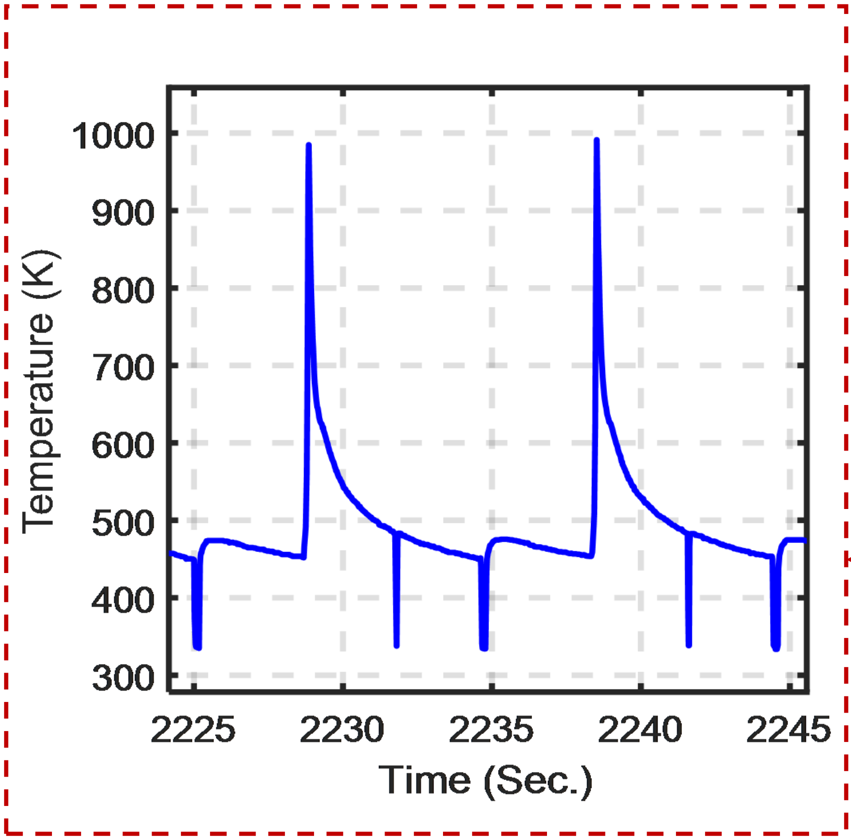

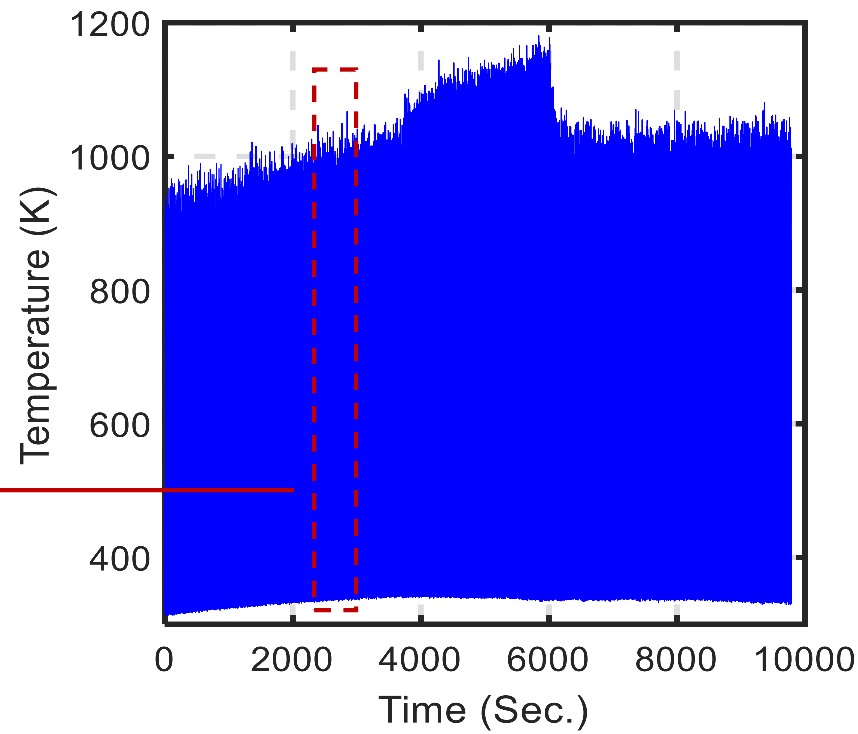

Raw IR camera measurements includes of several high and low peaks.

Removing Transients from IR Data

1 : Laser is located at the pixel traced by the IR-camera images

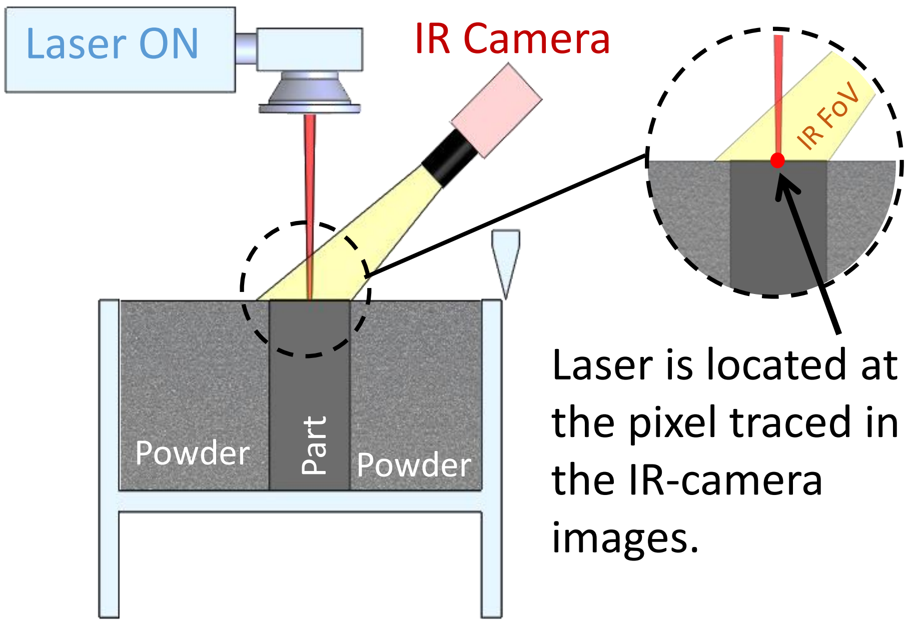

Laser is located at the pixel traced in the IR-camera images.

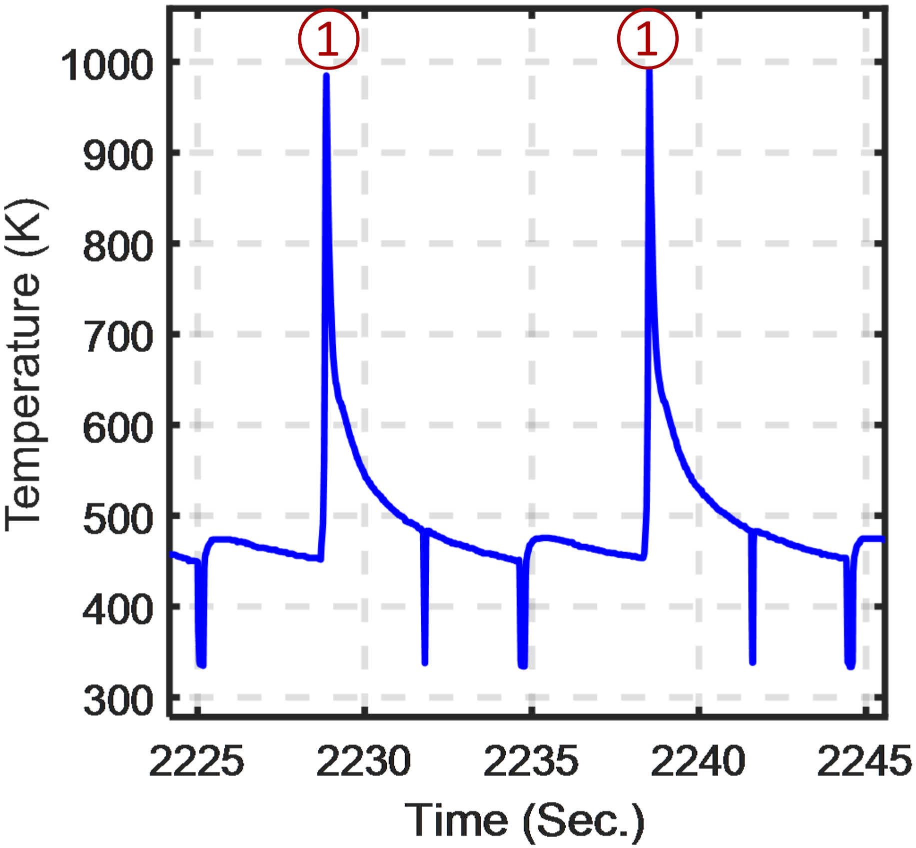

Removing Transients from IR Data

Inter-layer cooling time (ILCT): The time between successive scans, layer-to-layer.

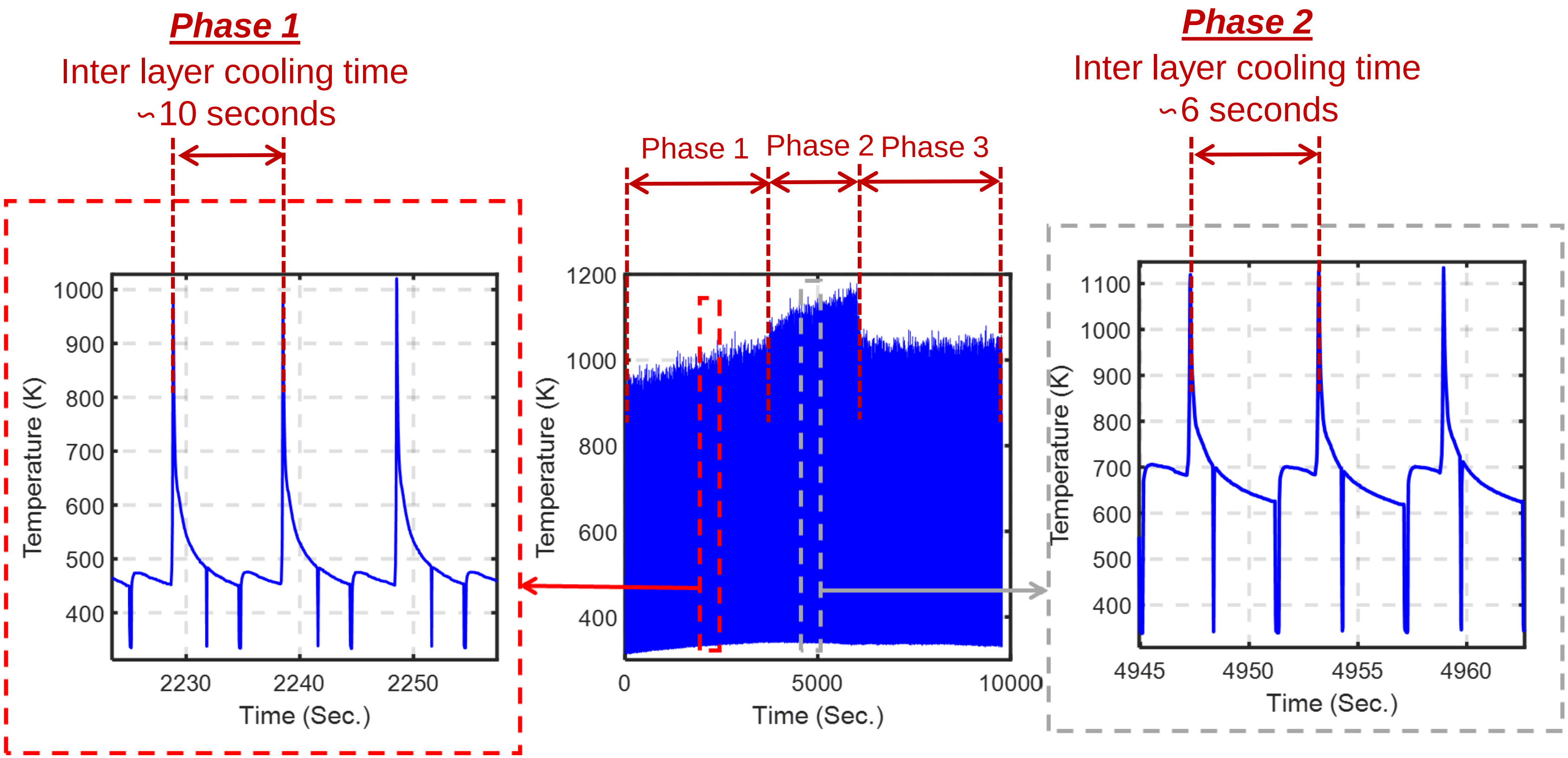

- Phase 1: 10 seconds
- Phase 2: 6 seconds
- Phase 3: 10 seconds

Removing Transients from IR Data

② : Recoater returns to back for powder

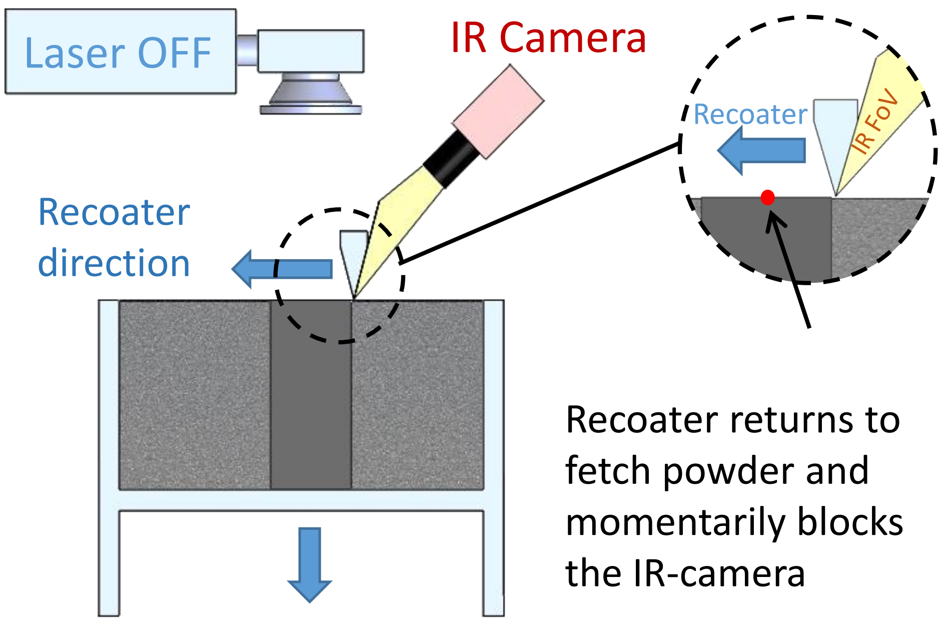

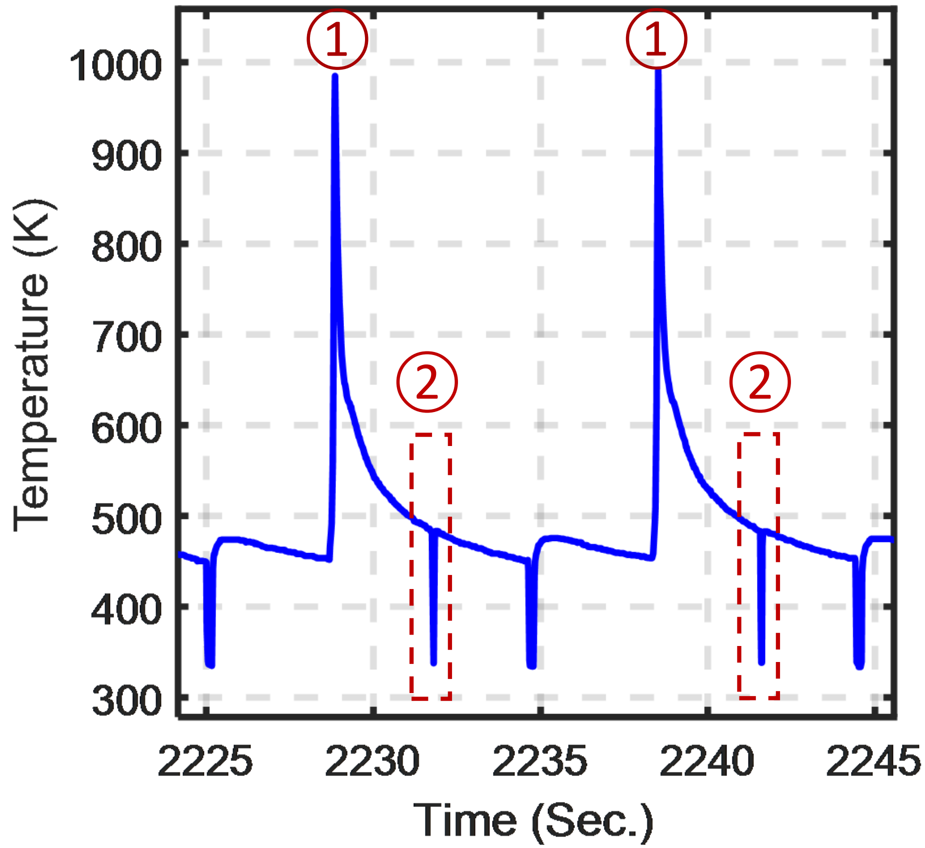

Removing Transients from IR Data

③ : Recoater spreads powder for a new layer

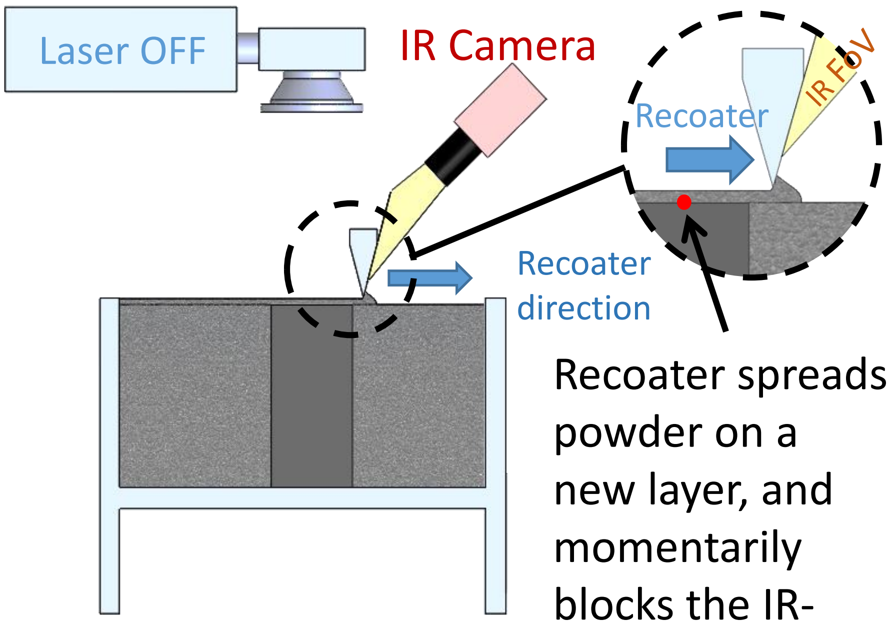

Recoater spreads powder on a new layer, and momentarily blocks the IR-camera.

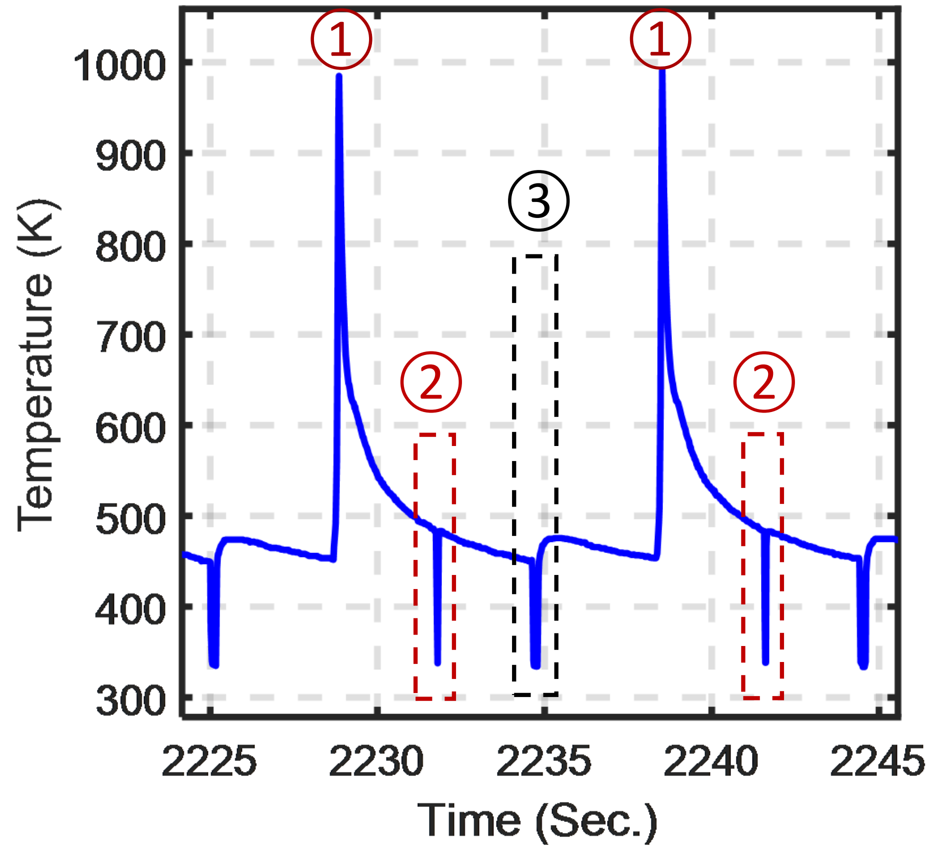

Calibration of IR Camera Measurements

- Calibration function applied to convert the raw IR camera data to temperature values.
- IR camera was calibrated empirically for both solid and powder.
- AM part temperature was controlled using a cartridge heater.
- Absolute temperature trends captured using thermocouples embedded in a cavity.

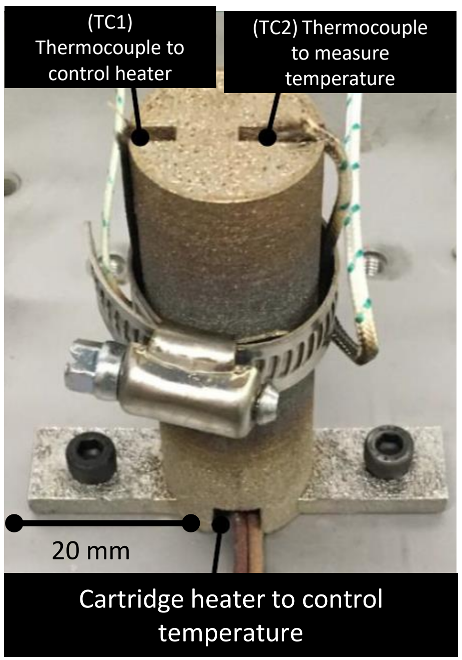

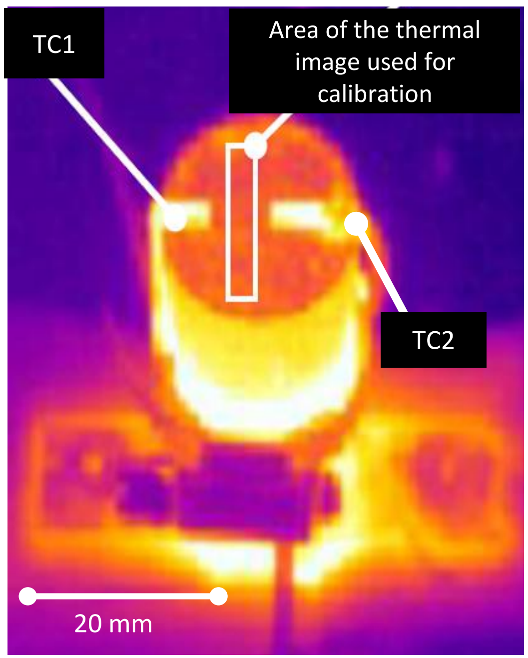

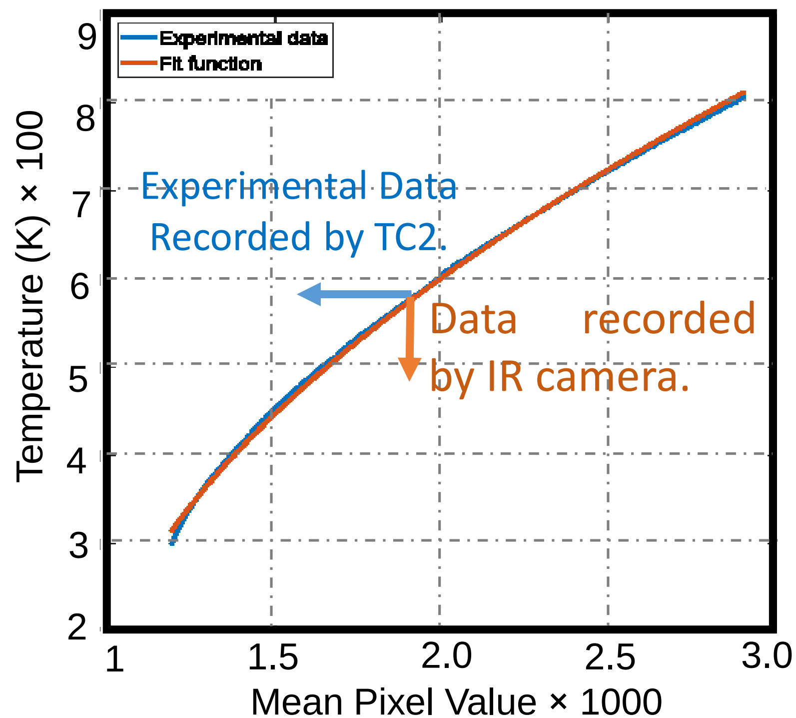

Williams, R., Piglione, A. , Ronneberg, T. , Pham, M. S., Davis, C. M. and Hooper, P. A. , 2019, "In-situ thermography for laser powder bed fusion: effects of layer temperature on porosity, microstructure and mechanical properties", *Additive Manufacturing*, In Press

Build 1 (Cylinder) Thermal Data

The temperature recorded at center pixel of the middle cylinder.

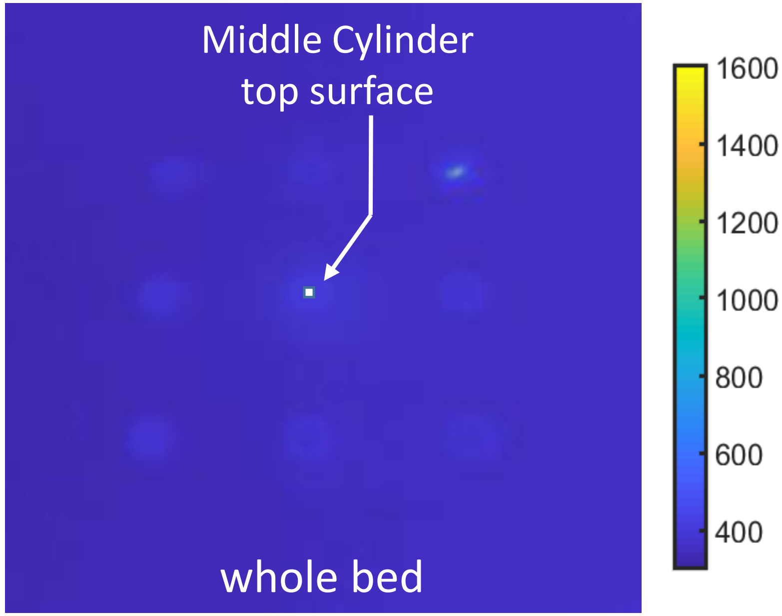

600,000 frames, 60 frames per second.

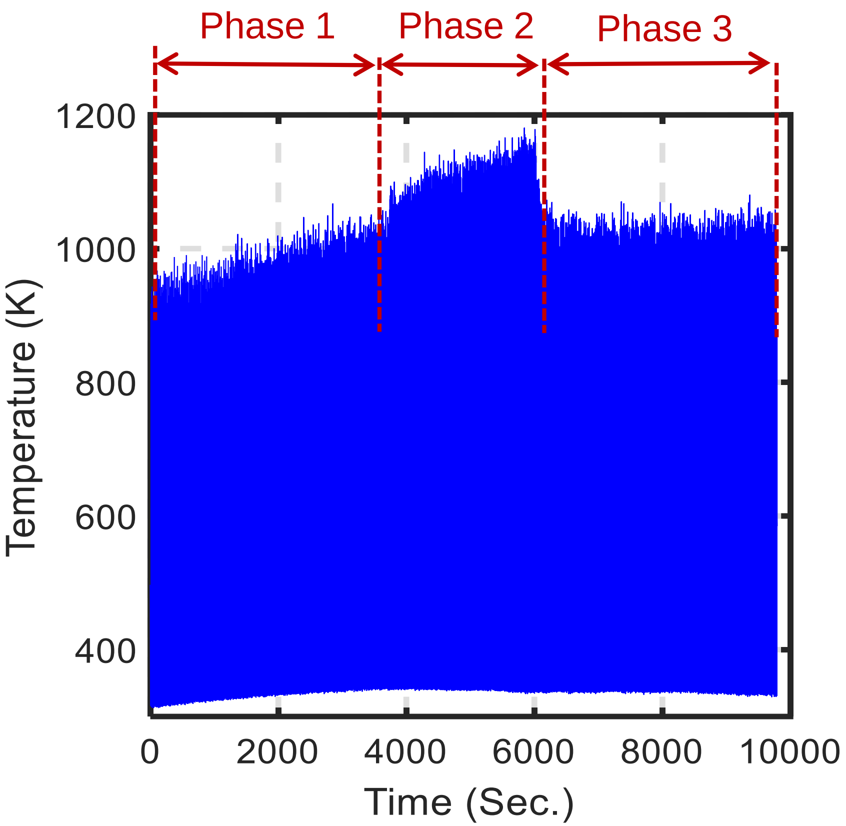

3 hours build time.

Thermal data is filtered to remove IR transients.